KfK 3028
Oktober 1980

KfK In-Pile Tests on LWR Fuel Rod Behavior During the Heatup Phase of a LOCA

E. H. Karb, L. Sepold,
P. Hofmann, C. Petersen, G. Schanz, H. Zimmermann
Hauptabteilung Ingenieurtechnik
Institut für Material- und Festkörperforschung
Projekt Nukleare Sicherheit

Kernforschungszentrum Karlsruhe

KERNFORSCHUNGSZENTRUM KARLSRUHE

HAUPTABTEILUNG INGENIEURTECHNIK
INSTITUT FÜR MATERIAL- UND FESTKÖRPERFORSCHUNG
PROJEKT NUKLEARE SICHERHEIT

KfK 3028

KfK In-Pile Tests on LWR Fuel Rod Behavior During the Heatup Phase of a LOCA

E.H. Karb
L. Sepold
P. Hofmann
C. Petersen
G. Schanz
H. Zimmermann

Kernforschungszentrum Karlsruhe GmbH, Karlsruhe

Kernforschungszentrum Karlsruhe GmbH
ISSN 0303-4003

Abstract

This report summarizes the results of the FR2 In-Pile Tests on LWR fuel rod behavior under LOCA conditions evaluated to date. The in-pile tests with the objective of investigating the influence of a nuclear environment on the mechanisms of fuel rod failure are being conducted with irradiated and unirradiated short-length single rods of a PWR design. The main parameter of the experimental program is the burnup, ranging from 2500 to 35000 MWd/t. Part I of this report describes the test results and the results of the non-destructive posttest examinations, part II presents the results of the metallographic evaluation of the unirradiated test specimens. The report also provides information on the condition of the UO_2 fuel after preirradiation and after the transient testing.

The test results with respect to the burst data, i.e. burst temperature, burst pressure, and burst strain, do not indicate major differences from out-of-pile data. No influence of burnup on the burst data was observed.

-.-.-.-.-.-.-.-.-.-.-.-

KfK-in-pile-Versuche zum Brennstabverhalten in der Aufheizphase eines LOCA

Kurzfassung

Dieser Bericht faßt die Ergebnisse der FR2 In-pile-Versuche, die bisher ausgewertet worden sind, zusammen. Mit den In-pile-Versuchen soll der Einfluß nuklearer Kenngrößen auf die Mechanismen des Brennstabversagens untersucht werden. Die Versuche wurden sowohl mit unbestrahlten als auch mit vorbestrahlten Prüflingen, die bezüglich der radialen Abmessungen DWR-Brennstäben entsprechen, durchgeführt. Hauptparameter des Versuchsprogramms ist der Abbrand, der von 2500 bis 35000 MWd/t variiert wird.

Teil I des Berichtes beschreibt u.a. die Ergebnisse aus den Versuchsdaten und aus der zerstörungsfreien Nachuntersuchung der Prüflinge. Teil II gibt die Ergebnisse der metallografischen Untersuchungen an unbestrahlten Teststäben wieder. Der Bericht enthält auch Information über Brennstoffzustand nach der Vorbestrahlung und nach den transienten Versuchen.

Die z.Z. verfügbaren Ergebnisse lassen bezüglich der Berstdaten, wie Berstemperatur, Berstdruck und Berstdehnung, keinen Unterschied zu Out-of-pile-Ergebnissen erkennen. Es wurde kein Einfluß des Abbrandes auf die Berstdaten gefunden.

Summary

This report summarizes the results of the FR2 In-Pile Tests on LWR Fuel Rod Behavior evaluated to date. It is used as a basis for our contribution to the planned CSNI * State-of-the-Art Report (SOAR) entitled "Fuel Behavior During a LOCA". The FR2 In-Pile Test results will be input for section B of the SOAR, which is concerned with ballooning behavior of irradiated cladding in in-reactor tests.

The in-pile experimental program is performed with single rods in the DK loop of the FR2 reactor at the Kernforschungszentrum Karlsruhe (KfK). The research is part of the Nuclear Safety Project's (PNS) LWR fuel behavior program. The main objective of the FR2 In-Pile Tests is to provide information about the effects of a nuclear environment on the mechanisms of fuel rod failure in the second heatup phase of a LOCA (Loss-of-Coolant Accident). The test rods are exposed to a transient heatup resulting in cladding ballooning and rupture.

The test rods used in the experiments have a heated length of 50 cm, and their radial dimensions are identical with those of a commercial German PWR (Pressurized Water Reactor). Tests are performed with unirradiated as well as with previously irradiated rods. Main parameter of the program is the burnup, ranging from 2500 to 35000 MWd/t. The test rods are filled with helium to internal pressures representing the range of PWR rod pressures.

To date, 39 in-pile tests have been completed and about half of the tested rods are post-examined. The test results available at this time do not indicate any influence of the nuclear environment on the mechanisms of fuel rod failure. In particular, the burst data of the in-pile test rods, i.e. the burst pressures, burst temperatures, and burst strains, lie in the data band obtained from out-of-pile experiments with electrically

*) Committee on the Safety of Nuclear Installations

heated fuel rod simulators. No influence of the burnup on the burst data was observed, also no difference between the unirradiated and the previously irradiated test specimens.

However, all tests with previously irradiated rods exhibited a fuel condition different from the experiments with unirradiated fuel rods. The fuel, already cracked during previous irradiation, fragmented during the transient tests due to cladding ballooning. The pellets in the ballooned regions lost their shape and the fragments filled the space in the fuel rod provided by the radial deformation of the cladding. As a consequence, the pellet stack length was significantly reduced for rods with major deformations.

The metallographic investigations are primarily based on the destructive posttest examination of the unirradiated test rods. Results on the mechanical behavior (local deformation) of the cladding, on the microstructural evaluation of the maximum clad temperature and its distribution around the circumference, on the cladding oxidation at the inner and outer surface, on the chemical and mechanical behavior of the fuel, and on the chemical behavior of the fission products are presented in part II of this report.

In addition, the fission gas behavior in the as-irradiated and in the LOCA-tested fuel pins has been investigated with respect to fission gas release, distribution of the retained fission gas, and swelling. Parallel to the in-pile experiments out-of-pile annealing tests with preirradiated but not LOCA-tested fuel samples were carried out. Up to now the post-irradiation examinations and the annealing tests of the test series F (20000 MWd/t) are completed.

KfK-in-pile-Versuche zum Brennstabverhalten in der Aufheizphase eines LOCA.

Zusammenfassung

Dieser Bericht faßt die Ergebnisse der FR2 In-pile-Versuche, die bisher ausgewertet worden sind, zusammen. Er dient als Grundlage für den Beitrag zum "State-of-the-Art"-Bericht für das CSNI (Committee on the Safety of Nuclear Installations). Der Beitrag bezieht sich auf das Thema des Beulverhaltens von vorbestrahlten LWR-Brennstabhüllen unter Störfallbedingungen.

Das In-pile-Versuchsprogramm ist Bestandteil des LWR-Brennstabverhaltens-Programms des Projektes Nukleare Sicherheit (PNS). Die Experimente werden im DK-Kreislauf des FR2-Reaktors im Kernforschungszentrum Karlsruhe (KfK) durchgeführt.

Mit den In-pile-Versuchen, in denen die 2. Aufheizphase eines Kühlmittelverlust-Störfalls simuliert wird, soll der Einfluß nuklearer Kenngrößen auf die Mechanismen des Brennstabversagens unter LOCA- (Loss-of-Coolant Accident) Bedingungen untersucht werden. Die Versuchsstäbe werden Temperaturtransienten (schnellen Aufheizungen) unterworfen, die in Hülldeformation (Ballooning) und Hüllbersten resultieren.

Als Versuchsstäbe werden Prüflinge verwendet mit einer aktiven Brennstofflänge von 50 cm und radialen Abmessungen, die denen von DWR- (Druckwasserreaktor-) Stäben entsprechen. Es werden Versuche sowohl mit unbestrahlten als auch mit vorbestrahlten Prüflingen durchgeführt. Hauptparameter des Versuchsprogramms ist der Abbrand, der von 2500 bis 35000 MWd/t variiert wird. Die Stäbe werden in den Versuchen mit Innendrücken beaufschlagt, die typisch für DWR-Brennstäbe sind.

Zur Zeit sind 39 In-pile-Versuche durchgeführt und etwa die Hälfte der getesteten Stäbe nachuntersucht. Die z.Z. verfügbaren Ergebnisse deuten nicht auf einen Einfluß der nuklearen Parameter auf die Mechanismen des Brennstabversagens hin. Ins-

besondere liegen die Berstdaten, wie Bersttemperatur, -druck und -dehnung, im Streubereich der Out-of-pile-Ergebnisse. Ein Einfluß des Abbrands auf das Berstverhalten konnte nicht beobachtet werden. Ebenso konnte kein Unterschied in den Berstdaten zwischen unbestrahlten und vorbestrahlten Prüflingen entdeckt werden.

Bezüglich des Brennstoffzustandes bestehen jedoch Unterschiede zwischen den unbestrahlten und den vorbestrahlten Prüflingen. Im Unterschied zu den Versuchen mit nicht vorbestrahlten Brennstabprüflingen zeigen die vorbestrahlten Versuchsstäbe nach dem Transientenversuch auseinandergefallenen Brennstoff, vor allem im Bereich deutlicher Hüllrohrdeformation. Der durch das Aufblähen der Hülle zusätzlich entstandene Raum für den Brennstoff füllt sich mit Bruchstücken der während der Vorbestrahlung schon zersprungenen Pellets. Innerhalb der gebeulten Zone haben die Tabletten ihre Form meist vollständig verloren, der Brennstoff liegt als Schüttung von Bruchstücken vor. Durch Nachrutschen von Brennstoff entstehen so z.T. ausgeprägte Verkürzungen der ursprünglichen Pelletsäule.

Die metallografischen Untersuchungen der unbestrahlten Prüflinge sind abgeschlossen. Über die Ergebnisse bezüglich des mechanischen Verhaltens der Hülle, der Hülltemperaturbestimmung aus dem Gefügebild, der Hülleninnen- und -außenoxidation, des chemischen und mechanischen Verhaltens des Brennstoffs und des chemischen Verhaltens der Spaltprodukte wird im Teil II berichtet.

Außerdem wurde das Spaltgasverhalten in den bestrahlten und LOCA-getesteten Brennstäben in Bezug auf die Spaltgasfreisetzung, die Verteilung der zurückgehaltenen Spaltgase und das Schwellen untersucht. Parallel zu diesen in-pile-Experimenten wurden out-of-pile-Glühversuche mit vorbestrahlten, aber nicht LOCA-getesteten Brennstoffproben durchgeführt. Bis jetzt wurden die Nachbestrahlungsuntersuchungen und die Glühversuche der Versuchsserie F (20000 MWd/t) abgeschlossen.

Contents

Contents (Continued)

Figures

Part I

Figures (Continued)

Part II

Figures (Continued)

Tables

Part I

Introduction

This report describes the results of the FR2 In-Pile Tests obtained from the test data of 39 in-reactor tests and from the posttest examinations of a part of the test samples, mainly of the unirradiated rods. The report serves as a basis for the contribution to the state-of-the-art report (SOAR) "Fuel Behavior During a LOCA" being initiated by the Committee on the Safety of Nuclear Installations (CSNI) of the OECD Nuclear Energy Agency (NEA). This contribution is to provide input on the knowledge of ballooning behavior of LWR (Light Water Reactor) cladding material. The particular section of the SOAR is concerned with ballooning behavior of irradiated rods in in-reactor tests.

The report is divided into two parts. Part I (written by E. Karb and L. Sepold) contains information on objectives, experimental hardware and procedures, test matrix, test results, and results of non-destructive posttest examinations. Part II (written by P. Hofmann, C. Petersen, G. Schanz, and H. Zimmermann) presents the results of the destructive posttest examinations of the test samples, i.e. the metallographic evaluation, and investigations on the fission gas release and fuel swelling.

Part I

OBJECTIVES, EXPERIMENTAL MATRIX AND PROCEDURES, TEST RESULTS, RESULTS OF NON-DESTRUCTIVE PTE

1. Research Objectives

The objectives of the FR2 in-pile tests are

- investigation of the possible influence of a nuclear environment on the known mechanisms of fuel rod failure,
- investigation if there are further failure mechanisms not uncovered in out-of-pile tests,
- quantification of such influences if there are any.

These objectives include a comparision with data obtained out-of-pile with electrically heated fuel rod simulators and thus provide a check of the simulation quality of such electrical simulators.

2. Experimental Hardware and Procedures

2.1 Fuel Rod Design

The design of the test fuel rod is presented in Fig. 1. It is identical to that of a German PWR (Pressurized Water Reactor) fuel rod for reactors of the 1300-MW_e class except for active length, fuel enrichment, and plena. The active length of the test fuel rod is 50 cm and approximately equals the axial distance between spacer grids. The U-235 enrichment of the test rods (see Table 1) is slightly higher than that of pellets used in PWR fuel rods. The test rod has only an upper plenum compared with the two plena of a German PWR fuel rod. The size

of the test rod plenum volume was chosen to equal the void volume of both plena in a PWR fuel rod. An analytical study on the time-dependent cladding strain with both rods, the test rod and PWR fuel rod, exposed to a LOCA transient resulted in best agreement for identical plenum volume sizes. The plenum spring of the test rod is designed and fabricated according to the PWR fuel rod standards.

2.2 Cladding Material Specifications and Dimensions

The specifications of the cladding material used for the test specimen are identical to those of commercial PWR fuel rods. The material was taken from a single lot fabricated for a commercial PWR.

The nominal dimensions of the test fuel rod are listed in Table 1.

2.3 Test Facility

The test facility is the DK loop in the FR2 reactor at the Karlsruhe Nuclear Research Center (Fig. 2). The loop is operated with superheated steam as coolant.

The loop is particularly suitable for experiments on fuel rod failure (rupture of the cladding), because it is equipped with condensation and filter systems for restraining fission products and retarding noble gases.

The test specimen is contained in the in-pile test section comprising several shrouds and a thick-walled pressure tube. The inlet and outlet connections of this tube to the loop system are both located at the upper end of the test section. The flow reverses at the bottom of the flow tube and moves up past the test rod (reentrant design, see Fig. 3).

Table 1: Nominal Test Fuel-Rod Data

Cladding	
Material	Zircaloy-4
Outside diameter, mm	10.75
Inside diameter, mm	9.3
Wall thickness, mm	0.725
Fuel pellets	
Material	UO_2
Diameter (nominal gap), mm	9.11
Diameter (small gap), mm	9.15
Length	11
Enrichment (active zone), %	4.7
Enrichment (end pellets), %	0.3
Height of pellet stack (active zone), mm	500
Density, g/cm³	10.35
Density, %T.D.*	94.4
Insulating pellets	
Material	Al_2O_3
Diameter, mm	9.15
Length, mm	8
Void Volumes	
Dishing per pellet, mm³	16
Gap Volume (nominal gap), cm³	1.57
Plenum (excl. spring), cm³	15.87
End plug, Capillary tube, and pressure transducer, cm³	12.25
Fillgas composition	100 % Helium

*) T.D. = theoretical density

2.4 Test Environment and Coolant Conditions

The test rod is surrounded by a cylindrical flow shroud (ID 18 mm). This shroud is not heated during the transient test and thus it remains at a significant lower temperature during the heatup of the fuel rod.

A test comprises two periods, the steady-state and the transient operation. During the steady-state phase the operating data of the coolant are as follows:

- mass flow 110 - 120 kg/h
- pressure ~ 60 bar
- temperature 290 - 340 °C.

After initiation of the transient phase the coolant flow decreases to a stagnant mode, and the depressurization of the coolant leads to less than atmospheric pressure within about 10 sec.

2.5 Test Assembly Power and Method of Control

The test rod power is governed by the inventory of fissionable material and the local fission neutron flux. Since for previously irradiated rods the concentration of fissionable material is not known exactly before PTE (Posttest Examination) and since the fission neutron flux is not measured, three different indirect methods for power determination are used, based on

a) energy balance of the coolant passing the test rod

b) measurement of undisturbed neutron flux and reactor power

c) measured heatup rate of test rod cladding.

(a) Coolant mass flow and temperature rise are measured and are combined with the specific heat of the coolant to the rod power. Possible error sources - besides the measurement uncertainties - are radial heat exchange and coolant bypass flow.

(b) The energy output of the reactor fuel elements surrounding the test section and the neutron flux in the vicinity of the test section are measured. These data are converted to a relative test rod power profile and an absolute test rod power value using a conversion factor determined by reactor physics calculations. Main error sources: Analytically determined conversion factor, basic assumption of proportionality of rod power to measured flux.

(c) The test rod power can be determined by a comparison between measured and calculated heatup rates based on the local cladding temperature histories during the transient. This is a posttest method. Error sources: Code assumptions,azimuthal variations in heatup rate.

Methods (a) and (b) are used during steady-state, (c) is a posttest method only. For the control of rod power during the test, method (b) was preferred after some empirical, facility-specific relations were developed. The posttest method based on the heatup rate is considered to be the most confidential one.

2.6 Temperature and Pressure Control and Typical Transients

During the steady-state period of the test the initial conditions for the transient are adjusted. The quantities controlled are rod power (controlled by reactor power), coolant mass flow, and inlet temperature. The test rod internal pressure is adjusted prior to the transient. During the transient the gas is confined and the internal pressure is measured but not controlled.

The transient is initiated by interruption of the coolant flow and depressurization of the coolant. During the heatup phase, the rod power is kept constant (Fig. 4, Test Procedure), and there is no control of the rod temperature and pressure up to the target cladding temperature of 920 to 950 °C when the rod power is rapidly reduced by reactor scram. The deformation and the burst of the rod cladding are monitored by means of the cladding temperature and internal rod pressure traces.

A typical transient is illustrated with Test B 3.1 in Fig. 5. The six cladding thermocouples (Nos. 131 to 136) located at six different axial positions of the rod show a rather flat temperature profile until major deformation starts. This is indicated by the change from pressure increase to decrease (at 36 s). When the fuel-cladding gap is enlarged drastically by radial deformation close to or at the moment of burst, all thermocouples show a temperature drop; the most pronounced drop occurs in thermocouples 131 and 132, which are located in the ballooned section. Heatup continues until the power is reduced at about 80 s. At 160 s quenching is initiated, causing the cladding temperatures to drop rapidly to coolant temperature level.

2.7 Measurement Techniques

a) Cladding Surface Temperature

For the measurement of the cladding surface temperature Inconel-sheathed Chromel/Alumel thermocouples (TC) are resistance spot welded to the outer rod surface at six different axial and azimuthal locations. Two different versions for the TC attachment are being used, Version A and Version B. The two TC versions are compared in Fig. 6. This schematic illustrates that, in both versions, a 30 to 35 mm long platinum tube is swaged onto the thermocouple sheath in order to avoid a eutectic formation between Zirconium and components of the TC sheath material at elevated temperatures. In addition, best welding results were accomplished with platinum material.

During steady-state and transient operation the surface-mounted TCs show lower temperatures than the real wall temperatures. The deviations were determined in calibration tests with electrically heated fuel rod simulators by comparing the readings of the clad surface TCs with those of TCs embedded in the cladding. Fig. 7 shows the deviations and the scatter (uncertainty), both being dependent on the rod power rate. The mean values are used as correction for the measured temperatures. Deviation and uncertainty are much smaller for TC version B as compared with version A.

b) Rod Internal Pressure

Internal rod pressure is measured dynamically by a strain-gauge-type pressure transducer, which is connected to the plenum by a capillary tube approximately 5 m in length with an inside diameter of 1.6 mm. This tube is coupled to the test rod plenum in a way that no fission gas produced during the pre-irradiation can escape from the interior of the rod (see Fig. 8). The signal delay caused by the connecting tube

was determined experimentally to be less than 10 ms for a rapid depressurization. Dynamic measurement of the internal rod pressure serves as an indication of the start of deformation and rupture of the cladding. The range of the pressure is 0 to 175 bars.

The uncertainty is estimated to be about $\pm$ 1 bar in the pressure range of 50 to 100 bars.

2.8 Irradiation of the Test Rods

All rods of series C, E, F, G1, and G2/3 were irradiated in the FR2 reactor prior to the transient testing. The burnup of the test rods was determined by a coolant enthalphy balance method during the irradiation, and by radiochemical analyses of fuel samples during posttest examinations.

The conditions for the test rod irradiation in the FR2 reactor are listed in Table 2 and compared with average values of a commercial PWR. Coolant pressure and coolant temperature are lower in the FR2 reactor. This results in lower cladding temperature and somewhat lower fuel temperatures of the test rods in the FR2 reactor compared with a PWR rod. No creep of the cladding towards the fuel due to external overpressure does occur in the FR2 test rods. There are more scrams and shutdowns in the FR2 research reactor than in a commercial PWR.

Inspite of these differences between FR2 and PWR the typicality of the test fuel rods is believed to be sufficient.

Table 2: Irradiation Conditions in FR2 and in a Commercial PWR

		FR2	PWR
Coolant inlet temperature	°C	60	290
Coolant pressure	bars	2,4	155
Linear rod power	W/cm	200 - 450	200 - 450
He fillgas pressure	bars	3	22,5

3. Definitions of Important Parameters

Burst temperature

The burst temperature is defined as the temperature of the cladding at the burst location at burst time. Since this temperature cannot be measured directly for the in-pile test rods, an interpolation is made between the readings of the thermocouples closest to the burst or an extrapolation from the signal of the closest thermocouple. The burst temperature is determined by adding a correction factor to the interpolated value in order to compensate for the deviations of the surface-welded thermocouples. In this method azimuthal temperature variations cannot be taken into account.

Burst Pressure

Burst pressure is defined as the rod internal pressure measured at the beginning of the fast pressure drop, i.e., when the pressure gradient dp/dt exceeds the value of minus 10 bars/s. The pertinent time after initiation of the transient is called burst time.

Heating rate

The heating rate is defined as the temperature gradient at 650 °C. It is determined for all cladding TCs. The heating rates determined from the readings of the thermocouple located closest to the burst location are given in Table 4.

Burst stress

The burst stress is defined as "engineering hoop stress", given by the equation

$$\sigma_B = P_B \cdot \frac{D_{i,o}}{2\ t_o}$$

where P_B = burst pressure
$D_{i,o}$ = initial cladding ID
t_o = initial wall thickness of the cladding.

Burst Strain

The burst strain of the Zry cladding is indicated by the maximum relative circumferential elongation $\Delta U/U_o$, where

$\Delta U = U_1 - U_o$ = increase in circumference
$U_o = \pi d_o$ = initial cladding circumference.

4. Test Matrix and Status

The main parameters are fuel burnup and rod internal pressure; these parameters were varied in the ranges shown in Table 3.

The heatup rate was not varied systematically, data range from 6 K/s to 20 K/s, with the majority of the tests from 9 to 13 K/s.

The cold diametral gap size was reduced from nominal 190 to 150 µm for test series G1, G3 (for comparison also in the B3 series) in order to compensate for the lack of cladding creep during irradiation in the low coolant pressure environment of the FR2 reactor.

All transient tests listed in the test matrix, Table 3, are completed plus a total of eight reference burst tests with electrically heated fuel rod simulators. There are no plans for further tests within this program.

Future work will comprise completion of the hot cell PTE of the remaining rods, evaluation and documentation of the data and compilation of the final test results.

Table 3

FR2 IN-PILE TESTS ON FUEL BEHAVIOR, TEST MATRIX

Type of Test	Test-Group	Number of Rods Irradiated	Nominal Gap Size µm	Number of Tests	Target Burnup MWd/t_U	Range of Internal Pressure at Steady State Temperature bar
I Calibration, Scoping	A	-	190	5	-	25 - 100
Unirradiated Rods						
II (Main Parameter:	B1	-	190	7	0	55 - 90
Internal Pressure)	B3	-	150	2	0	
Irradiated Rods	C	6	190	5	2500	25 - 110
	D	6	190	-	5000	cancelled
III (Main Parameter:	E	6	190	5	8000	25 - 120
Burnup)	F	6	190	5	20000	45 - 85
	G1	6	150	5	35000	50 - 90
	G2	2	190	2	35000	60 - 125
	G3	4	150	3	35000	

5. Principal Results

Table 4 shows the main test results. Since hot cell post-test examinations are not complete for a part of the test rods, some deformation data are still to be determined.

Another important result, the effect of fuel pellet fragmentation, is described in section 6 of this document.

Burst Temperature

Burst temperatures are plotted versus burst pressures in Fig. 9. In this figure the different heating rates as well as the degree of burnup are indicated by different symbols. For comparision two dashed curves approximating the out-of-pile ORNL Multirod Burst Test single-rod results /3/ are included.

In many cases it is more meaningful to compare burst stresses rather than burst pressures, in order to eliminate design-specific dimensional effects. Therefore, the measured burst pressures were converted to burst stresses according to the relation given in section 3. The results are listed in Table 4 and plotted in Fig. 10.

Burst Strain

In Fig. 11 the measured circumferential burst strains are plotted vs. burst temperatures, the heating rates being indicated by different symbols. For comparison, results of burst tests with irradiated cladding tubes performed by BMI /4/ are presented in the same plot.

Views of the ruptured regions are presented in Fig. 12 through 15, for the unirradiated test rods as well as for the irradiated test rods of series F, G1, and G2/3. The individual burst temperatures and burst pressures are also indicated on those figures. No systematic relation between the burst shape and the burst temperature was found.

TABLE 4

Test No	Rod No	Cold diametral gap size	Thermo-couple-version	Burnup	Heatup rate at 923 K	Time to burst	Burst Tempe-rature	Maximum cladding temperature	Burst pressure	Maximum pressure	Maximum total circumferential strain	Volume increase	Calculated engineering burst stress	Test No.
		µm		GWd/t	K/s	s	K	K	bars	bars	%	%	MN/m^2	
A1.1	15	191	A	-	7,1	79	1083	1275	50	54	64	24	31,98	A1.1
A1.2 a)	14	182	A	-	11,5	a)		1281						A1.2 a)
A2.1	16	181	A	-	20,0	20	1093	1323	88	100	36	47	56,43	A2.1
A2.2	17	179	A	-	12,1	38	1133	1301	58	75	56	83	37,43	A2.2
A2.3	18	184	A	-	13,0	55	1288	1288	25	27	35	38	15,84	A2.3
B1.1	20	190	A	-	17,0	40	1173	1304	52	59	30	44	33,59	B1.1
B1.2	21	191	A	-	8,7	72	1188	1283	45	55	25	39	28,99	B1.2
B1.3	22	187	A	-	12,7	37	1118	1258	61	71	34	52	39,26	B1.3
B1.4 b)	23	184	A	-	9,3	b)		1291						B1.4 b)
B1.5	24	193	A	-	9,2	72	1183	1282	45	58	60	98	28,65	B1.5
B1.6	25	184	A	-	8,2	56	1098	1288	80	90	38	44	51,04	B1.6
B1.7	30	191	B	-	11,5	41	1113	1163	61	71	e)	48	39,37	B1.7
B3.1	1	154	A	-	10.0	46	1098	1289	79	91	37	40	50,87	B3.1
B3.2	2	159	A	-	12,1	55	1188	1284	50	61	50	69	32,13	B3.2
C1	56	188	B	2,5	14,0	47	1173	1290	46	56	e)	e)	29,32	C1
C2	57	190	B	2,5	12,6	58	1218	1223	30	34	e)	e)	19,34	C2
C3	59	197	B	2,5	13,2	32	1022	1046	98	112	e)	e)	63,00	C3
C4	60	197	B	2,5	12,1	41	1088	1284	65	81	e)	e)	41,95	C4
C5	63	193	B	2,5	9,3	78	1189	1276	22	25	e)	e)	14,06	C5
E1	44	187	B	8	12,5	59	1183	1282	23	26	e)	e)	14,90	E1
E2	45	196	B	8	11,7	29	981	1272	113	129	e)	e)	72,71	E2
E3	46	202	B	8	11,2	47	1133	1273	49	56	e)	e)	31,74	E3
E4	47	200	B	8	11,6	35	1054	1278	72	86	e)	e)	46,10	E4
E5	48	197	B	8	11,5	57	1202	1206	24	26	e)	e)	15,18	E5
F1	37	208	A	20	10,6	43	1163	1289	56	72	59	76	36,22	F1
F2	38	204	A	20	8,7	57	1166	1280	53	62	38	43	34,26	F2
F3	39	198	A	20	10,1	57	1205	1290	42	46	27	27	27,19	F3
F4	40	195	A	20	11,1	37	1108	1322	72	84	34	46	46,44	F4
F5	43	200	A	20	10,1	49	1153	1279	60	72	41	60	38,75	F5
G1.1 a)	3	158	A	35	10,1	a)		1283			2	5		G1.1 a)
G1.2 d)	4	154	A	35	15,0 c)d)	55	1003	1282	68	75	30	32	43,86	G1.2 d)
G1.3	5	158	A	35	9,0	70	1163	1250	41	51	62	71	26,41	G1.3
G1.4	7	150	A	35	6,1	58	1058	1244	83	91	33	34	53,40	G1.4
G1.5 d)	9	154	B	35	12,0 d)	60	1053	1200	52	60	41	52	33,08	G1.5 d)
G2.1	35	199	B	35	13,6	38	1142	1225	37	f)	32	20	23,71	G2.1
G2.2	36	194	B	35	13,0	31	1119	1213	66	75	28	41	42,51	G2.2
G3.1	12	145	B	35	12,3	55	1173	1203	33	f)	e)	57	20,91	G3.1
G3.2	11	128	B	35	15,4	33	1111	1213	57	74	41	77	36,55	G3.2
G3.3	10	142	B	35	9,8	29	1023	1220	111	128	e)	39	71,02	G3.3

a) Rod leaked; no burst

b) No internal overpressure; no burst

c) Heatup rate at 743 K

d) Abnormal heatup; burst during temperature plateau

e) Not yet determined (status: Sept. 1980)

f) Rod leaked, no max. pressure

The cross sections of the location representing the maximum circumferential strain (burst strain) are compiled in Figs. 16 through 19 (Test series A/B, F, G1, and G2/3).

Circumferential Temperature Gradients at Burst

No measured data are available on the circumferential temperature difference at the location of burst.

TC measurements in the less deformed section of a test rod indicate a maximum azimuthal temperature difference of approx. 50 K. The results from the metallographic examinations on the circumferential temperature gradients are in the same order of magnitude; methods and results are described in Part II.

Axial Distribution of Cladding Temperature

Information on the axial temperature distribution is drawn from the cladding surface thermocouples, positioned as described in 2.7. This means that measured data are available between 200 and 450 mm above the bottom of fuel stack.

Fig. 20 as an example presents the axial temperature distributions at different times during the transient test F4: The axial power profile causes a rather flat temperature distribution at steady state (0 sec.), which is maintained without major changes during the heatup until the moment of burst. Then the thermocouples in the region of maximum deformation indicate a temperature drop and continue to show lower temperatures during the remainder of the heatup.

Axial Distribution of Strain

Fig. 21 shows the strain profiles obtained with test series F. They are typical for tests with unirradiated rods as well as with previously irradiated rods: All samples exhibit deformation on the entire heated length (500 mm); in most of the cases the ballooned part is between 200 and 400 mm above the bottom of fuel stack, i.e. within the instrumented section of the rod.

Fig. 21 shows also the normalized axial power profiles for each of the F-Tests. The position of maximum strain is usually at or close to the position of maximum rod power. However, the very flat power profile observed in most of the tests may have allowed other parameters, e.g. wall thickness, fuel eccentricity, increase of cladding mass and heat transfer surface by TC leads, to have influenced the position of maximum strain.

This is also demonstrated in Fig. 22 with a flat power profile for most of the tests with unirradiated test rods. The influence of the TC leads on the strain profile can also be noticed in this figure. In contrast to the flat profiles of Fig. 22, Fig. 23 presents the power and strain profiles of Tests A 1.1 and A 2.2. The maximum deformation of Test A 1.1 fuel rod was forced to the lower end of the fuel stack where the relatively steep power profile (peaking factor 1.4) had its maximum.

For completion, the strain profiles of the test Series G1 and G2/3, both performed with a burnup of the test rods of about 35.000 MWd/t, are given in Figures 24 and 25. The power profiles are not yet determined because the axial burnup profiles are not available yet. The procedure for the evaluation of the axial power profile of pre-irradiated rods is illustrated in Fig. 26.

6. Discussion of the Test Results

6.1 Effect of Test Parameters, Similarities and Contrasts with Unirradiated Test Results

a) Internal pressure

The influence of the internal pressure on burst temperature (see Fig. 9) and on the other burst data is very similar to out-of-pile test results.

b) Irradiation, Burnup

The test results do not show an influence of irradiation or even burnup on the burst data; i.e. on burst temperature, burst pressure, burst strain.

One difference between previously irradiated and unirradiated test rods was observed: As in commercial fuel rods, the pellets in the test rods are cracked during irradiation, and the fragments are held together by the cladding, When, during the transient test, the cladding pulls away from the fuel because of radial deformation, the pellet fragments fall into the thus generated additional space. In the ballooned sections the pellet shape is completely lost, the cladding tube is filled with pellet fragments. The neutron radiographs taken pretest and posttest of Test-F1 fuel rod are given in Fig. 27 as an example for this phenomenon.

An important question is, whether this type of relocation of the fuel occurs before the burst and thus may affect the deformation, or after the burst when the deformation process is essentially terminated. The information from two tests demonstrated, that the fuel movement happens at or immediately after the burst, so that the cladding deformation is not affected by the fuel fragmentation. These results were accomplished by using a special TC instrumentation at the upper end of the fuel stack in the two tests E3 and E4, shown schematically in Fig. 28. The clad temperature histories during Test E4 are illustrated in Fig. 29. The rapid temperature drop of the upmost cladding thermocouples T137 through T139 at the time of burst and the slow heatup thereafter indicate that the movement of the pellet column is initiated with the burst.

The size of the pellet fragments was not changed by the transient testing of the rods. This is clearly demonstrated in Figs. 30 and 31 presenting the particle size distributions for the transient tested rods and the pertinent reference rods. The data are derived from sieve analyses. The mean fragment size resulted in about 3 mm for the test series F and G1.

c) Heatup Rate, Gap Size

An effect of the heatup rate on the in-pile fuel rod behavior could not be observed as demonstrated in Figs. 9, 10, and 11 It must be stated again, however, that the range of heatup rates covered with these tests is rather small. If there is an influence of the heatup rate it seems to be smaller than the data scatter of the test results.

The same statement holds for a possible influence of the pellet/cladding gap size, which was not varied systematically either.

6.2 Accuracy of Test Parameters

The evaluated uncertainties of the test parameters and of some of the important test data are listed in Table 5.

Table 5

Parameter	Max. Uncertainty	Remarks
Rod internal pressure	± 1 bar	
Burnup	± 4 %	
Heatup Rate	± 1 K/s	
Burst temperature		
α) from temperature measurement	± 35 K	TC Version A
	± 10 K	TC Version B
β) from axial and azimuthal inter/extra-polation	approx. ± 40 K	Estimated
γ) Total	± 75 K	TC Version A
	± 50 K	TC Version B
Burst pressure	± 1,5 bar	
Burst strain	± 4 %	Percentage of measured strain

7. Major Conclusions

From the FR2 In-Pile Tests evaluated to date the following statements can be made:

- All pressurized rods ruptured during the heatup phase.
- All ballooned rods exhibit circumferential strains over their entire heated length.
- All specimens burst at the location of maximum strain.
- Some specimens burst at an axial location that coincided with the location of a thermocouple.
- The maximum deformation is located at or near peak power position.
- The axial power profile influenced the ballooning shape.
- The burst data, i.e. burst temperature, burst pressure, and burst strain are similar to results from various out-of-pile tests.
- No influence of burnup or heating rate on the burst data was detected.
- The tests with pre-irradiated rods resulted in fragmented fuel pellets. The pellet fragments relocated outward and downward filling the space in the fuel rod created by the radial clad deformation.
- Fuel pellet fragmentation does not seem to have affected the cladding deformation process.

With respect to the test objectives, the tentative conclusion can be drawn:

- No influence of the nuclear environment on fuel rod failure was found.

8. References

/1/ Karb, E.H.: In-pile Tests at Karlsruhe of LWR Fuel-Rod Behavior During the Heatup Phase of a LOCA. Nuclear Safety 21(1): 26 - 37 (Jan.-Febr. 1980)

/2/ Karb, E.; Prüßmann, M.; Sepold, L.: In-pile-Experimente zum Brennstabverhalten beim Kühlmittelverluststörfall; Bericht über die Versuchsserie F, Report KfK-2956, Kernforschungszentrum Karlsruhe, May 1980 (in German)

/3/ Champman, R.H.: Multirod Burst Test Progress Report for January-March 1978, NRC Report NUREG/CR-0225 (ORNL/NUREG/TM-217), Oak Ridge National Laboratory, NTIS, August 1978

/4/ Bauer, A.A. et al.: Evaluating Strength and Ductility of Irradiated Zircaloy. Task 5. Quarterly Progress Report , October-December 1977, NRC-Report NUREG/CR-0026 (BMI-1992) Battelle Columbus Laboratories, NTIS, January 1978

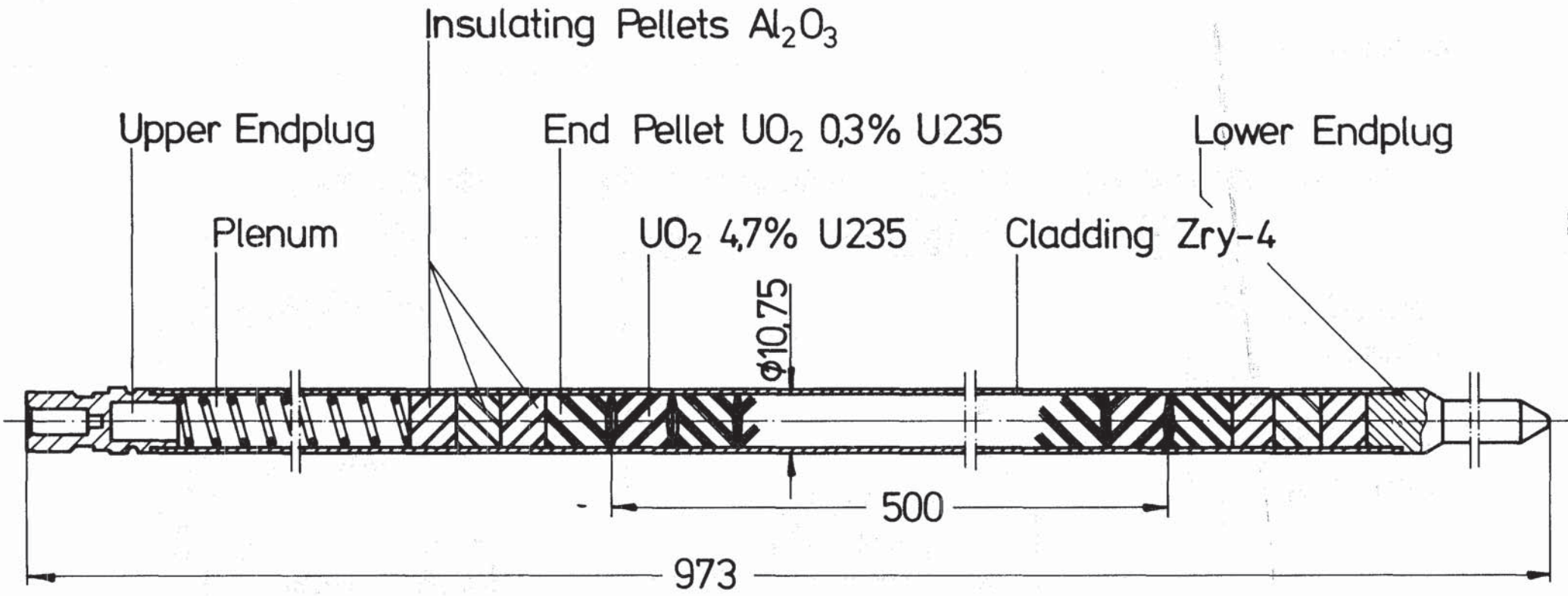

Dimensions in (mm)

KfK IT 79 PNS4237-109.1

FR2 In-Pile Tests Test Rod Design

FIG. 1

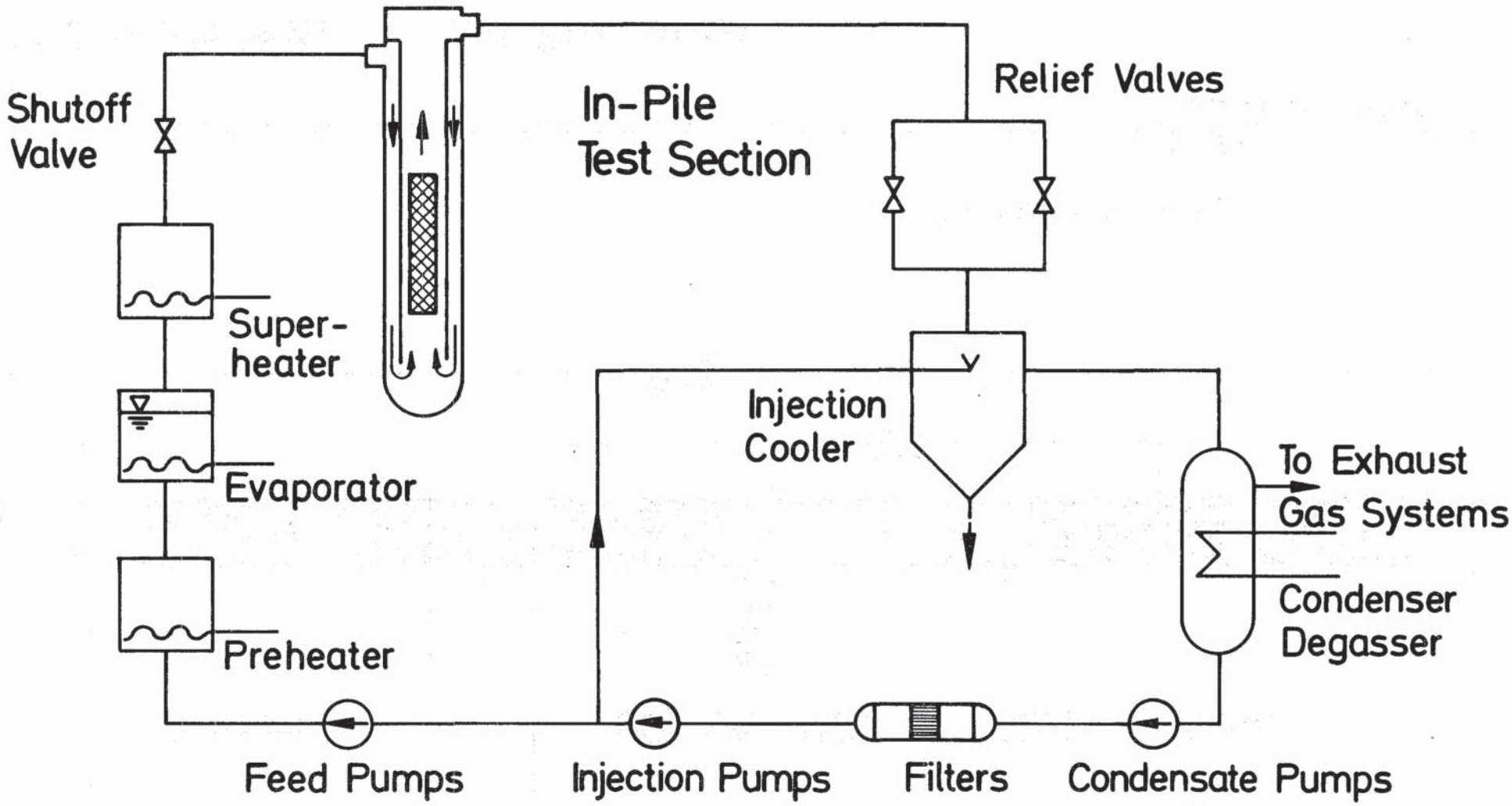

KfK IT 80 PNS 4237-291

FR2 In-pile Tests Simplified Flow Scheme Fig. 2

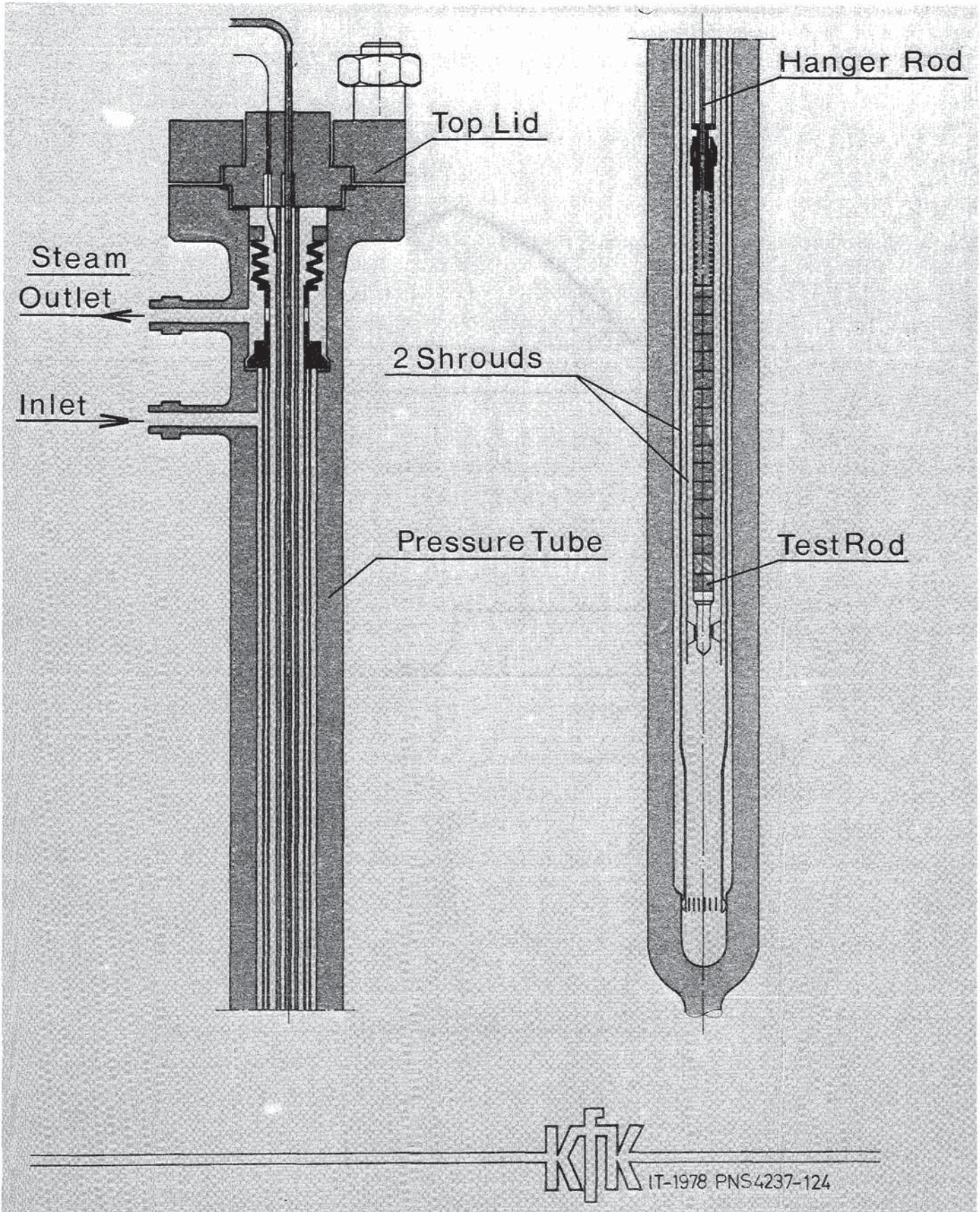

IN PILE TEST SECTION
DK-LOOP FR2 (Simplified)

Fig. 3

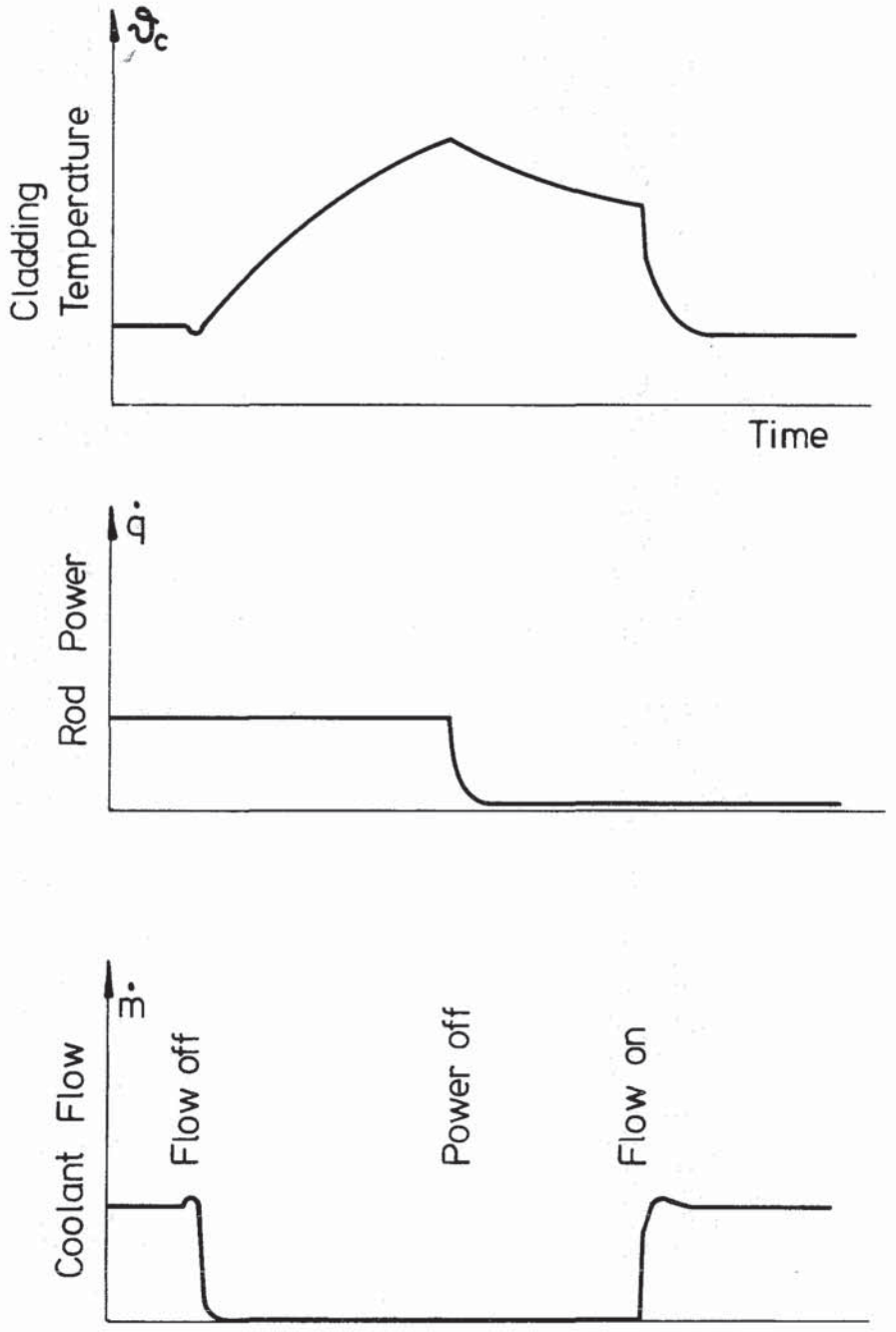

FR2 In-Pile Tests

Test Procedure, Schematic

Fig. 4

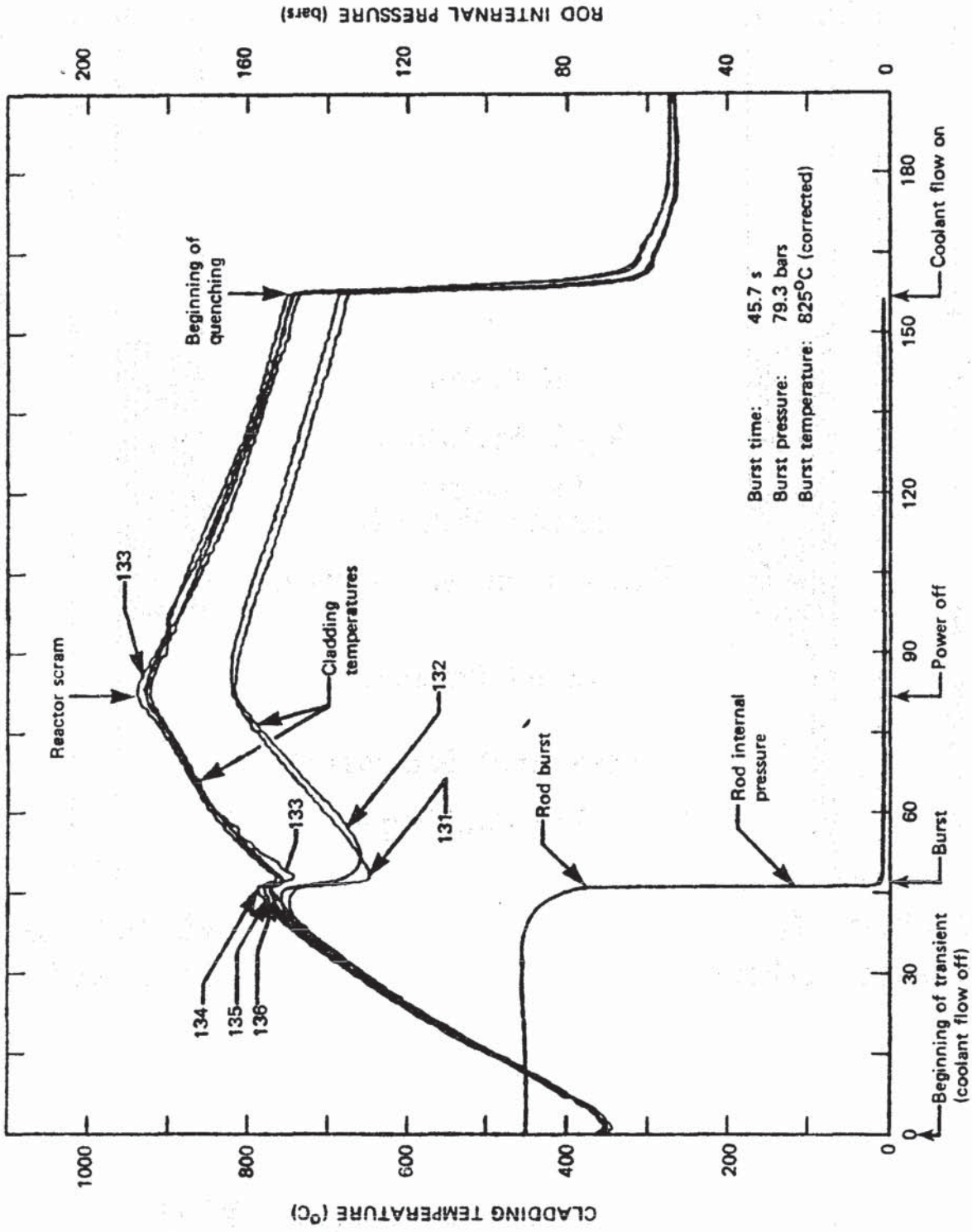

FR2 in-pile test. Typical temperature and pressure histories; measured data of test B3.1.

IT - 1980
PNS 4237-304

Fig. 5

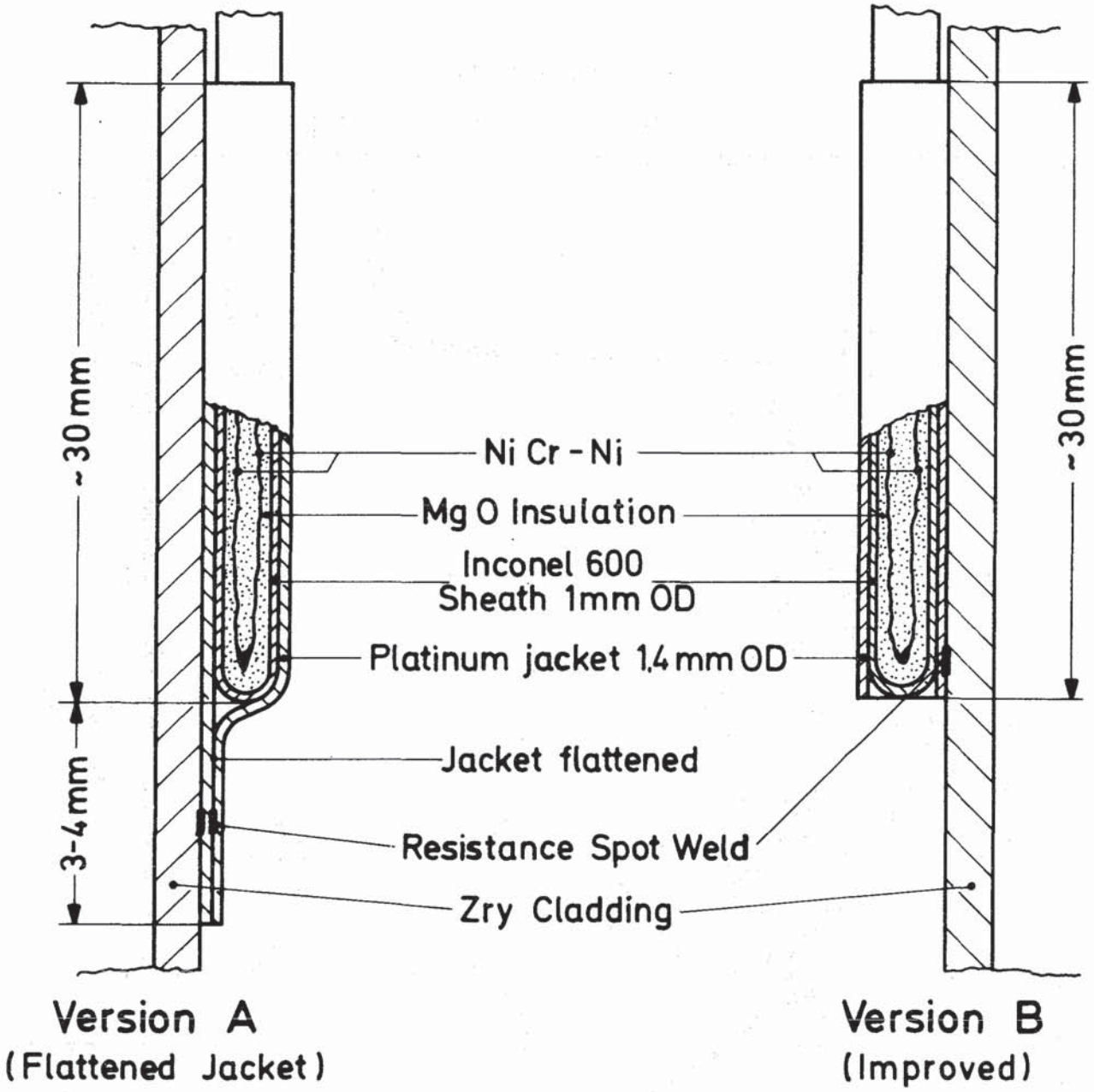

FR2 In-Pile Tests:
Cladding Thermocouple (Schematic)

Fig. 6

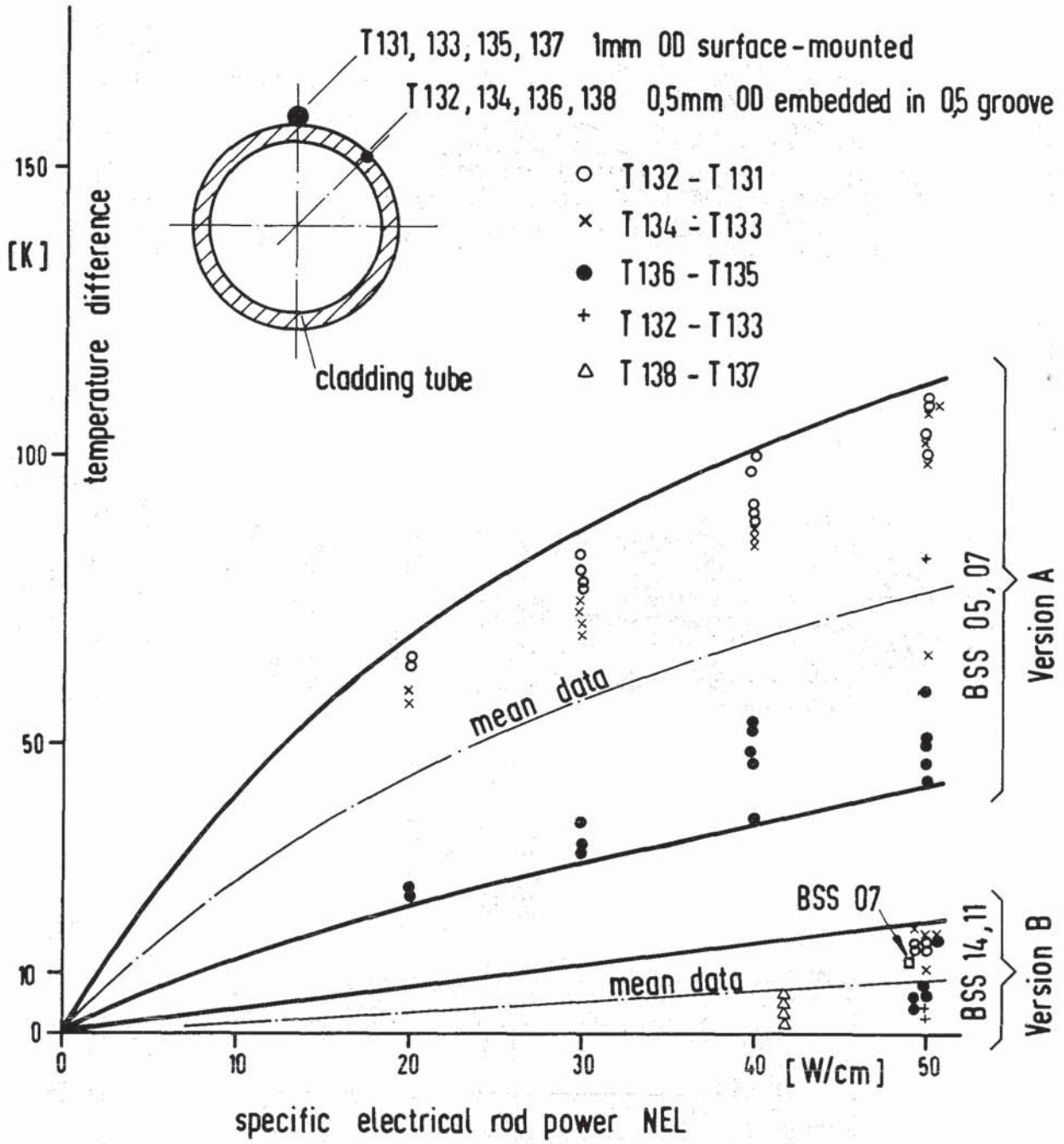

KfK IT80 PNS 4237-399

FR2 In-Pile Tests.
Temperature differences between embedded and surface-mounted TCs vs. rod power during the transient test Fig.: 7

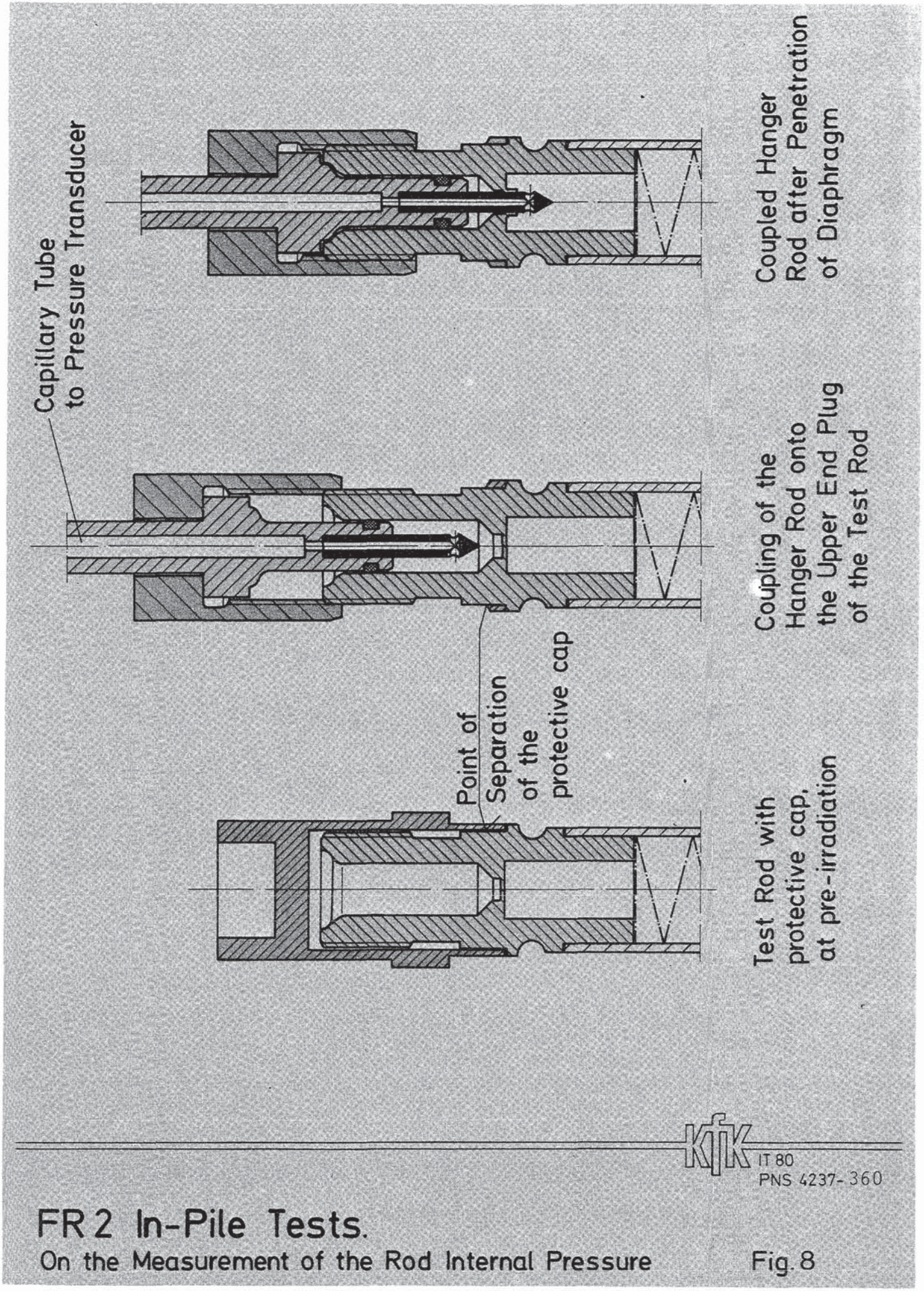

FR 2 In-Pile Tests.

On the Measurement of the Rod Internal Pressure

Fig. 8

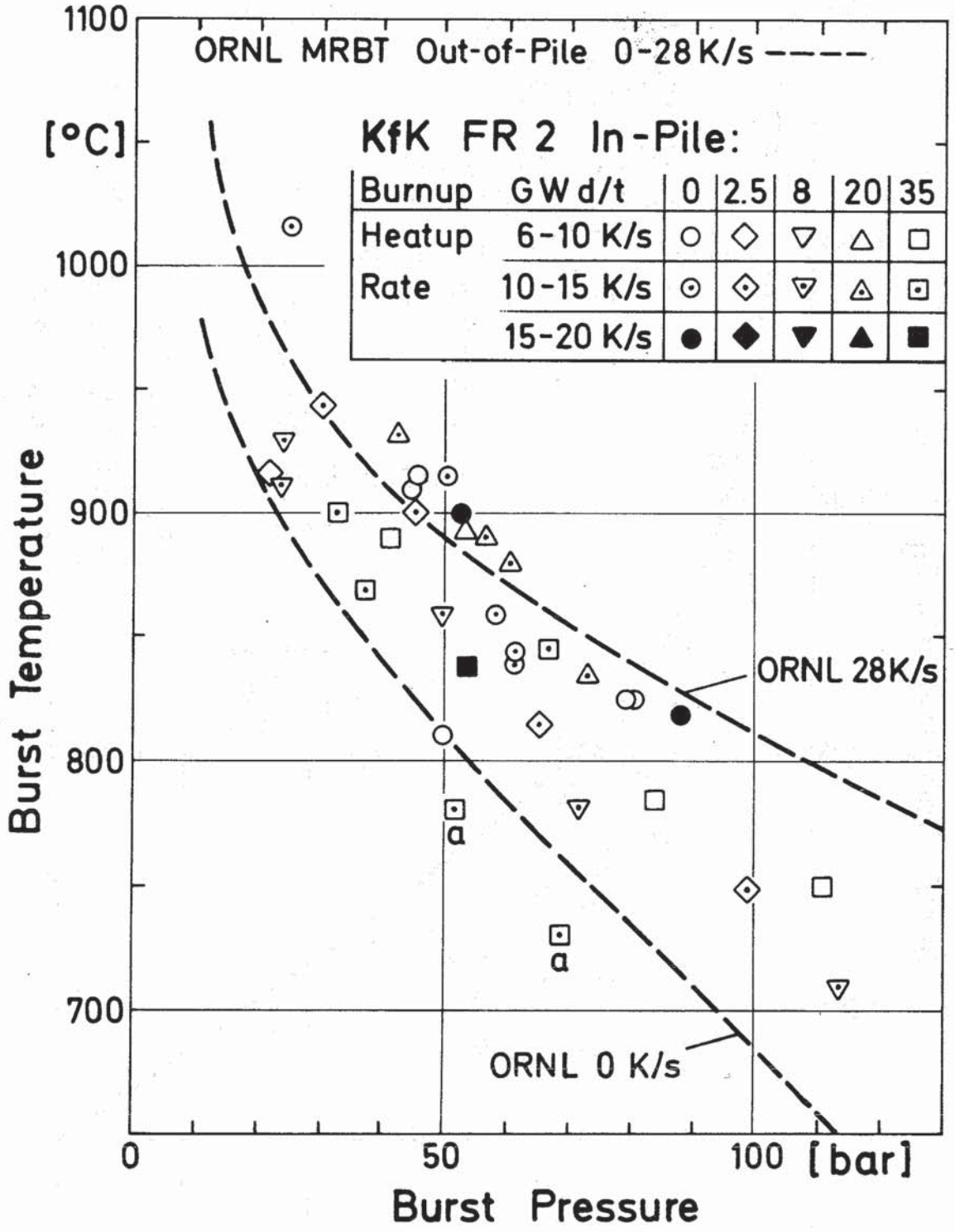

a) burst during temperature plateau

KfK IT-80
PNS4237-298

FR2 In-Pile Tests:

Burst Temperature vs. Burst Pressure Fig. 9

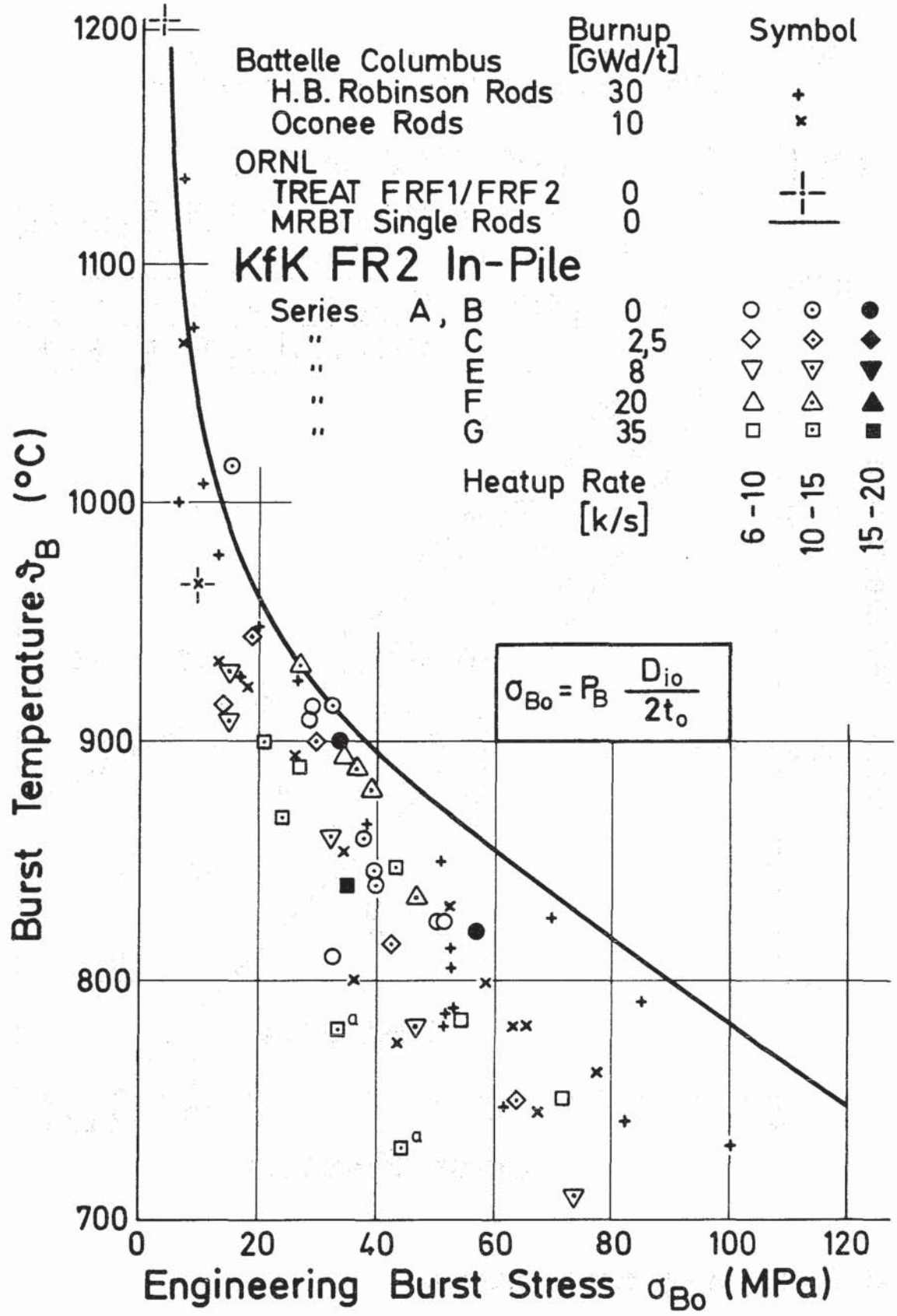

a) Abnormal heatup; burst during temperature plateau

KfK IT-80
PNS4237-305

FR2 In-Pile Tests:

Burst Temperature vs. Engineering Burst Stress Fig.10

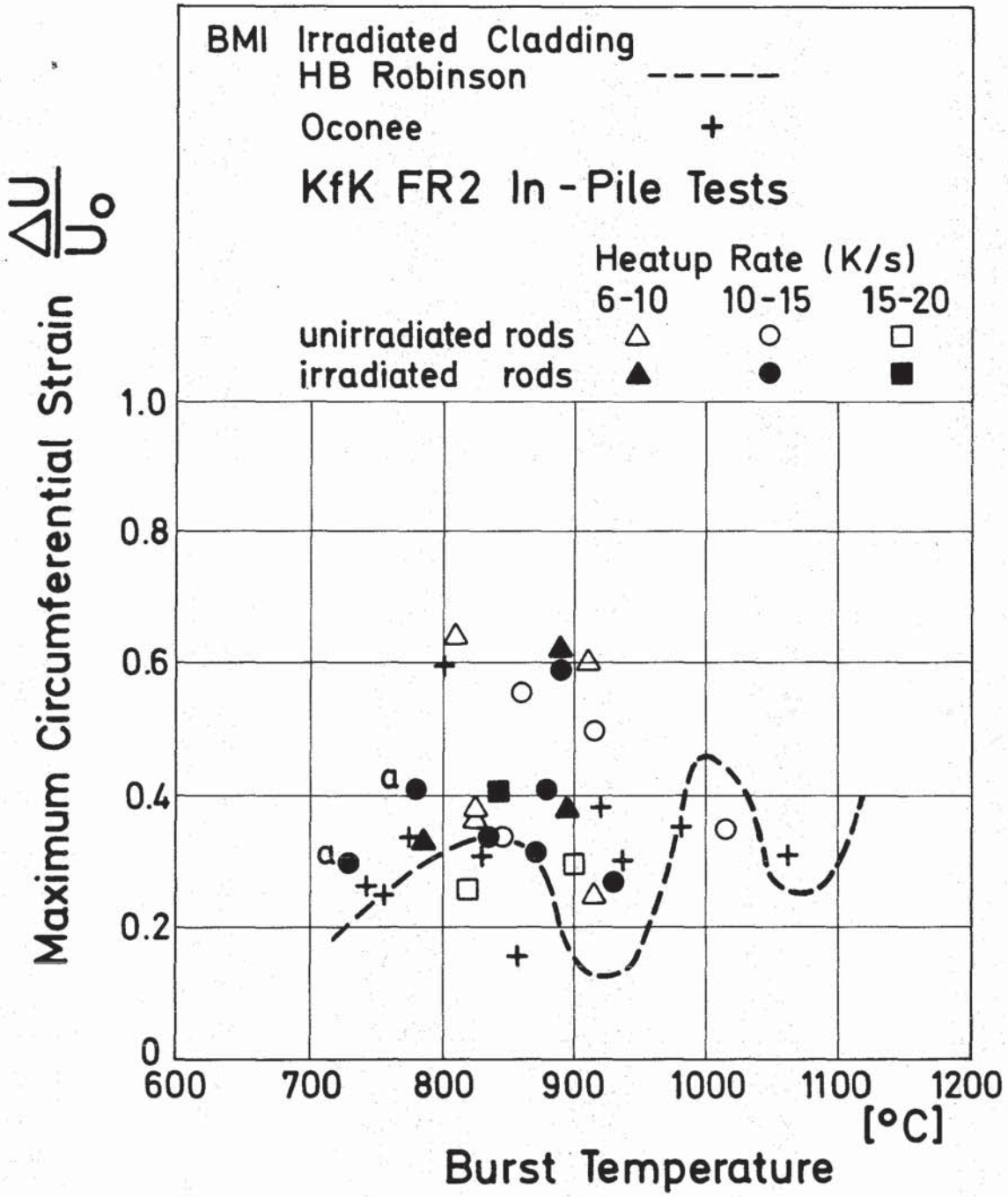

a) burst during temperature plateau

KfK IT-80
PNS4237-297

FR 2 In-Pile Tests:
Max. Circumferential Strain vs. Burst Temperature Fig. 11

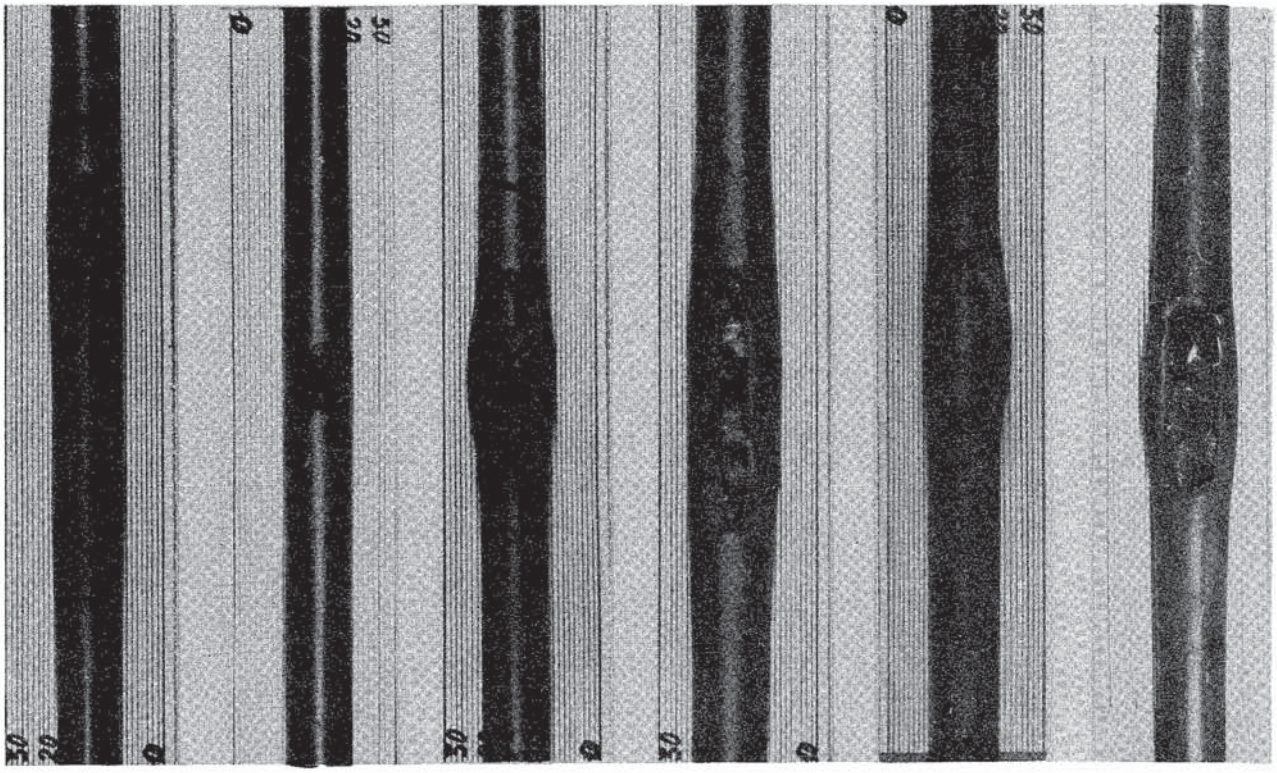

	A2.3	B1.2	B1.1	A2.2	B1.3	A2.1
T_B	1015 [°C]	915	900	860	850	820
P_B	24,7 [bar]	45,2	52,4	58,4	61,2	88

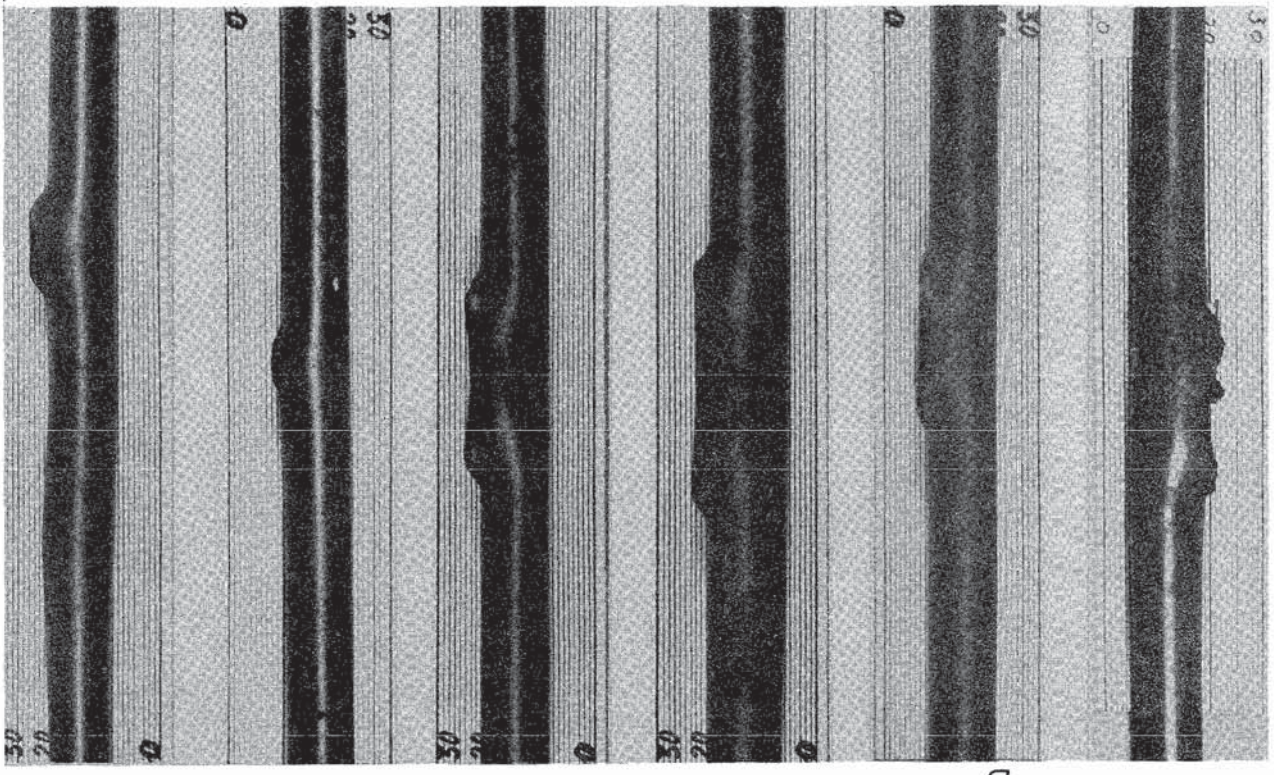

KfK

IT 1980
PNS 4237-365

FR 2 In-Pile Tests. Unirradiated Rods
Views of the Ruptured Regions Fig. 12

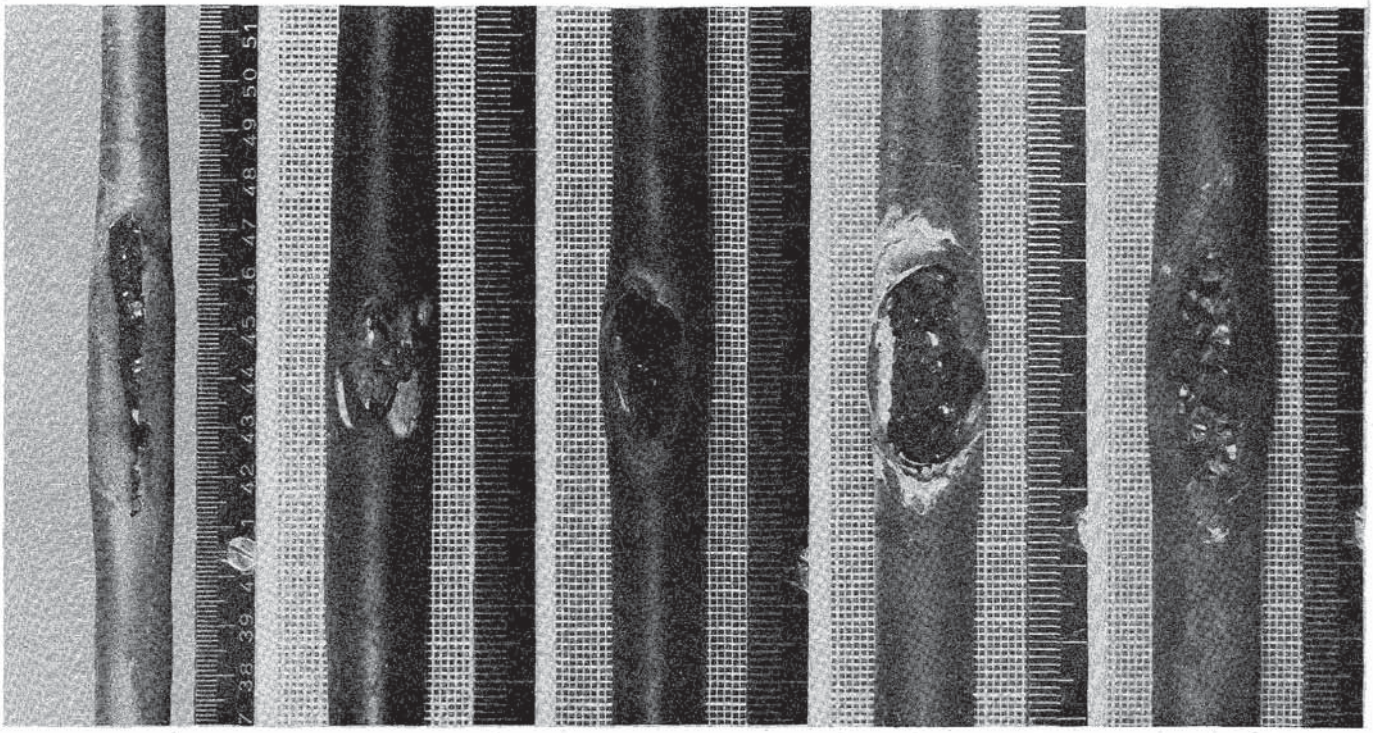

	F1	F2	F3	F4	F5
T_B(°C)	890	893	932	835	880
P_B(bar)	56	53	42	72	60

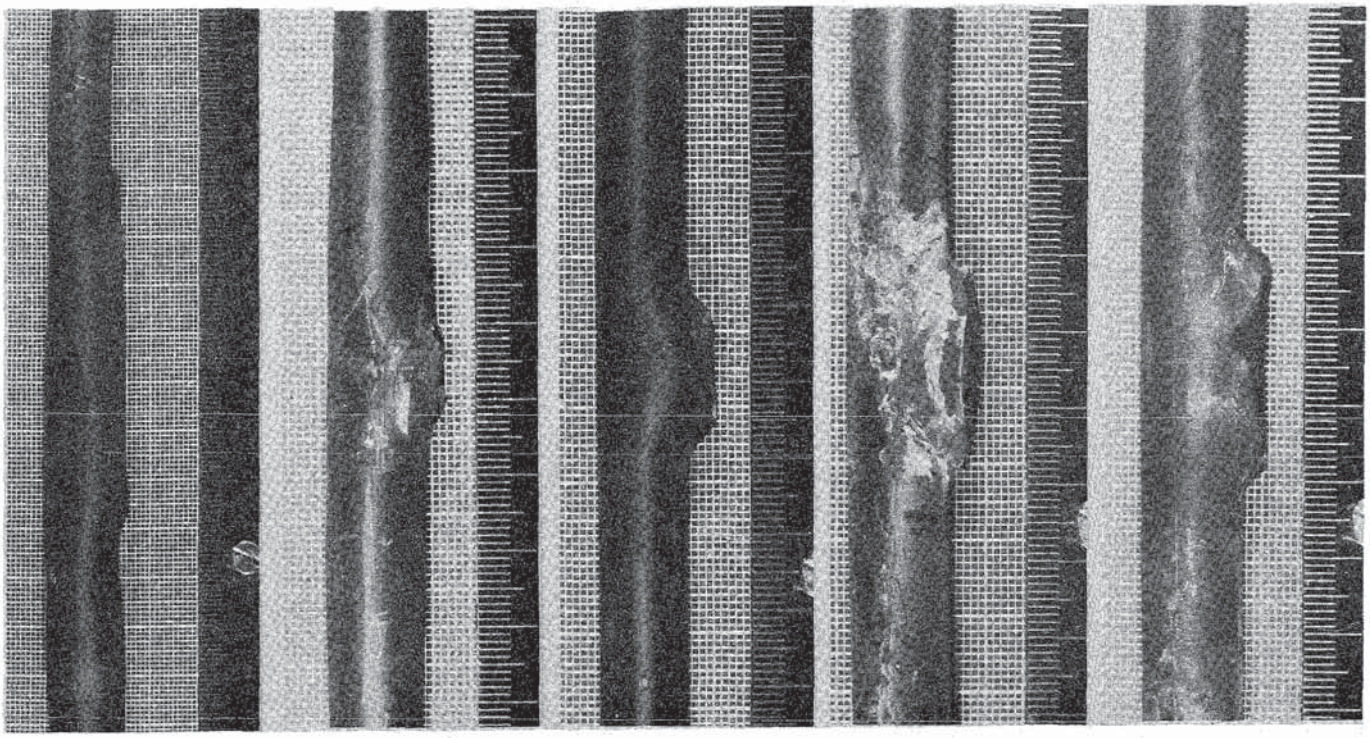

KfK

IT 1980
PNS 4237-362

FR 2 In-Pile Tests. Test Series F

Views of the Ruptured Regions

Fig.13

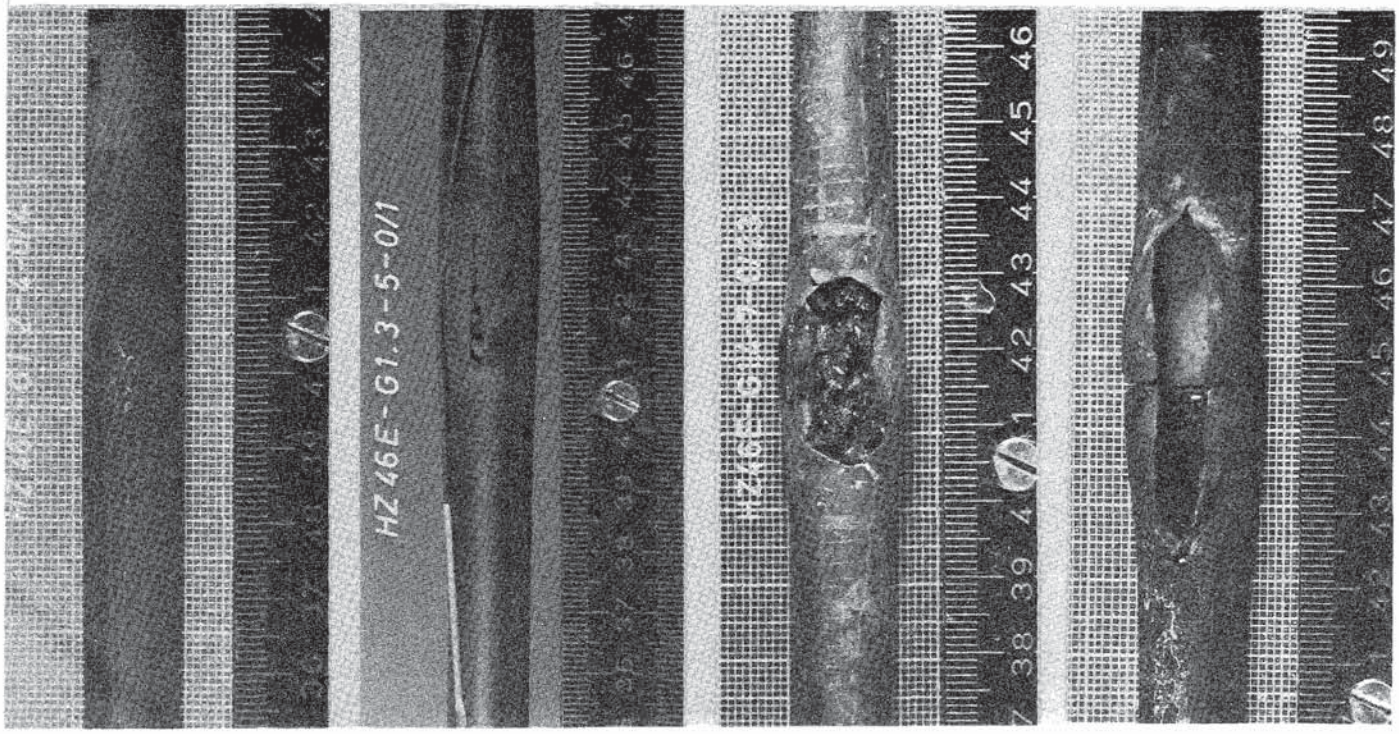

	G1.2	G1.3	G1.4	G1.5
T_B(°C)	730	890	785	780
P_B(bar)	68	41	83	52

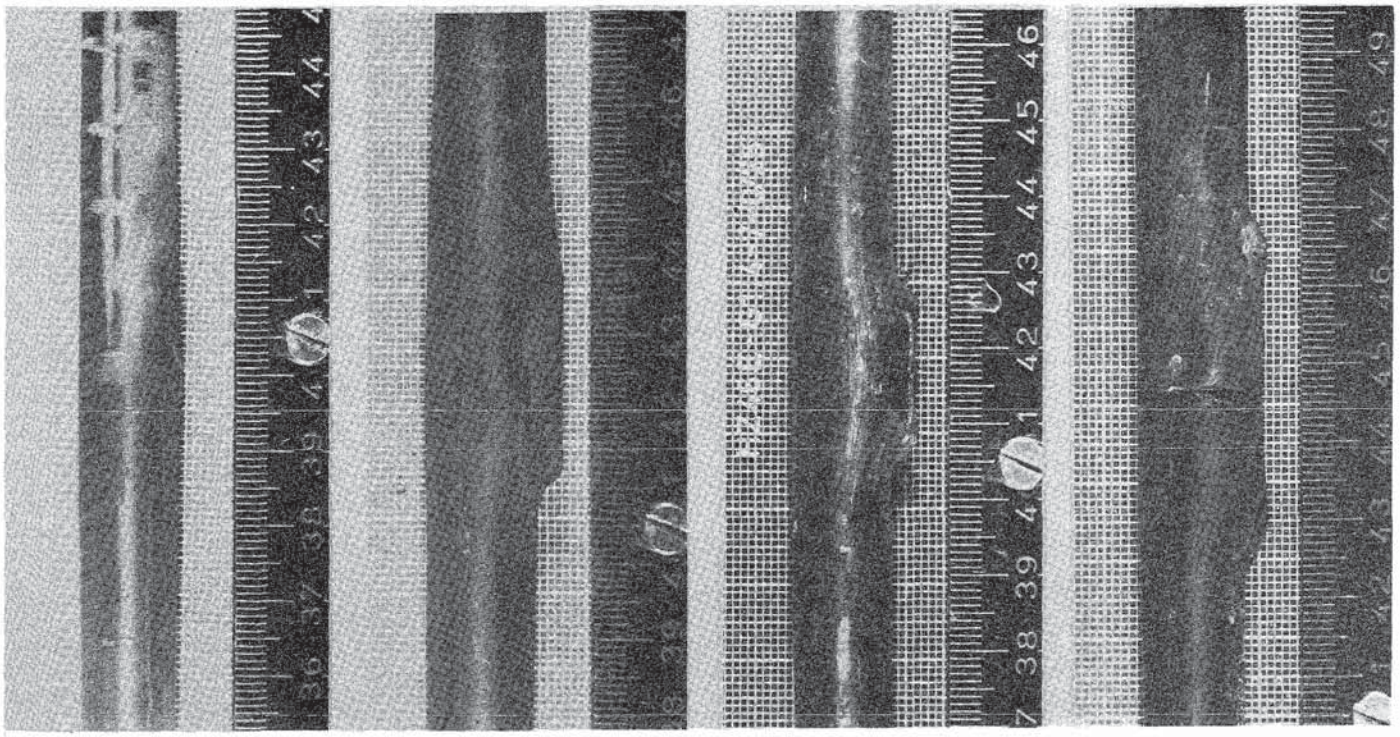

KfK

IT 1980
PNS 4237-363

FR 2 In-Pile Tests. Test Series G 1

Views of the Ruptured Regions Fig. 14

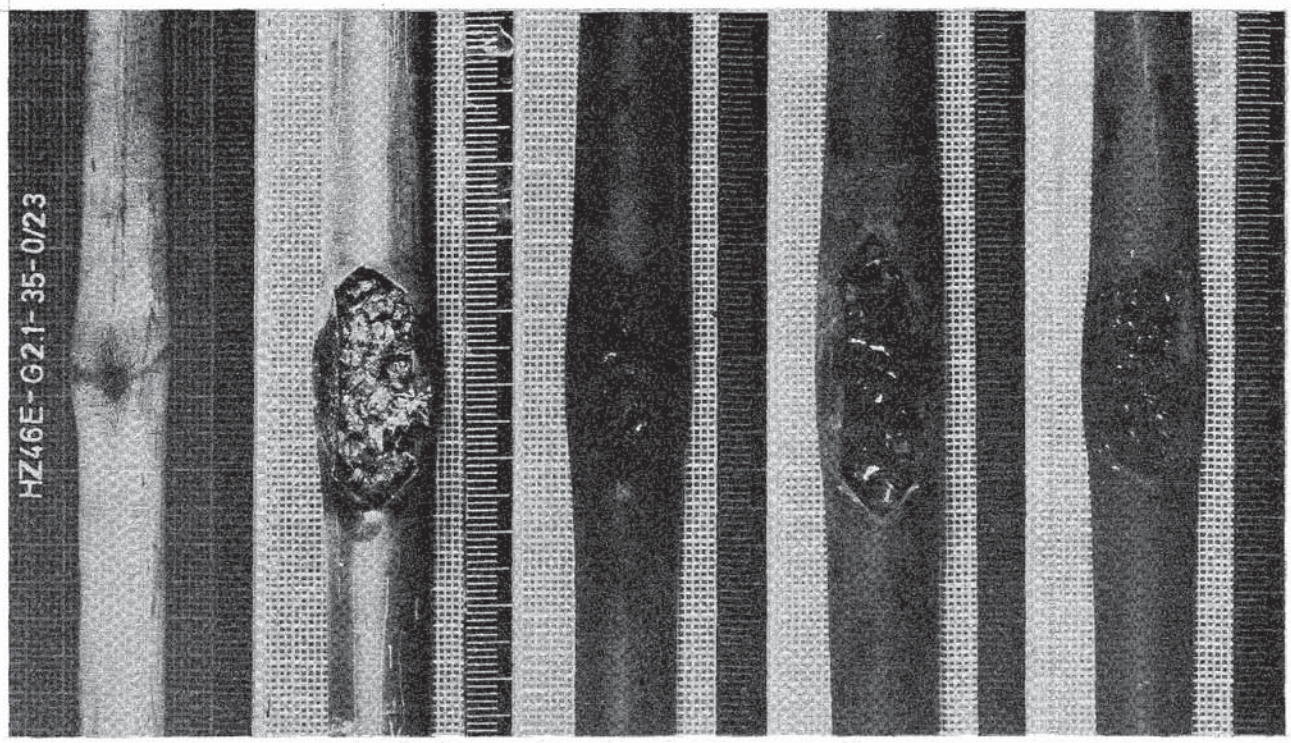

G 2.1	G 2.2	G 3.1	G 3.2	G 3.3
869 T_B(°C)	846	900	838	750
37 P_B(bar)	66	33	54	111

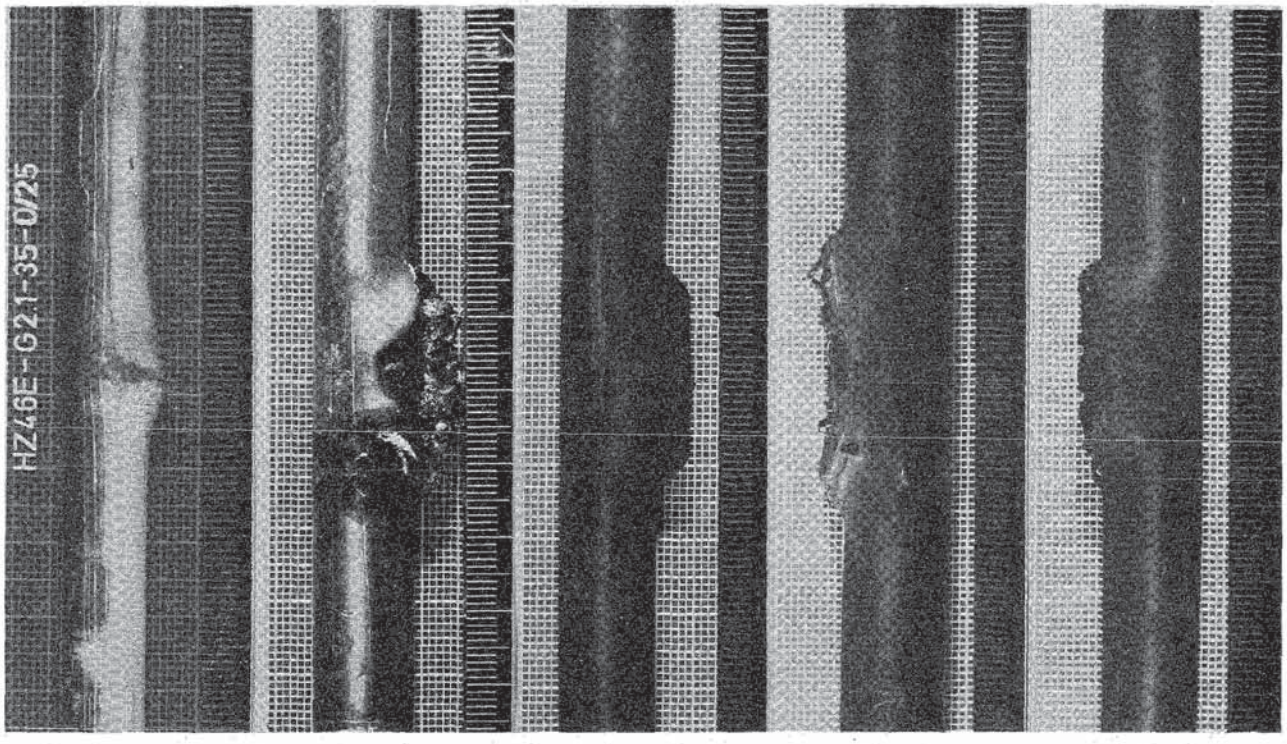

KfK IT 1980
PNS 4237-364

FR 2 In-Pile Tests. Test Series G2/3

Views of the Ruptured Regions Fig. 15

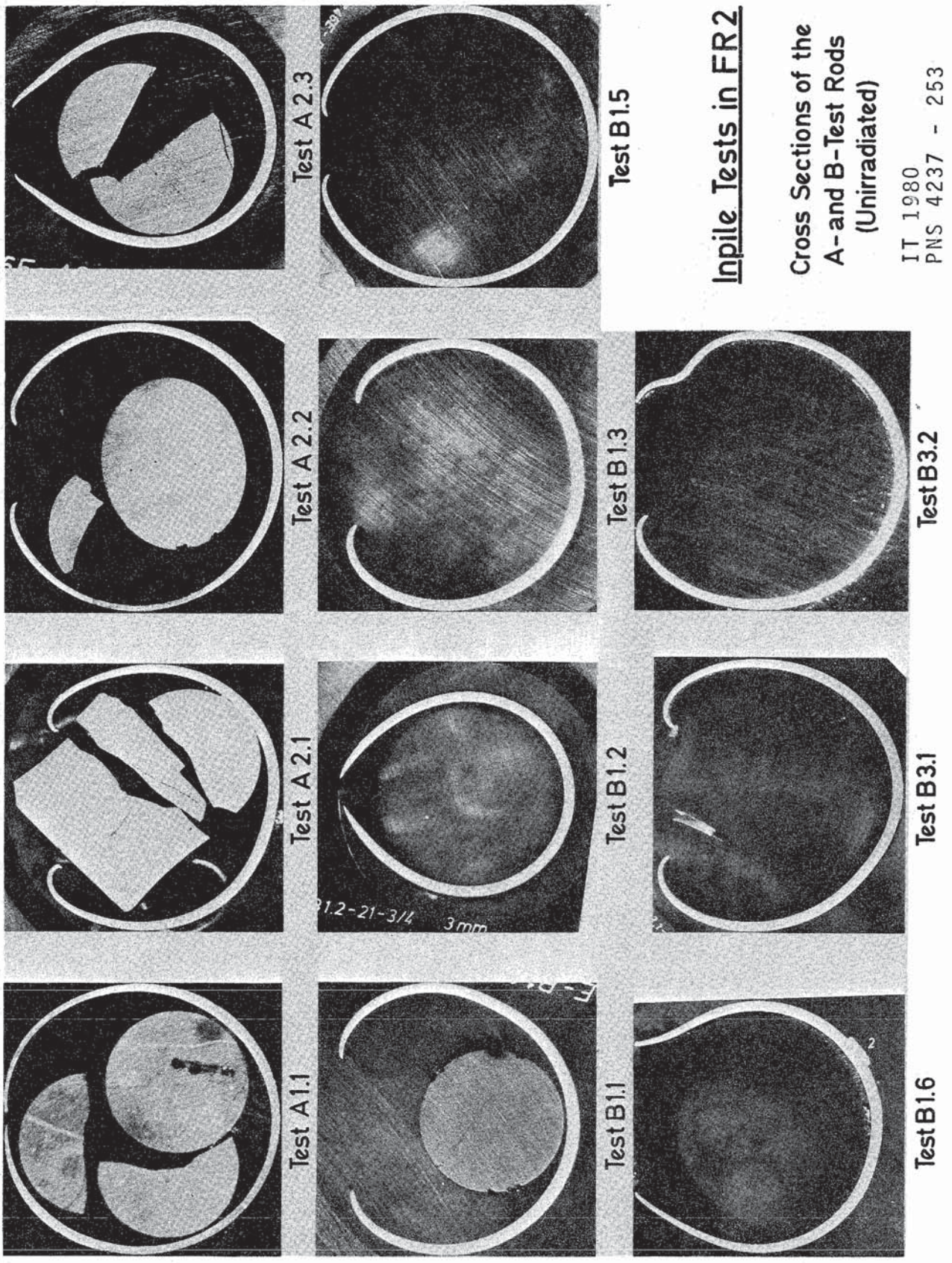
Test A1.1
Test A2.1
Test A2.2
Test A2.3
Test B1.1
Test B1.2
Test B1.3
Test B1.5
Test B1.6
Test B3.1
Test B3.2
3mm
Inpile Tests in FR2
Cross Sections of the
A- and B-Test Rods
(Unirradiated)
IT 1980
PNS 4237 - 253

Fig.16

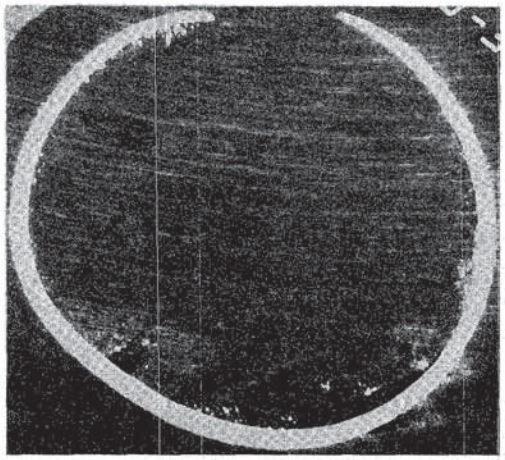

Test F 1

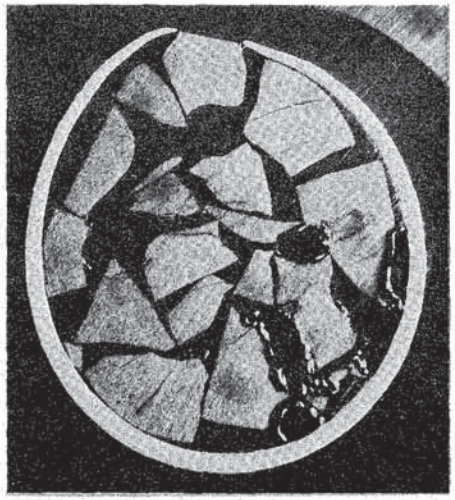

Test F 2

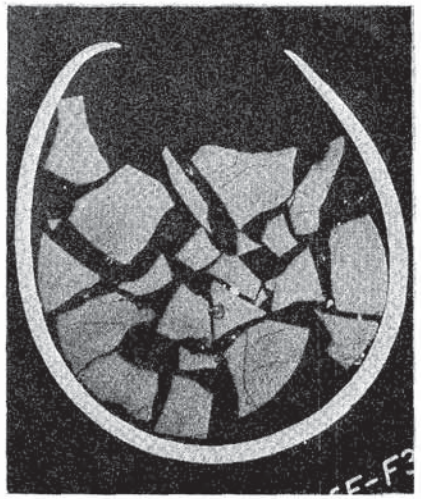

Test F 3

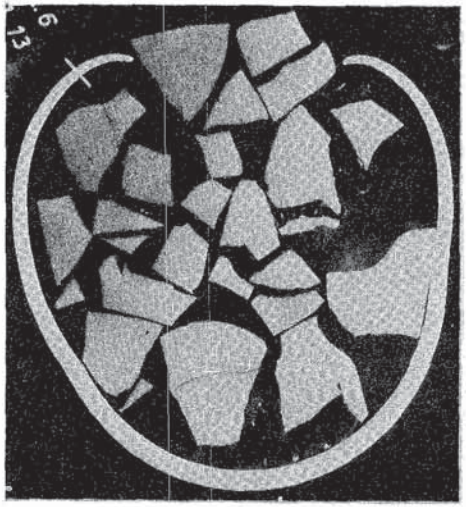

Test F 4

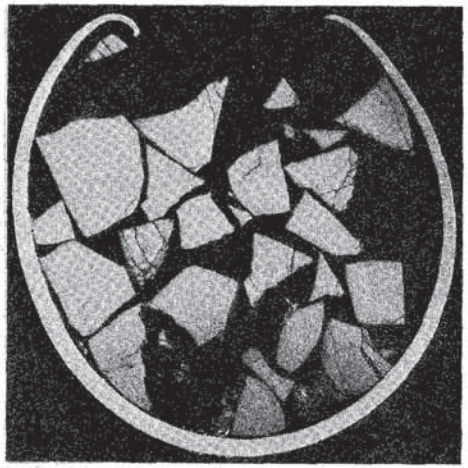

Test F 5

FR2 In-Pile Tests.

Cross Sections of the
Test Rods Series F
(20000MWd/t Burnup)

IT-80
PNS4237-357

Fig. 17

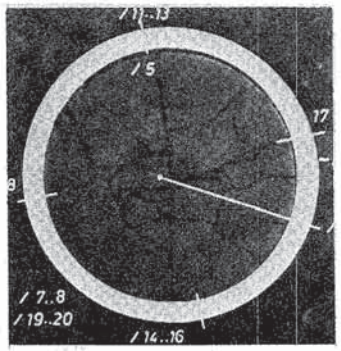

Test G1.1
(No Burst)

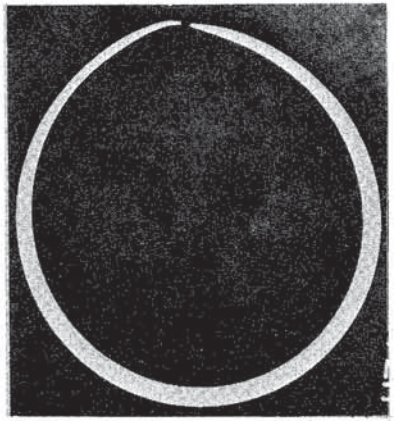

Test G1.2

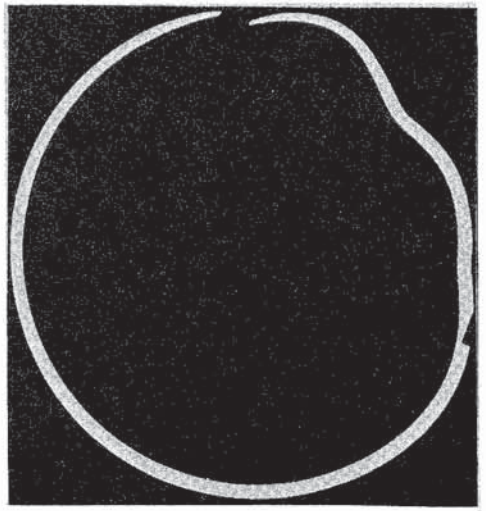

Test G1.3

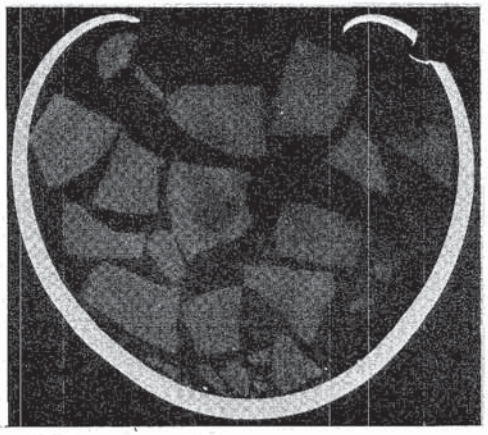

Test G1.4

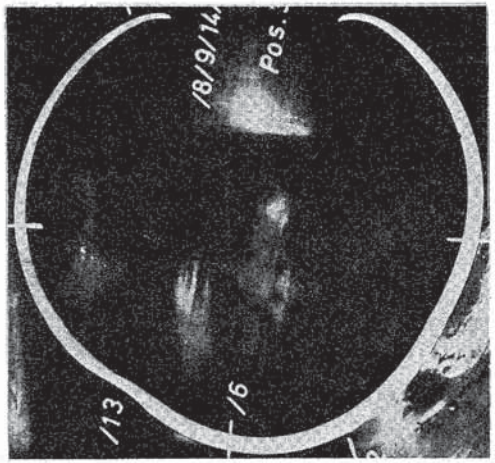

Test G1.5

FR2 In-Pile Tests.

Cross Sections of the Test Rods Series G1 (35 000MWd/t Burnup)

Fig. 18

IT-80
PNS4237-358

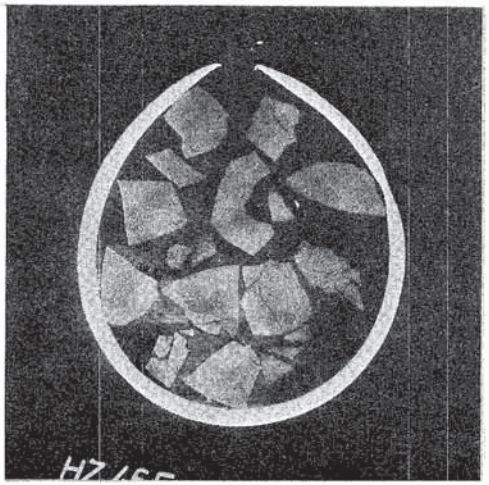

Test G 2.1

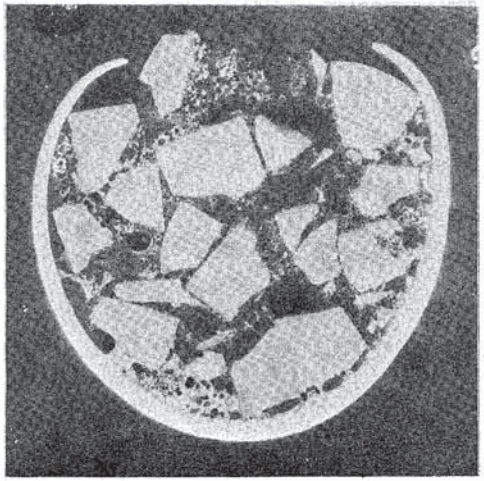

Test G 2.2

FR 2 In-Pile Tests

Cross Sections of the Test Rods, Series G 2 / G 3 (35 000 MWd/t Burnup)

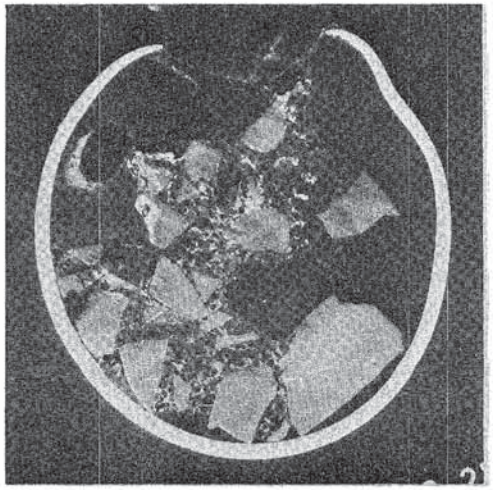

Test G 3.1

Test G 3.2

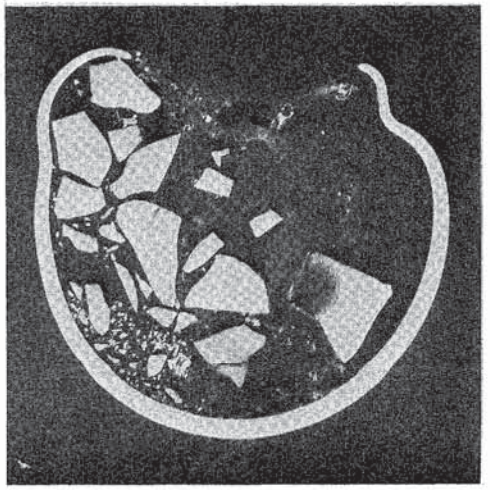

Test G 3.3

IT 1980
PNS 4237-397

Fig. 19

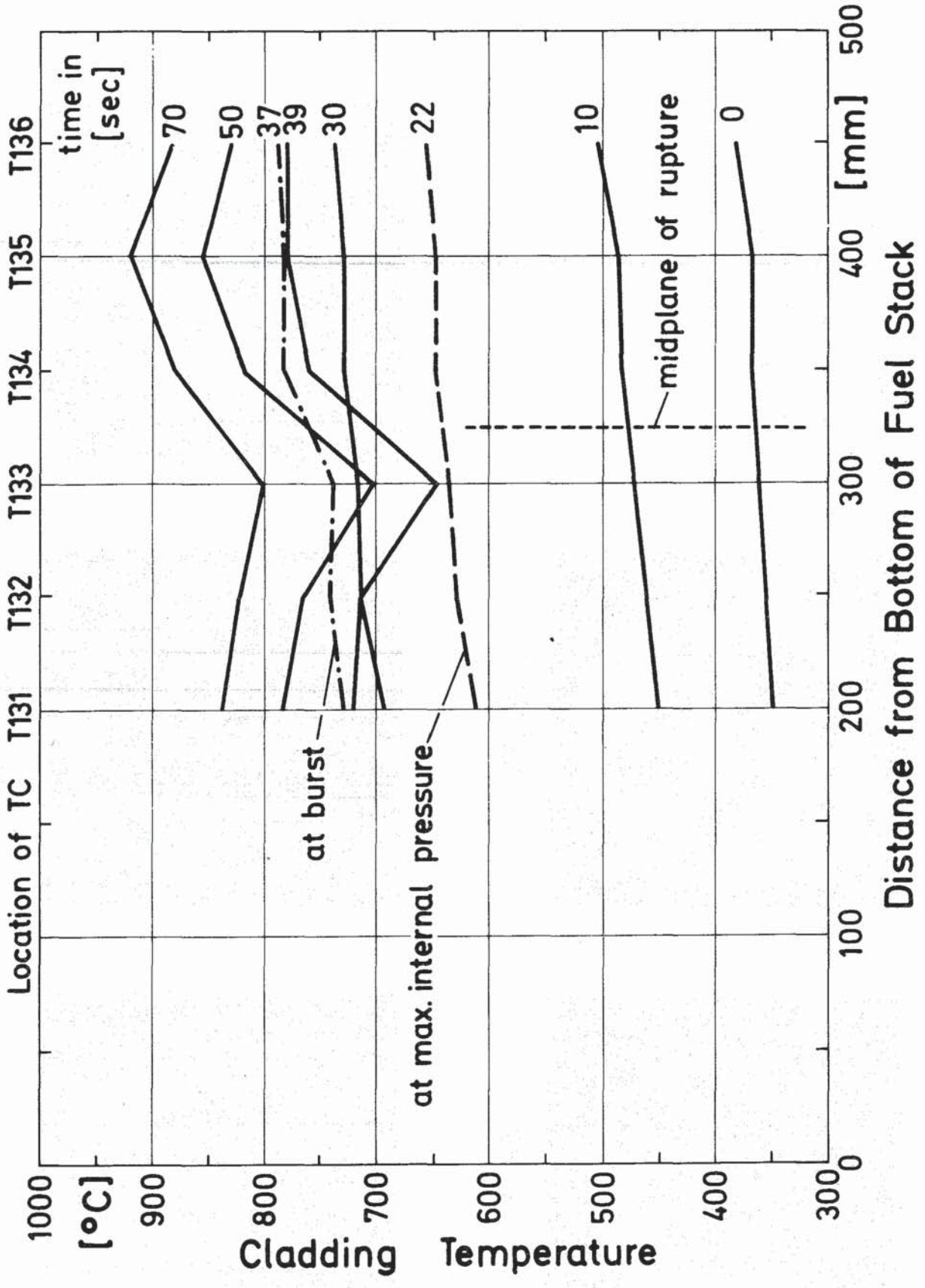

FR2 In - Pile Tests:

Axial Temperature Profiles during Test F4

Fig. 20

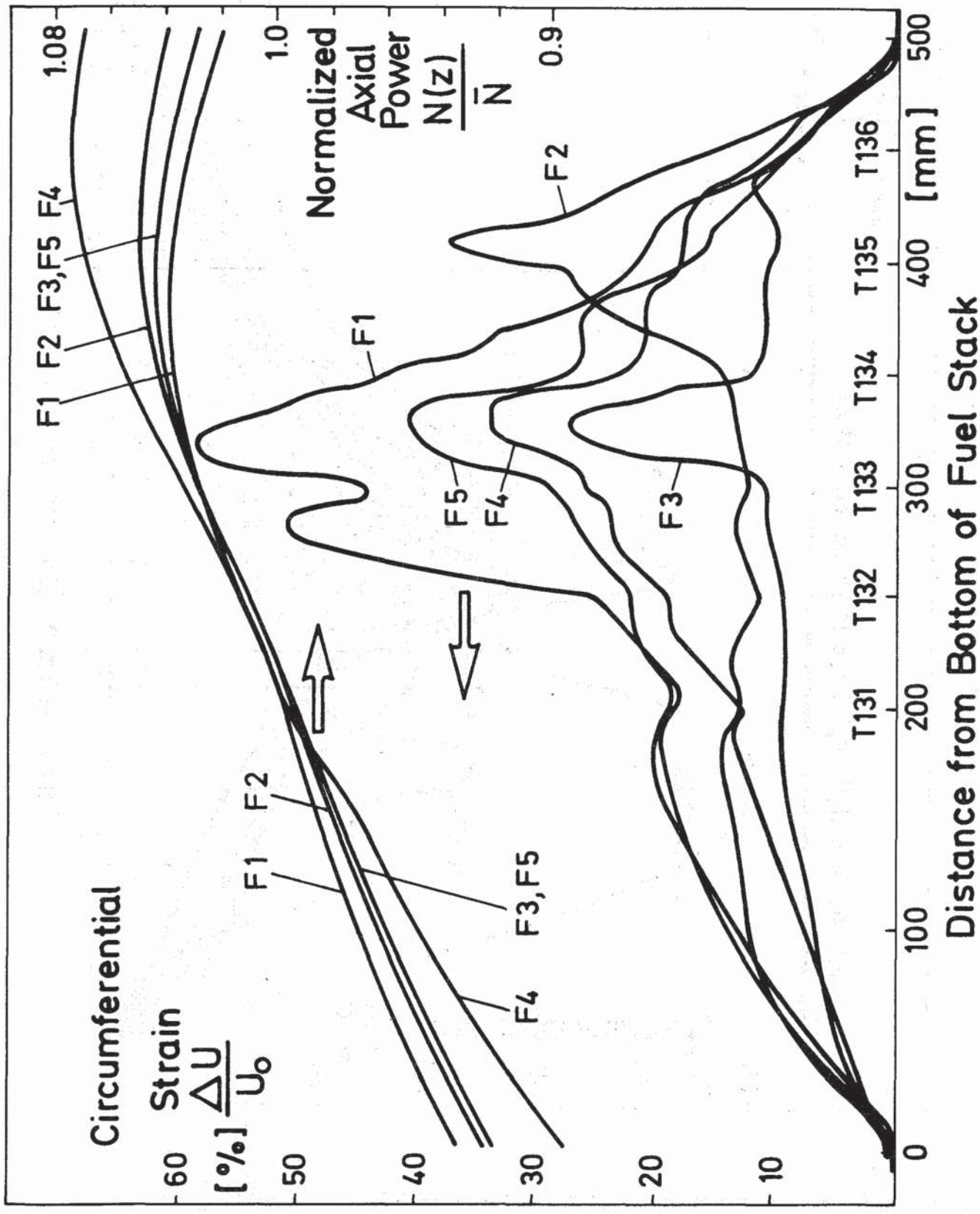

KfK IT-80
PNS4237-284

FR2 In-Pile Tests: F1 through F5

Circumferential Strains and Axial Power Profiles

Fig. 21

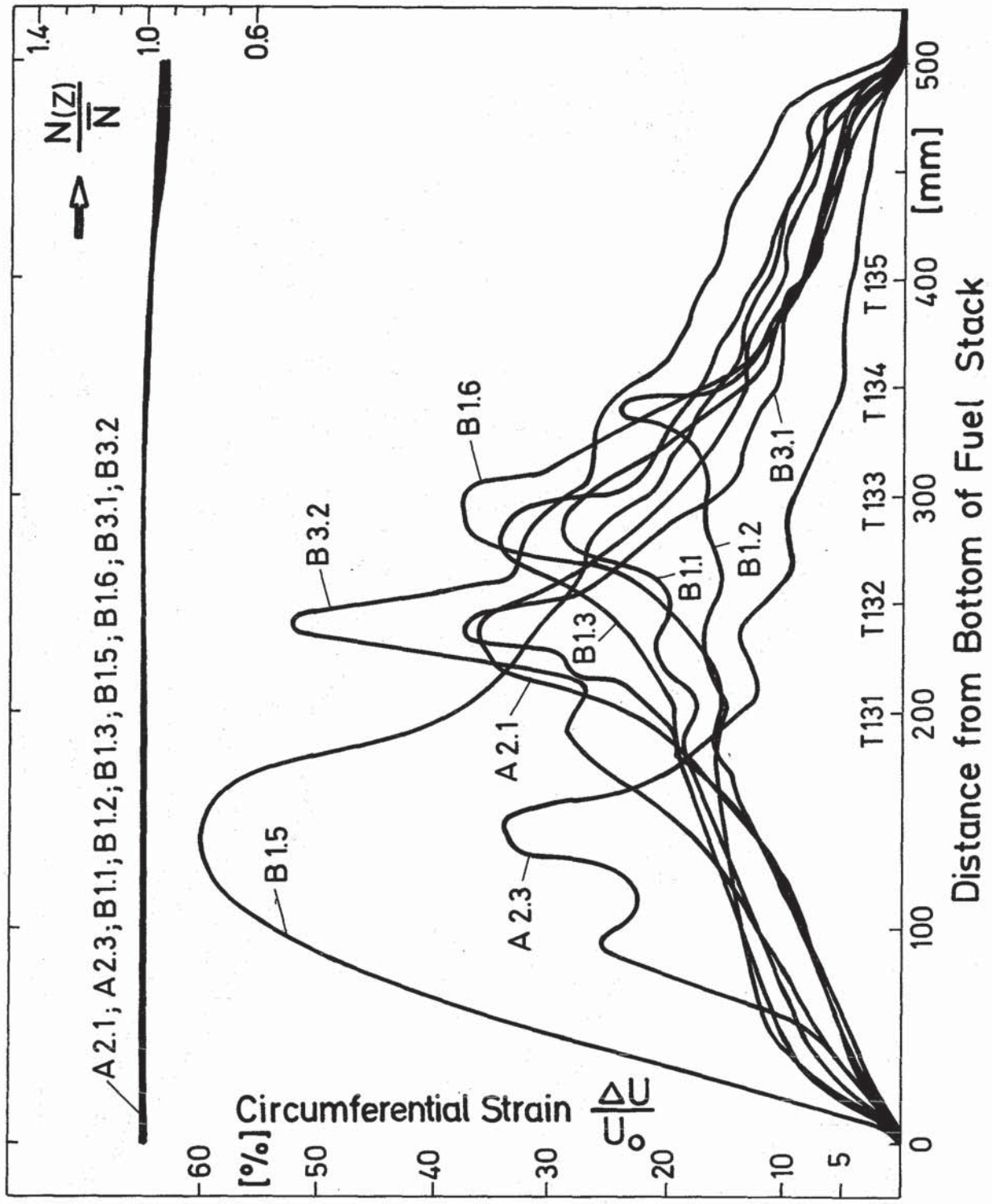

KfK IT-80
PNS4237-341

FR 2 In-Pile Tests.

Circumferential Elongations and Axial Power Profiles of the A and B Tests (unirradiated)

Fig. 22

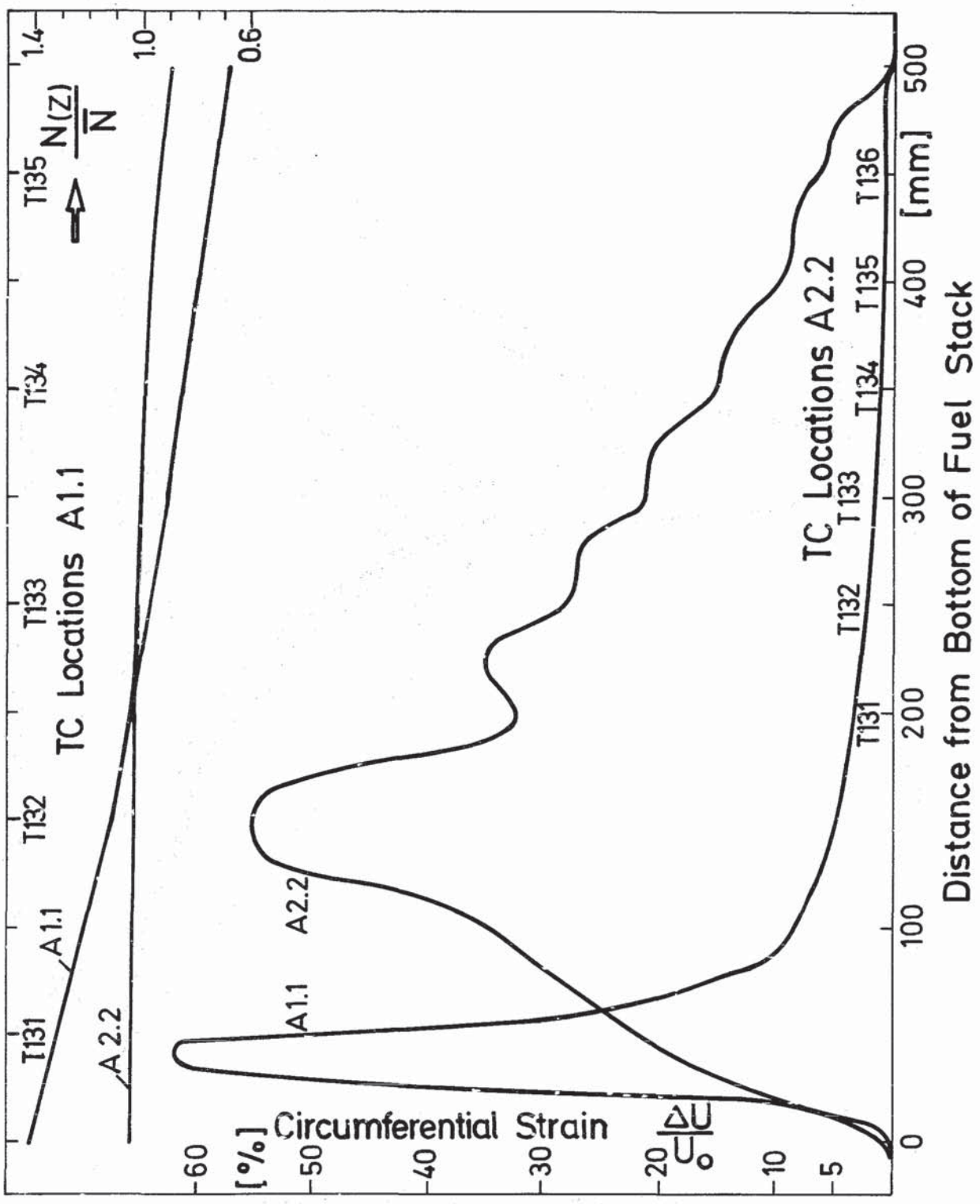

KfK IT-80
PNS4237-342

FR2 In-Pile Tests.

Circumferential Elongations and Axial Power Profiles of the A1.1 and A2.2 Tests (unirradiated)

Fig. 23

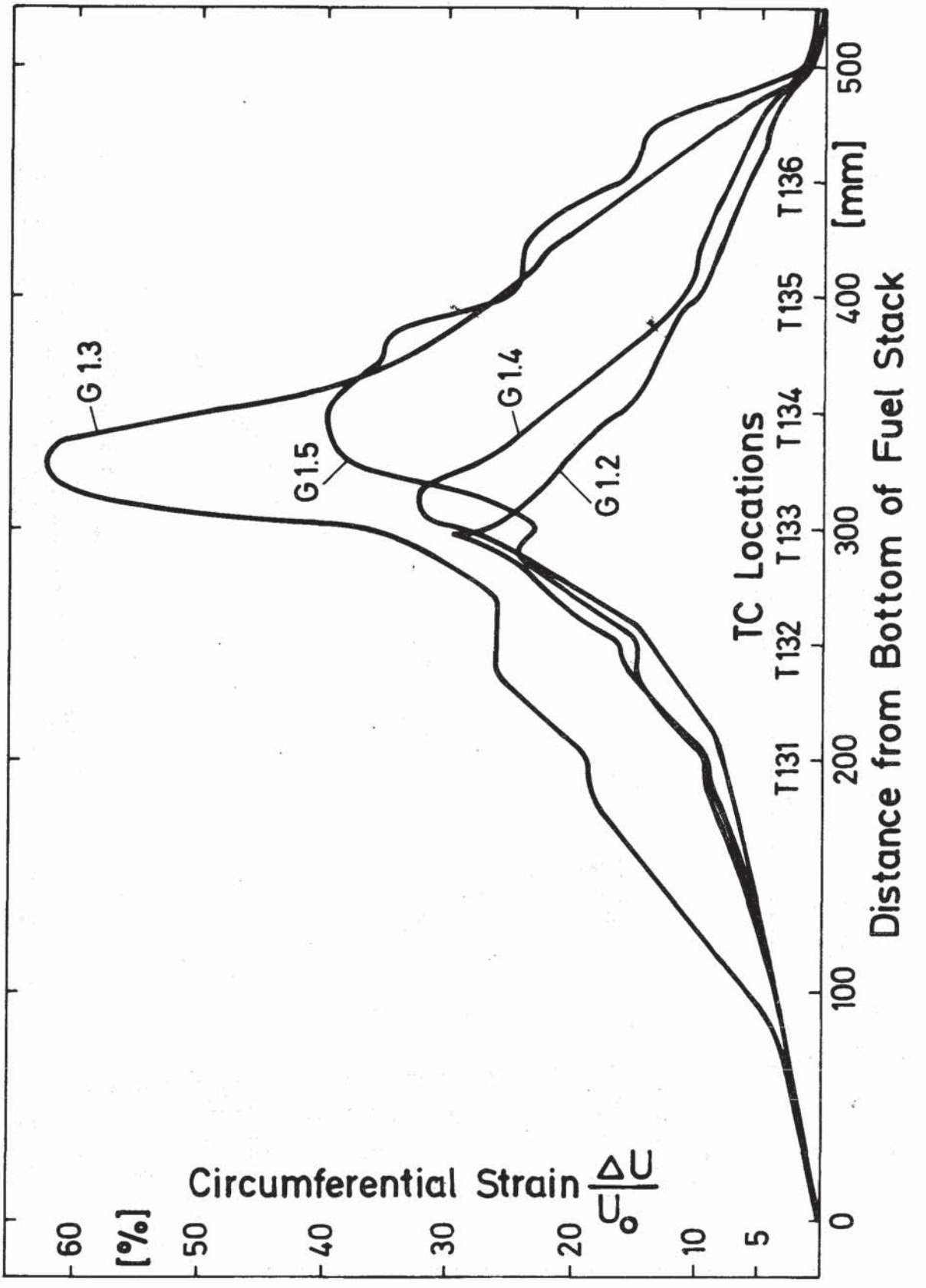

KfK IT-80
PNS4237-344

FR 2 In-Pile Tests.

Axial Profile of Circumferential Strain, Tests G1 Fig. 24

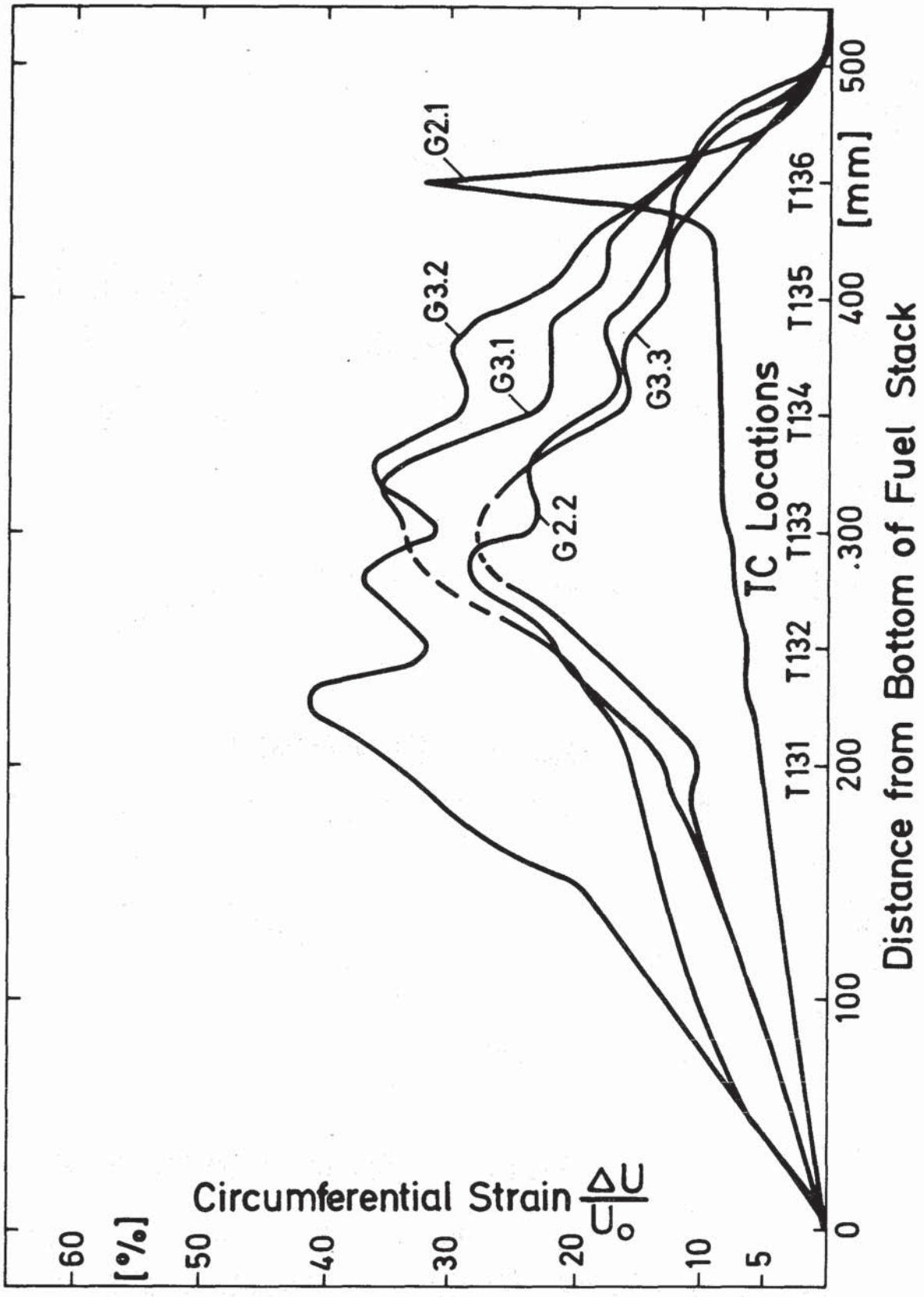

KfK IT-80
PNS 4237-343

FR2 In-Pile Tests.

Axial Profile of Circumferential Strain, Tests G2 and G3 Fig. 25

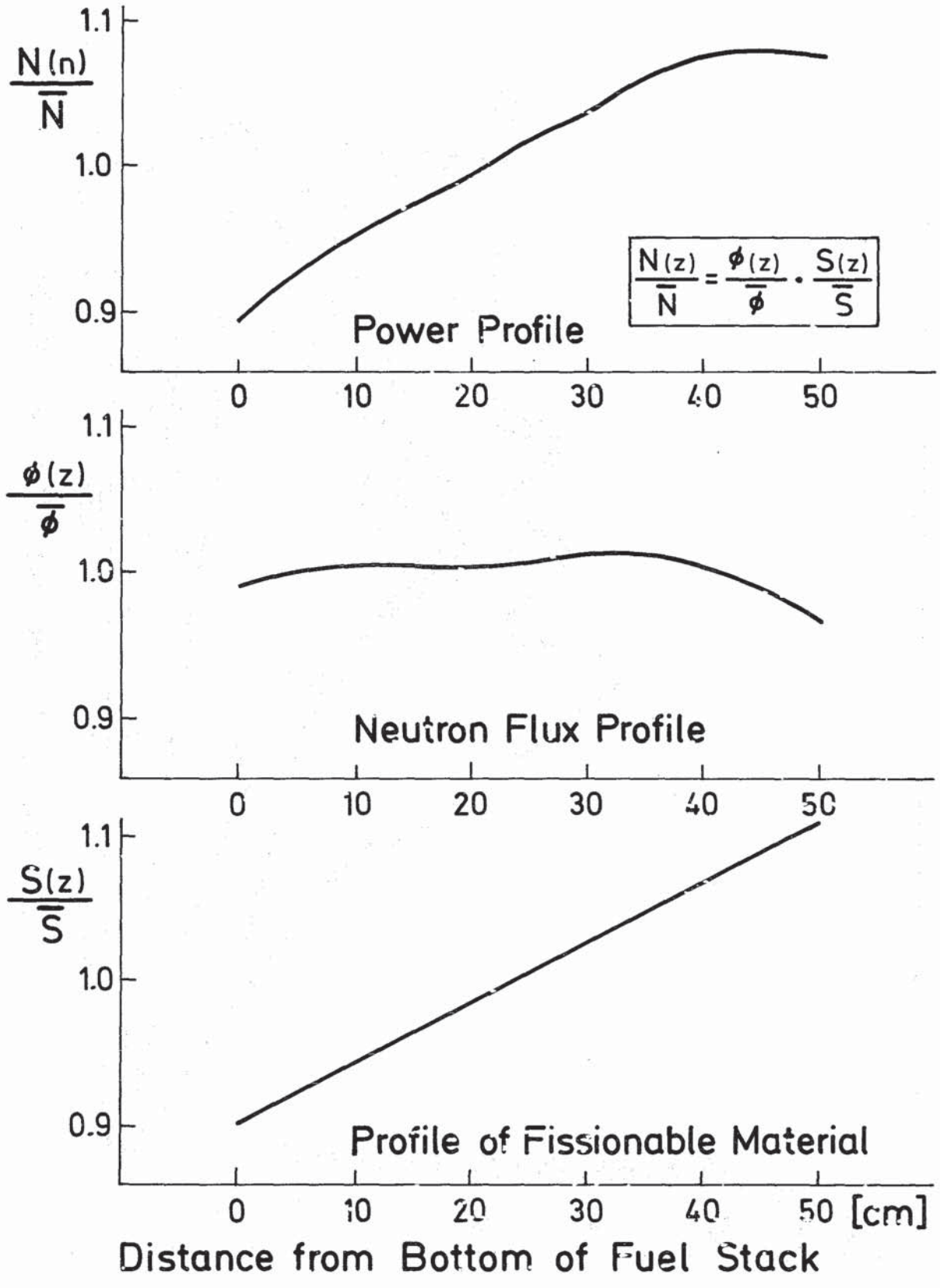

FR2 In-Pile Tests:

Normalized Axial Profiles, Test F4 Fig. 26

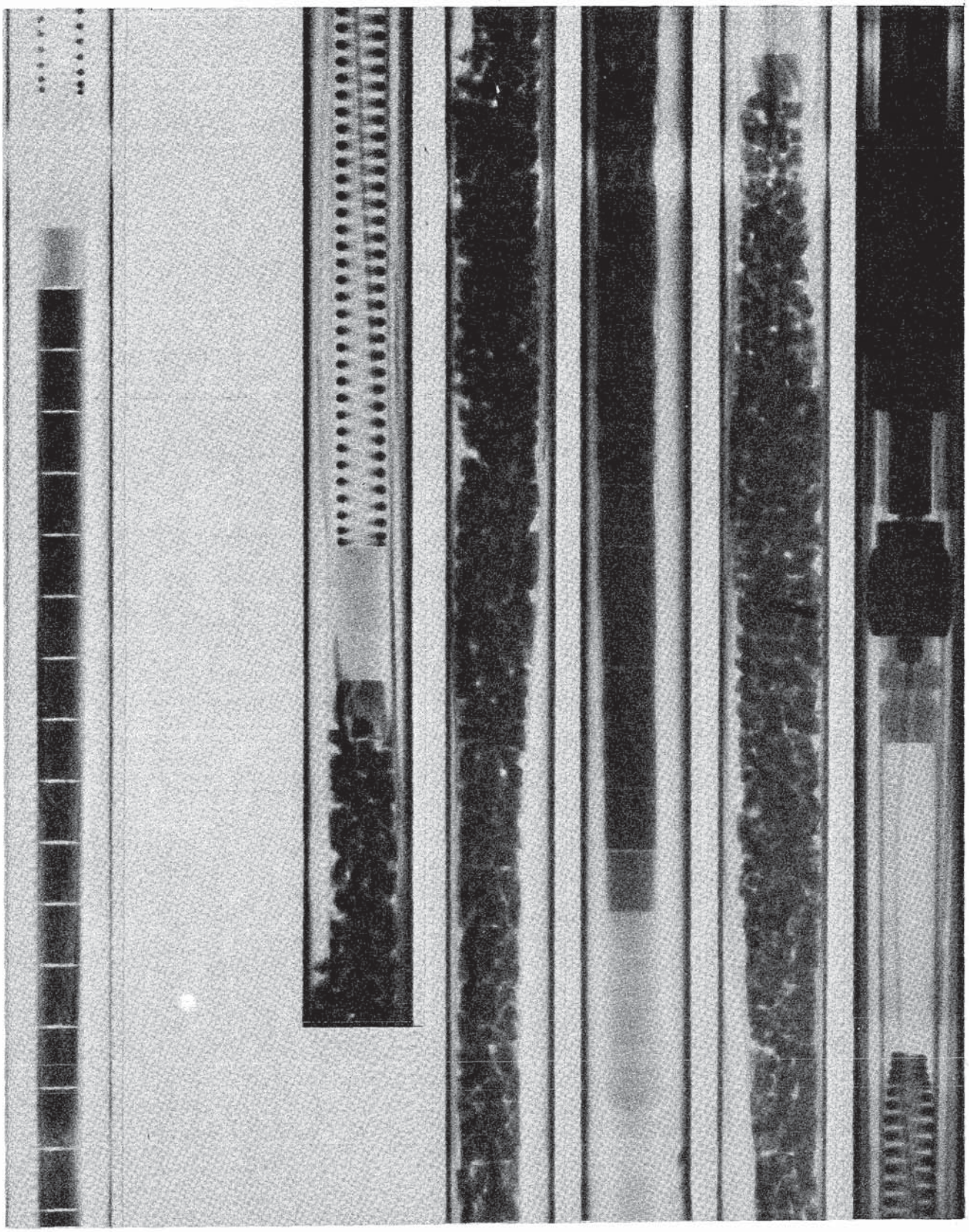

Pre-Transient

Post-Transient

KfK IT80
PNS 4237-366

FR2 In-Pile Tests

Neutrographs of Rod F 1, burnup 20 GWd/t_u

Fig. 27

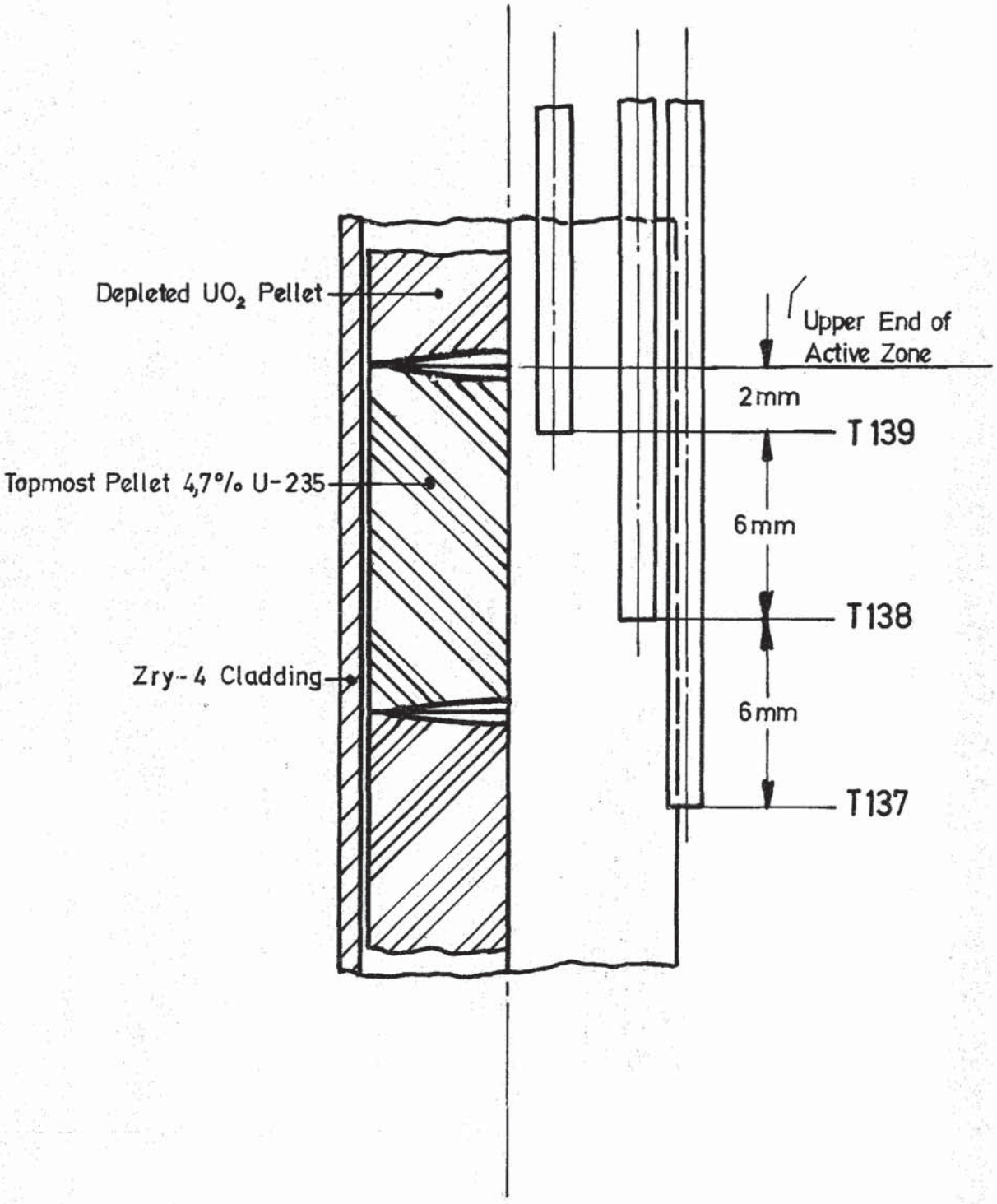

KfK IT-80
PNS4237-306

FR2 In-Pile Tests.

TC Instrumentation in Tests E 3 and E 4 Fig. 28

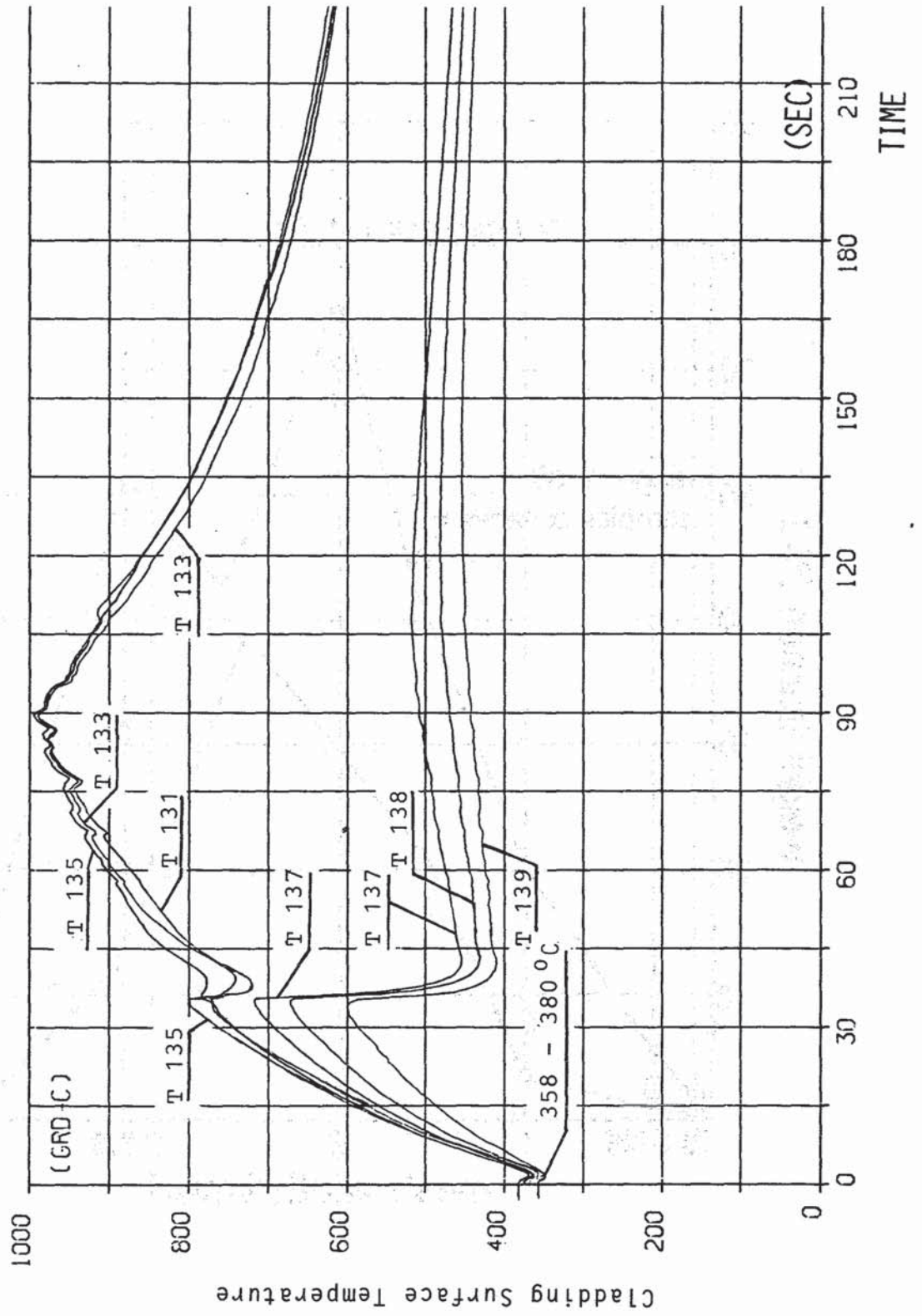

FR2 IN-PILE TESTS: TEST E4

CLADDING TEMPERATURE HISTORIES

KfK IT 1980
PNS 4237-339

Fig. 29

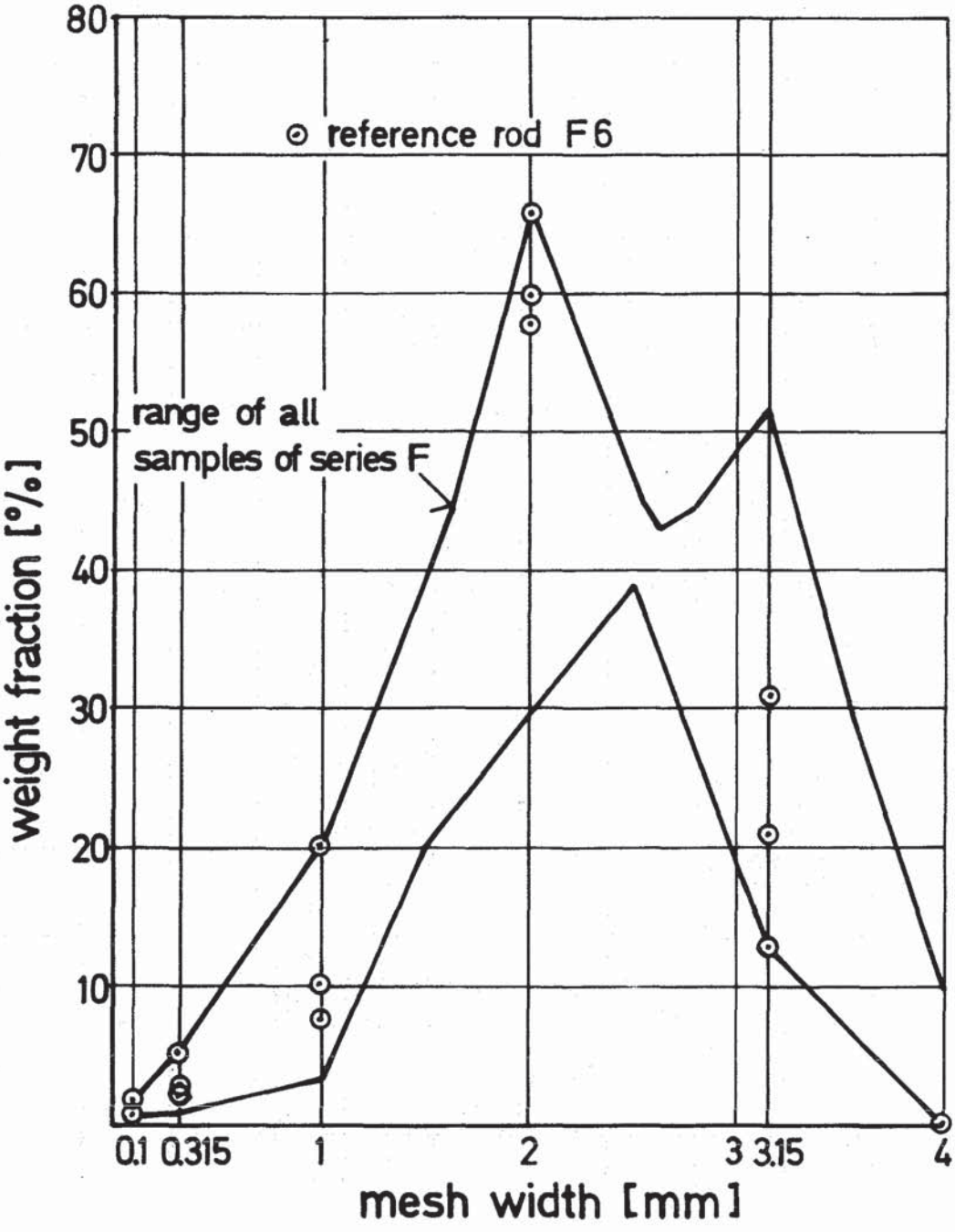

KfK IT-80
PNS4237-398

FR2 In-Pile Tests: Series F

Fuel Particle Size Distribution, Sieve Analyses Fig. 30

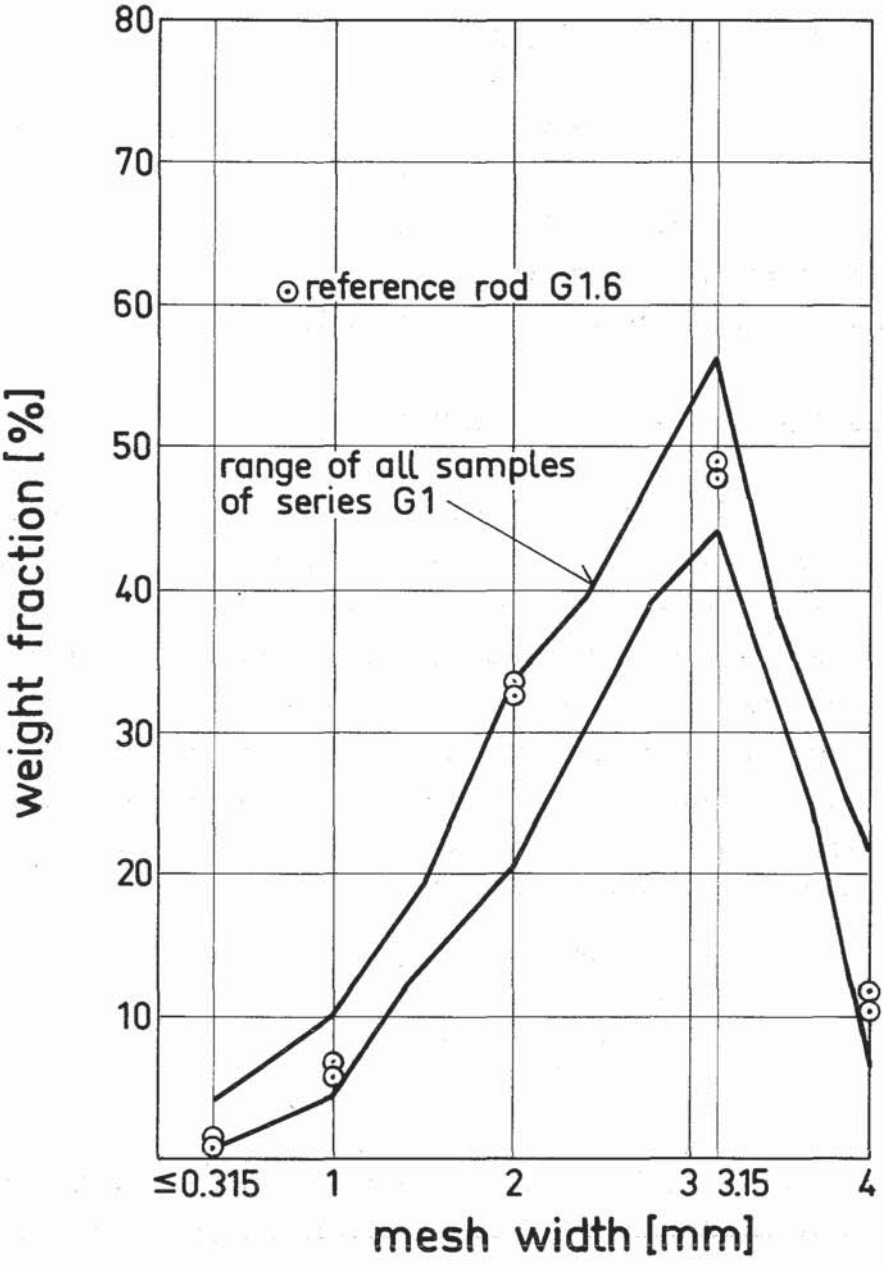

KfK IT-80
PNS 4237-301

FR2 In-Pile Tests: Series G1

Fuel Particle Size Distribution, Sieve Analyses

Fig. 31

Part II

RESULTS OF DESTRUCTIVE PTE

1 Analysis of Deformation of Zircaloy-4 Cladding

To describe the complex nature of Zircaloy-4 deformation two quantitative methods are used: The radial strain localization parameter to quantify the deformation in the region of maximum circumferential strain and the axial strain localization parameter to quantify the deformation along the axis of the tube.

1.1 Radial strain localization parameter

The radial strain at fracture can be correlated with the heating rate and the maximum circumferential temperature variation for the cladding at burst temperatures < 1000°C. It should be possible to correlate the maximum circumferential strain with a quantitive measure of the extent of radial strain localization, such that the circumferential strain decreases as the radial strain becomes more localized. This method had been presented by H.M. Chung and T.F. Kassner [1]. For this purpose, a radial-strain-localization parameter W_Θ can be defined by

$$W_\Theta = 1 - \frac{1}{2\pi} \int_{\Theta/2\pi=0}^{1} \frac{\psi_W(\Theta)}{\psi_W^B} \, d\,\Theta \qquad (1)$$

where Θ is the tangential angle from the fracture tip, $\psi_W(\Theta)=\ln(s_1/s_o)$ is the true local radial strain at different Θ-positions around the circumference of the cladding and $\psi_W^B = \ln(s_R/s_o)$ is the true fracture radial strain (s_o = initial wall thickness, s_1 = actual wall thickness at different Θ-positions and s_R = thickness of the fracture tip). Thus, W_Θ can be calculated from measured values of the cladding thickness from each experiment. Fig. 1 shows a cladding cross section from test B3.2 and lists some $(\psi_W(\Theta)/\psi_W^B)$-values as a function of normalized angular position $\Theta/2\pi$.

The $(\psi_W(\Theta)/\psi_W^B)$-values were plotted against $\Theta/2\pi$ and integrated according to eq. 1 with a computer-aided digitizer. The result is shown

in Fig. 2, where the shaded area correspond to the parameter W_Θ.

Fig. 3 is a plot of the parameter W_Θ versus the maximum circumferential strain. All eleven in pile tests of series A and B(without preirradiation) are shown and compared with ANL-data which include the following conditions: Out of pile test, steam environment,300 mm length, Al_2O_3 pellet constrained, 0,07 and 0,5 mm diametral gap and direct heating. The correlation between the circumferential strain and the parameter W_Θ is the same found by H.M. Chung and T.F. Kassner [1] i.e. the circumferential strain increases as the parameter W_Θ decreases.

The values of the KfK tests are above the scatterband of the ANL-data (dotted lines in Fig.3). An influence of the irradiation can be excluded, because the temperature transient was very fast and therefore irradiation time very short. The most important difference between the two kinds of tests is the heating method: KfK tests are in-pile tests with indirect heating, ANL-data are from out-of-pile tests with direct heating.

In direct heating the decrease of wall thickness in the balloon leads to higher temperatures in this area and supports an overall thinning of the wall, i.e. lower W_Θ-value. In indirect heating, we know, if the ballooning is started the cladding lifts off and the material flows on that side where the contact with the pellets is better. The consequence is a non-uniform deformation with long necking zones, i.e. higher W_Θ-values. In both cases the circumferential strain can be the same.

Therefore we assume, that W_Θ is not the general parameter to describe the deformation behavior of all burst tests.

1.2. Axial-strain localization parameter

The shape of balloons of burst Zircaloy-4 cladding looks very different. Depending on the boundary conditions of the deformation like temperature and temperature variation (axial and circumferential) an axialy localized balloon or a homogeneous distribution of the circumferential strain along the tube could be achieved respectively. Most cases are inbetween. A quantitative measure of the extent of axial strain localization was

defined by an axial-strain localization parameter W_z

$$W_z = 1 - \frac{1}{Z_o} \int_{z/z_o=0}^{1} \frac{\varepsilon_\Theta(z)}{\varepsilon_{\Theta,Max}} \, dz \qquad (2)$$

where z is the distance from the lower end of fuel, z_o = 500 mm (length of the heated zone), $\varepsilon_\Theta(z) = \ln(d_1/d_o)$ is the true local circumferential strain at different z-positions along the axis of the tube and $\varepsilon_{\Theta,Max} = \ln(d_{max}/d_o)$ is the true maximum circumferential strain (d_o = initial diameter, d_1 = actual diameter at different z-positions, and d_{max} = maximum diameter).

The procedure to get the W_z-values is nearly the same as that to get W_Θ. Fig. 4 shows as an example a diameter measurement plot from test B3.2. In Fig.5 the $(\varepsilon_\Theta(z)/\varepsilon_{\Theta,Max})$-values were plotted against the normalized axial position z/z_o and integrated according to eq. 2 with the digitizer, the shaded area corresponds to the parameter W_z.

In Fig. 6 the parameter W_z versus the time to burst is plotted. This plot contains the eleven in pile tests of A and B series and for comparison tests which had been conducted in RFL [2]. Those conditions had been: Out of pile tests, steam environment, 470 mm heated length, Al_2O_3 pellet constrained, direct heating.

The values from RFL scatter very much, but most of the values especially for higher times to burst are below W_z = 0,5 and show therefore a homogenious distribution of the circumferential strain along the axis ("sausages"). Below a time to burst less than 45 sec even RFL had test conditions (high internal pressure and or fast temperature transients) where onecould not get "sausages".

In the case of W_z an influence from the different heating methods is not remarkable. As a final remark it should be said, that at test conditions which lead to higher times to burst i.e. low internal pressure and or slow temperature transients the possibility to get long sausages will increase.

2 Microstructural Evaluation of Cladding Maximum Temperature

2.1 Intention and Procedure

As part of the destructive investigation of fuel rods after in-pile transients, the Zircaloy 4 (Zry) cladding tube microstructure was studied. In addition to the performed temperature measurements an independent estimation of local maximum cladding temperatures reached during the LOCA transient was intended. This evaluation has shown to be practicable for the 800 - 1050°C temperature range.

According to the Zry-oxygen phase diagram 820 - 970°C is the $\alpha + \beta$ two-phase region for non-oxidized Zry (Fig. 7). Approximately this range holds also for mid-wall positions of slightly oxidized tubes. The relation $T_{max} = 820 + 150 \cdot f_\beta$ [°C] between peak temperature T_{max} and β-Zry volume fraction f_β was used as approximate microstructure/temperature correlation. Further the micrographs were compared to those of laboratory oxidation test specimens as standards. Those have shown, that equilibrium f_β values are quickly established after heating. Prior β to α' retransformation is occurring during cooldown from higher temperatures, whereas cooling from lower temperatures (two-phase range), lower cooling rates and high deformation seem to favour the β to α transformation by growth of α nuclei. Main difficulty of the temperature estimation procedure is the correct identification of the prior β volume fraction.

In the high α-Zry temperature range (up to 820°C) recrystallisation and grain growth help to estimate the maximum temperature. In the lower β-Zry range (970 - 1050°C) fast growth of β grains after complete α-grain dissolution is temperature indicative (Fig. 7).

2.2 Results

Eleven not pre-irradiated fuel rods from the A and B series tests have been evaluated for local maximum temperatures and azimuthal and axial temperature variations. The estimated temperatures are in general judged to be reliable within less than ± 30°C of scatter. At about 950°C the Zry microstructure is most temperature sensitive. Two independent evaluations have shown that the temperature uncertainty may be relatively higher for the lower temperature region and high local deformation.

Fig. 8 shows the field of maximum cladding temperatures for the B 1.3 test rod as example, which is seen from the inside after cutting in axial direction and unfolding. As far as a direct comparison with thermocouple (T 131 - T 136) measurements, corrected by addition of 75°C, is possible, the relative axial temperature profile is corroborated, whereas in most cases the microstructural evaluation has resulted in about 40°C lower maximum temperatures than measured. It may be concluded, that the thermocouple correction is too high, so that the burst temperatures of the tubes should equally be reduced. Only for test A 2.3 this was directly indicated; the burst temperatures of the other tubes could not be microstructurally evaluated due to the continuation of heatup after bursting for those tests. Azimuthal temperature differences up to about 60°C have been found for different tubes in the evaluated axial positions.

3 Cladding Oxidation

3.1 Outer Surface

Hot-cell metallography of the not pre-irradiated fuel rods after in-pile tests has verified the steam oxidation aspects studied by out-of-pile laboratory investigations [3],[4]. Cladding temperature, oxidation time and deformation mainly determine the local oxidation.

The oxide layer is found to be dense and adherent. Cross sections show the axial, deformation-induced cracks to be narrow or extremely widened, respectively, depending on the local amount of deformation (Fig.9). For highest deformation partial oxide loss is seen and oxidation after the burst is identified by crack-free, smooth oxide layers (Fig.10). The α-Zr(O) layer between oxide and bulk $\alpha + \beta$ or β-Zry has about the same thickness as the oxide and varies with local temperature-time conditions (Fig.11).

Measured local mean values of oxide layer thickness at positions relatively undisturbed by cracks have been drawn against the corresponding local maximum temperatures as estimated on the basis of bulk Zry microstructural appearance. The results are seen in Fig.12 to form a scatter band common for all tubes of the test series A and B. This indicates, that the temperature is the parameter of main influence and its microstructural evaluation seems to be reliable. In the upper region of the scatter band the results for the relatively longest tests (A 1.1 and B 1.5) are found as well as thickness results for tube positions with seriously cracked oxide. This demonstrates the relative importance of the oxidation time and of the strain-induced oxide damage. The absolute amount of oxidation, ca. 2 - 7 µm oxide was to be expected for this kind of tests according to the existing knowledge of the Zry oxidation kinetics and in comparison to out-of-pile investigations. The limited steam supply in the in-pile tests did not reduce the reaction, so that additional supply via steam bypass for some tests was of no detectable influence.

First results for some pre-irradiated rods of the F and G test series have shown rare events of very locallized forms of oxide failure. Enhanced oxide growth during the transient at those spots was the result. Corresponding forms of local oxide failure during pre-oxidation have been revealed in out-of-pile laboratory oxidation tests.

It is concluded that no in-pile specific influences on morphology and kinetics of the Zry oxidation have been revealed for the evaluated test rods.

3.2 Inner surface

The inner surface of the Zry tubes shows relatively smooth and dense oxide layers. The oxide cracks typical for the outside are not encountered. But some of the micrographs show fine and shallow cracking of the outer and therefore oldest part of the oxide. The layer thickness varies with the maximum temperature locally reached but it is generally smaller than the oxide at the outer tube surface (Fig. 13). The thickest oxide is found in the vicinity of the tube burst, and with growing distance from it the oxide is generally thinner. At more than 100 mm apart from the burst position oxide has in no case been identified. But a thin seam of α-Zr(O) or at least the oxygen uptake, having modified the border of the bulk $\alpha + \beta$ or β Zry microstructure, indicate the at least slow oxidation reaction (Fig. 14).

It has to be concluded that the oxidation of the tube inside is mainly caused by steam access via the burst. This explains the absence of gross oxide cracking, the generally lower level of oxidation compared to the outside and the favouring of the burst vicinity. The steam seems to be consumed essentially in this range or at least to be delayed, to reach others in form of a mixture with fill-gas and released hydrogen. The above mentioned shallow oxide cracking (Fig. 13) indicates that oxidation commenced before the burst time, and the oxidation, identified far from the burst (Fig. 14), also seems to be not the result of steam. Those items are judged to be the effect of cladding oxidation in contact with the fuel. The relative contribution of fuel/clad reaction is however widely obscured by the steam access.

4. Assessment of Cladding Tube Inner Corrosion

4.1 Chemical Behavior of the Fuel

Zircaloy (Zry) has a very high affinity for oxygen and, therefore, it is capable of reducing the slightly hyperstoichiometric oxide fuel (UO_{2+x}) while forming oxygen stabilized α-Zr(O) and ZrO_2 (α-Zr(O) and ZrO_2 being more stable thermodynamically than hyperstoichiometric and stoichiometric UO_2. However, under normal reactor operating conditions, the temperatures of the cladding material are so low that due to the slow reaction kinetics the chemical interactions between UO_2 and Zry can be tolerated. This is not the case in a loss-of-coolant accident (LOCA) in which the normal cladding temperature will be clearly exceeded. Therefore, in a LOCA transient, the cladding tube inner surface might undergo oxidation by UO_2 in addition to the oxidation of the cladding tube outer surface caused by steam. However, the extent of the inner cladding oxidation descisively depends - besides on the temperature and time - on the solid contact between the fuel and the cladding material. In case of direct solid contact the UO_2-Zry reactions are considerably faster than in reactions going via the gas phase. Since in a LOCA the cladding is generally detached from the fuel, the oxygen can be transported from UO_2 to Zry via the gas phase only. For this reason and because of the relatively short duration of a LOCA transient, the chemical interactions between UO_2 and Zry will be not particularly pronounced /5/.

4.2 Chemical Behavior of the Fission Products

In the course of in-pile ramp experiments and in out-of-pile experiments it was demonstrated without any doubt that reactive fission products such as iodine, are susceptible to causing failure of the Zircaloy cladding material due to stress corrosion cracking (SCC). Although in the ramp experiments the expected iodine concentration is much lower than the necessary iodine concentration determined in out-of-pile experiments cladding tube failure due to SCC can occur, especially with fuel rods of

medium and high burn-up rates. However, the prerequisite is, in addition to the presence of chemically reactive fission products, a sufficient high tensile stress in the cladding tube.

Laboratory experiments on the behavior of LWR fuel rods in LOCA transients have shown that - also under these conditions - iodine can cause a strong reduction in burst strain up to temperatures of about 800°C. For these reasons it had to be expected that also in in-pile LOCA experiments involving fuel rods with high burnups the fission products exert an influence on the rupture behavior of the cladding tubes below 850°C /6/.

However, in the FR 2 in-pile experiments no influence of fission products on the burst strain of the Zircaloy cladding tubes has sc far been detected despite the partly high burnups reached (35,000 MWd/t). The reasons might be of a different nature. A major reason could be that iodine is not present in the fuel rod at a sufficient concentration. Starting from balance considerations, a sufficient amount of iodine should be present in the fuel at high burnup rates. However, the availability of iodine on the cladding tube inner surface highly depends on the release of fission products during pre-irradiation and in the LOCA transient. Measurements of fission gas release which might be considered as a measure of iodine release, yielded for the LOCA transient values $\leq$ 6%. A comparision of these release values with the critical iodine concentration which result in a low ductility failure of the cladding tube shows that the iodine concentrations in the fuel rod are too low (under the assumption that the iodine is homogeneously distributed in the fuel rod). Moreover, the chemical state of iodine in the fuel rod plays a decisive role. It has not been definitely clarified to which extent the conditions of pre-irradiation, the preconditioning of the fuel before the transient (buildup of short-lived fission product isotopes and the steady state fission product chemistry), and the course of the LOCA transient exert an influence on the release of fission products and the chemical state of the fission products. Considering these facts, a final statement cannot yet be made on the possible influence of fission products on the burst strain of the cladding tubes. It is possible that a different mode of conduct of the experiment (changing over from full reactor power to the LOCA transient) and/or a practice relevant preconditioning of the fuel rod might give other test results.

5. Mechanical Behavior of the Fuel

In the course of irradiation the fuel undergoes physical and chemical changes which are due to the fission products generated. On account of the poor thermal conductivity of UO_2 the heat produced in the fuel gives rise to a steep temperature gradient with an elevated fuel central temperature. The fuel central temperature and the temperature gradient are determined by the linear rod power of the fuel rod and they exert a high influence on the migration and release of fission products during reactor operation. Moreover, the temperature gradient causes mechanical stresses in the fuel which result in the formation of cracks in the fuel. The degree of crack formation depends primarily on the linear rod power and on the number of power cycles in the reactor (startup and shutdown, changes of reactor power). The state of burnup of the fuel rod has but a slight influence on crack formation. Due to the radial, tangential and transversal cracks in the fuel the latter disintegrates into fragments which considerably increases the free fuel surface.

5.1 Fuel not Subjected to Pre-Irradiation

As regards the mechanical behavior of the UO_2 fuel pellets it can be observed in the tests involving UO_2 not subjected to pre-irradiation that the UO_2 pellets during the LOCA transient do not rupture at all or into a few large fragments only occuring in the zone of ballooning (Figs.15,16) However, in most cases only microcracks can be found in the UO_2 pellets (Fig.16). Since the fuel rod had not been preconditioned at normal rod power ($\geq$ 200 W/cm), fragmentation of the fuel during the LOCA transient is not to be expected. The low rod power of about 50 W/cm for simulating the decay heat, is not sufficient to cause UO_2 fragmentation. Most probably the fragmentation of the UO_2 pellet in the burst zone was caused by mechanical interactions between the fuel rod and the shroud after bursting.

5.2 Pre-Irradiated Fuel

During irradiation fuel fragmentation is unavoidable. The pattern of cracks, i.e., the number of radial, tangential and transversal cracks in UO_2 and, hence, the size and shape of the fuel particles, are mainly determined by the rod power. Typical crack patterns of the fuel after irradiation (35,000 MWd/t) can be seen in Fig.17.

During the LOCA transient the cladding material is detached from the fuel since there is no close bond between the UO_2 and the Zircaloy. This means that the outer structure of the fuel gets lost so that the fuel pellets in the zone of ballooning fall apart (Fig.18,19). This seems to occur after major deformation has taken place, or, when the cladding tube bursts by mechanical action. The post-irradiation examinations did not provide indications that the disintegration of the fuel exerts an influence on the size of the balloon and its shape. During the LOCA transient some additional microcracks are formed in the fuel particles although the particle size is generally maintained (compare Fig. 19 with Fig. 17).

6. Fission Gas Behavior and Fuel Swelling

The swelling was evaluated by measurements of the fuel immersion density in carbon tetrachloride before and after irradiation and LOCA-testing, respectively. The density increased during irradiation up to about 3% burnup. This is due to a volume-averaged swelling rate of about 1% per % burnup and an irradiation-induced densification to about 2% residual porosity. There was no noticeable swelling during the LOCA-tests.

Fission gas determinations were carried out after irradiation and after LOCA-testing. The amount of fission gas was measured in the three steps as (1) released fission gas, (2) fission gas retained in pores and bubbles and (3) fission gas retained in the matrix. The released fission gas was removed from the capsules by puncturing the can. The quantities of xenon and krypton were evaluated by gas chromatography. Because of the cladding defects in the LOCA-tested fuel pins it was not possible to measure exactly the fission gas release during the LOCA. The release values could only be deduced from the measurements of the retained fission gas. To evaluate the retained fission gas the fuel was ground in a ball mill to particle sizes smaller than 1 µm. The fission gas released during grinding is called "gas in pores". It orginates from pores and bubbles and from grain boundaries. After grinding the powdered fuel was dissolved in nitric

acid. The fission gas released in this step was in fission-induced solution and in very small intragranular bubbles. This gas is called "gas in the matrix".

The mean fission gas release in the fuel pin F 6 with 2.4% burnup was about 3.5%. As deduced from measurements of the retained fission gas there was a slight dependence of the release on the axial position according to the axial profile of burnup and linear rod power. The fission gas release during the LOCA tests was between 0 and 6%. The LOCA fission gas release is primarily caused by crack formation.

In order to investigate fission gas and fuel behavior under "small break LOCA" conditions fuel samples of the preirradiated but not LOCA-tested fuel pins are annealed for various times at temperatures between 1200 and 1600°C. Up to now the annealing test with samples of the fuel pin F 6 are completed. The observed effects were small at temperatures up to 1400°C. After a 3 hours annealing at 1400°C the swelling was 0.5% and the fission gas release was 3%. With increasing temperature fission gas release and swelling increase. Fig.20 shows the fission gas release during the annealing tests at 1500 and 1600°C as a function of annealing time. Fig.21 shows the swelling.

The time dependence of the fission gas release during the LOCA and the annealing tests supports the conclusion that different release mechanisms are effective:

- crack formation,
- grain boundary separations caused by bubble growth and coalescence,
- diffusion, i.e. transport of single gas atoms or small bubbles to free surfaces or grain boundaries.

The fission gas fraction, i.e. the released gas, the gas in pores, and the gas in the matrix, in fuel samples of the test series F after different treatments are shown in Fig.22.

The mircrostructure of the fuel samples annealed at 1500 and 1600°C is characterized by grain boundary separations. The effect intensifies with increasing annealing temperature and time.

7. References

[1] H.M. Chung and T.F. Kassner
Deformation Characteristics of Zircaloy Cladding in Vacuum and Steam under Transient-Heating conditions: Summary Report ANL-77-31, July 1978.

[2] K.M. Rose, C.A. Mann and E.D. Hindle
Axial distribution of deformation in the cladding of pressurized water reactor fuel rods in a loss-of-coolant accident Nucl. Technol. 46, 2 (220-227) Dec. 1979.

[3] S. Leistikow, G. Schanz and H. v. Berg
Kinetik und Morphologie der isothermen Dampf-Oxidation von Zircaloy-4 bei 700-1300°C ,KfK 2587, March 1978.

[4] S. Leistikow, G. Schanz and H. v. Berg
Untersuchungen zur temperatur-transienten Dampfoxidation von Zircaloy-4-Hüllmaterial unter hypothetischen DWR-Kühlmittelverlust -Störfallbedingungen, KfK 2810, April 1979.

[5] P.Hofmann, C.Politis
The kinetics of the uranium dioxide-Zircaloy reactions at high temperatures
Journal of Nucl.Materials 87, No. 2&3, (1979) pp. 375-397

[6] P.Hofmann
Influence of iodine in the burst strain of Zircaloy-4 cladding tubes under simulated reactor accident conditions
Journal of Nucl.Materials 87, No. 1, (1979) pp.49 - 69

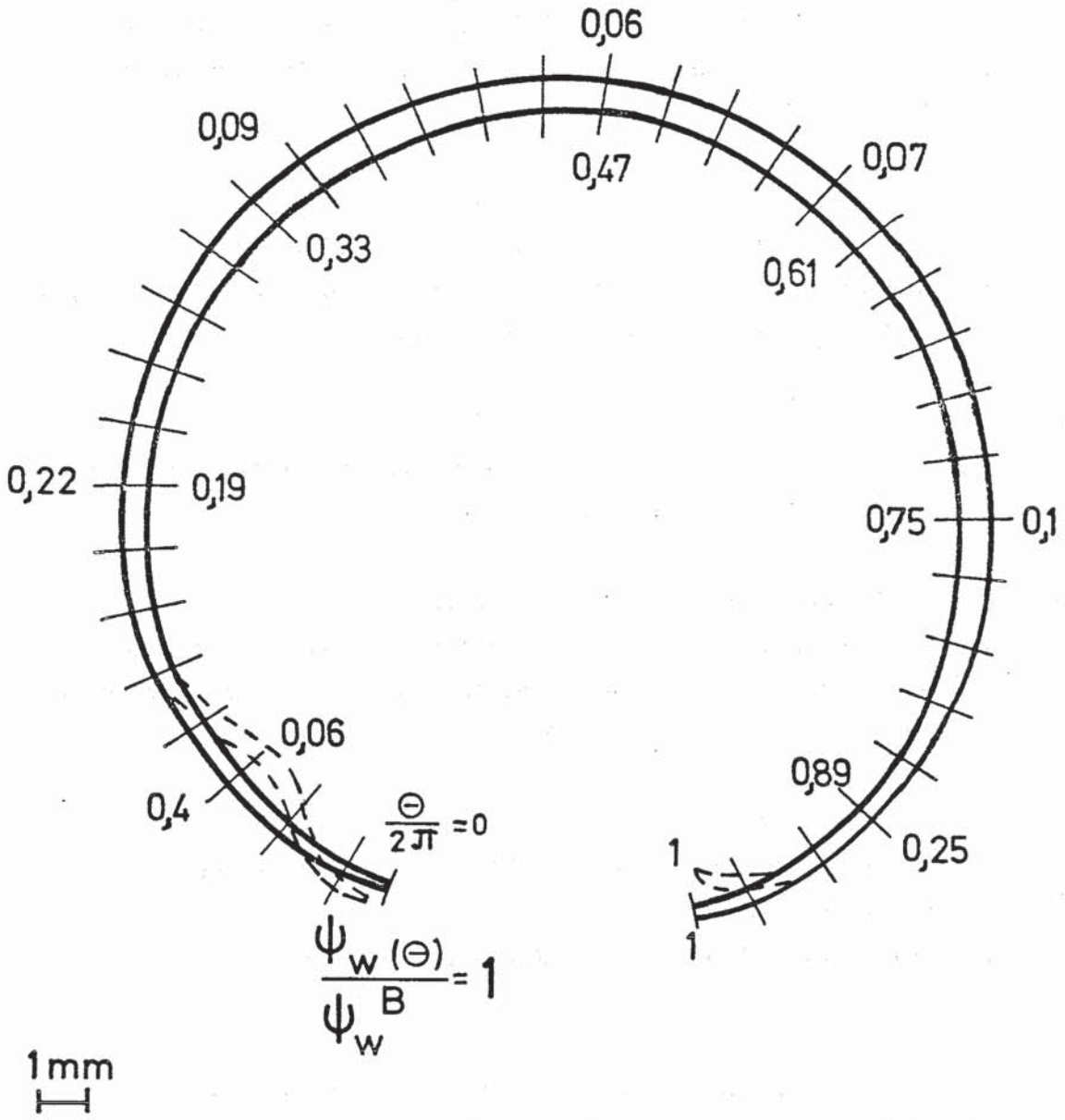

Fig. 1: Cross section of maximum circumferential strain from test B3.2 indicating the radial strain measurement steps.

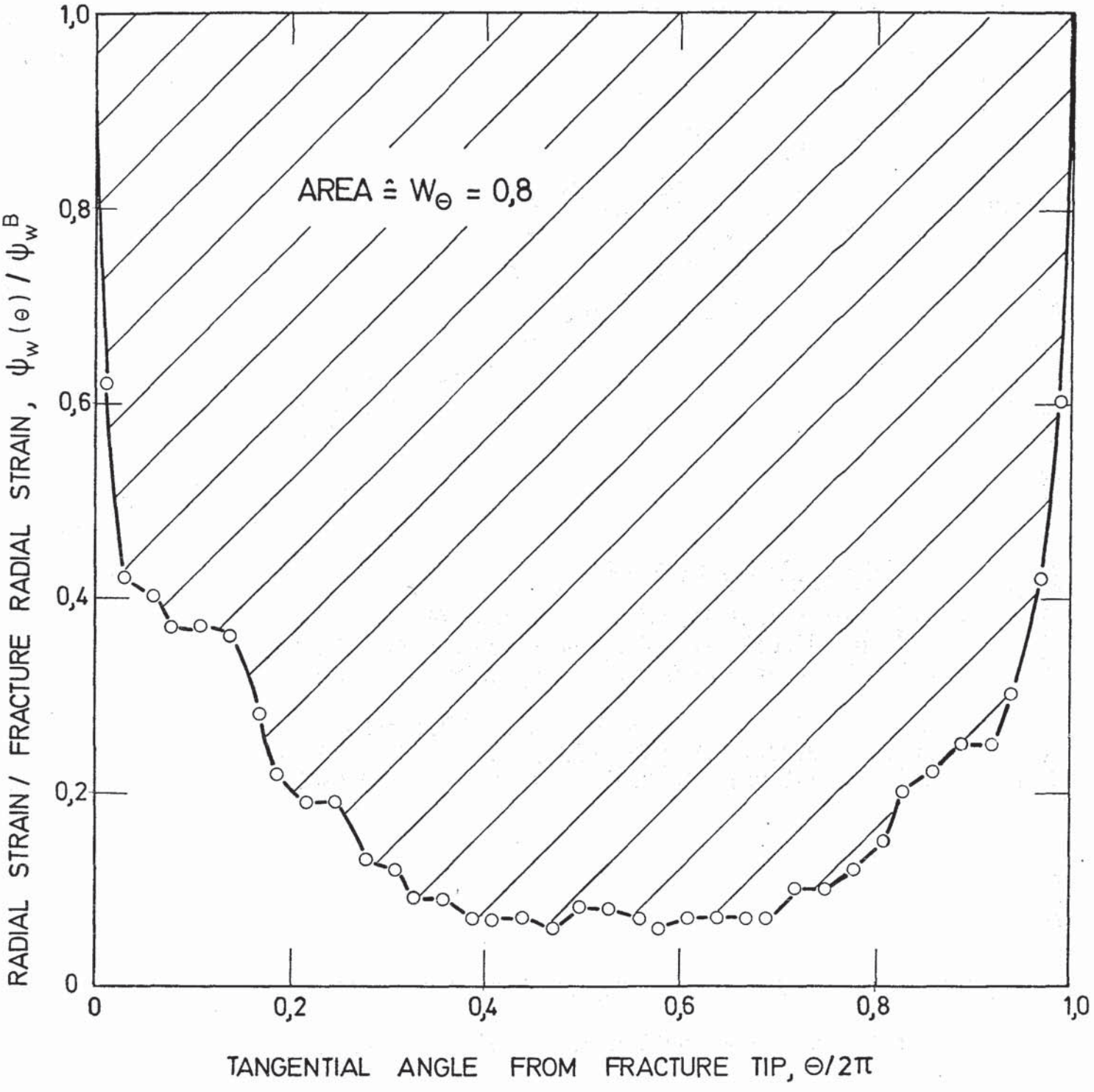

Fig. 2: Method of determining the radial strain localization parameter W_Θ (Test B3.2).

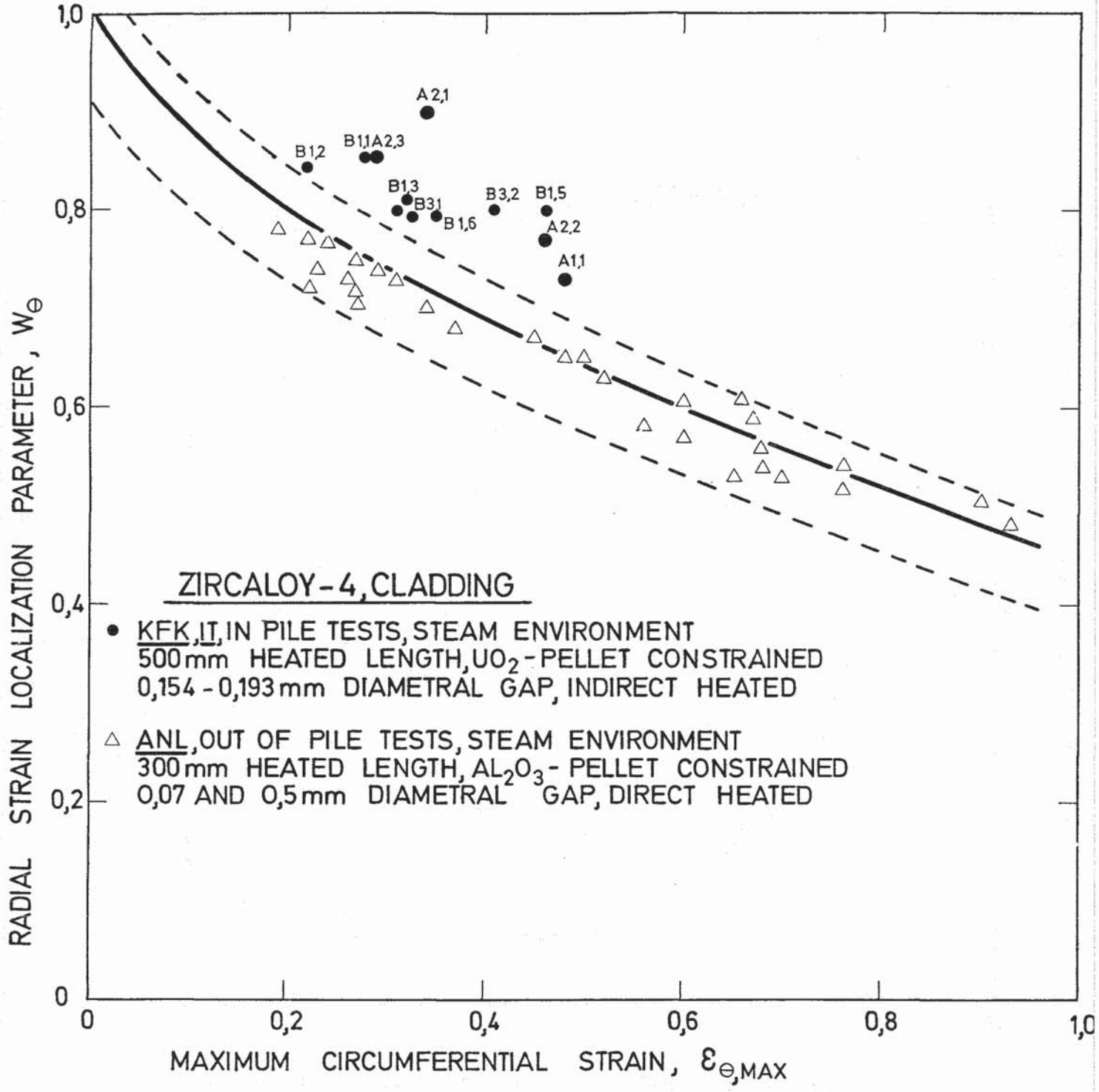

Fig. 3: Maximum circumferential strain vs. W_Θ. Tests of A and B series compared with ANL-data [1].

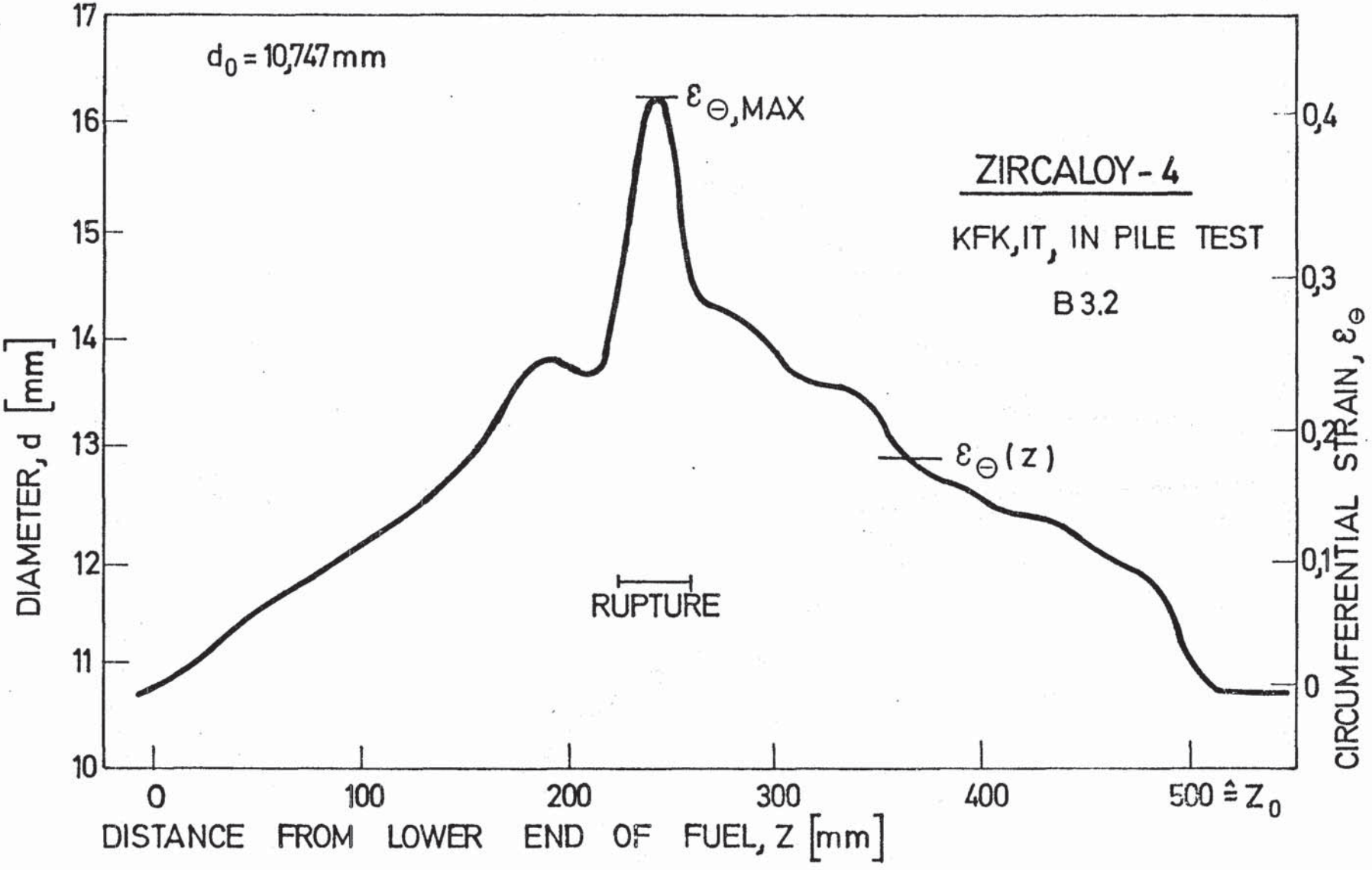

Fig. 4: Change in diameter along the heated zone (Test B3.2).

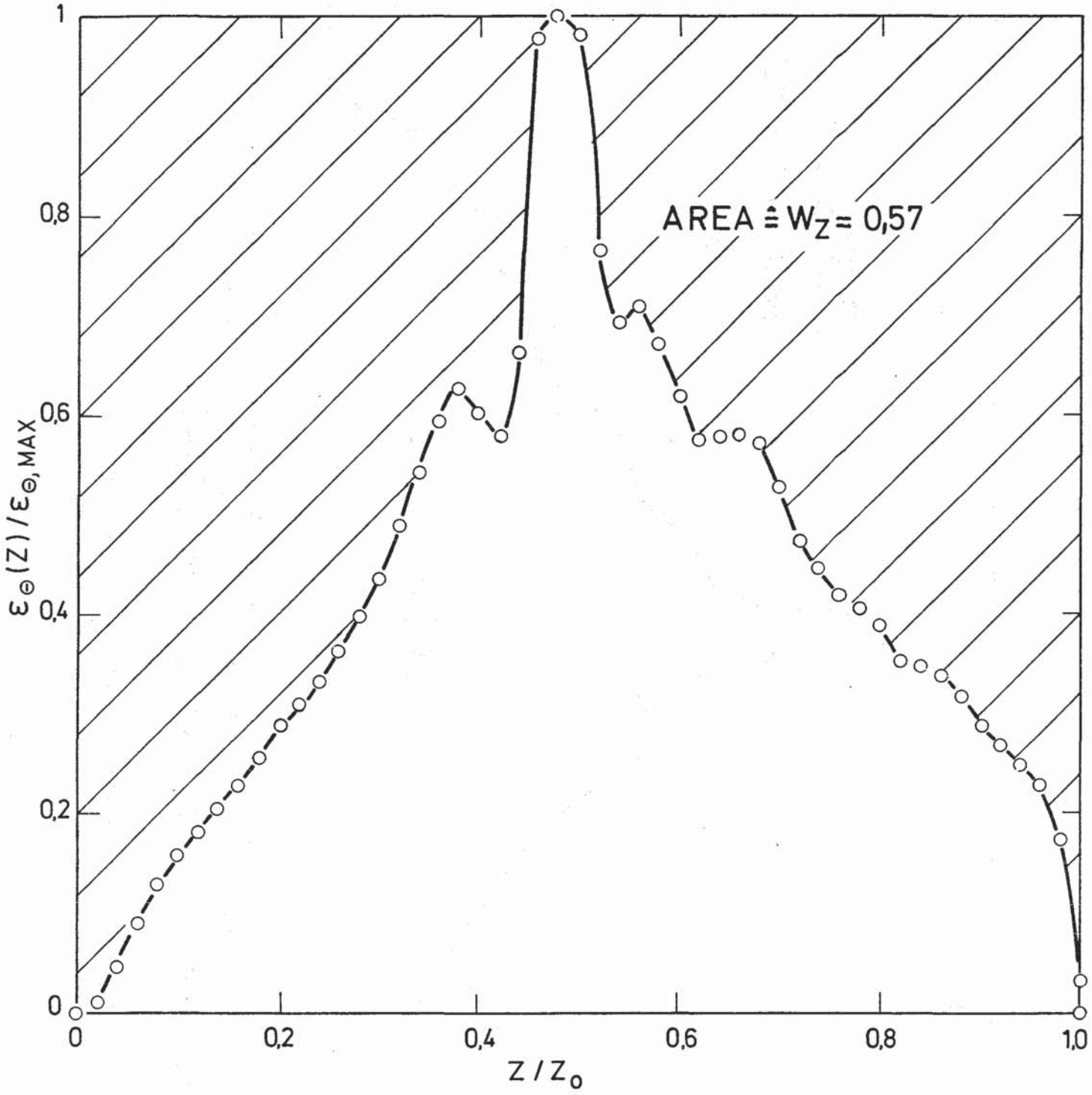

Fig. 5: Method of determining the axial strain localization parameter W_z (Test B3.2).

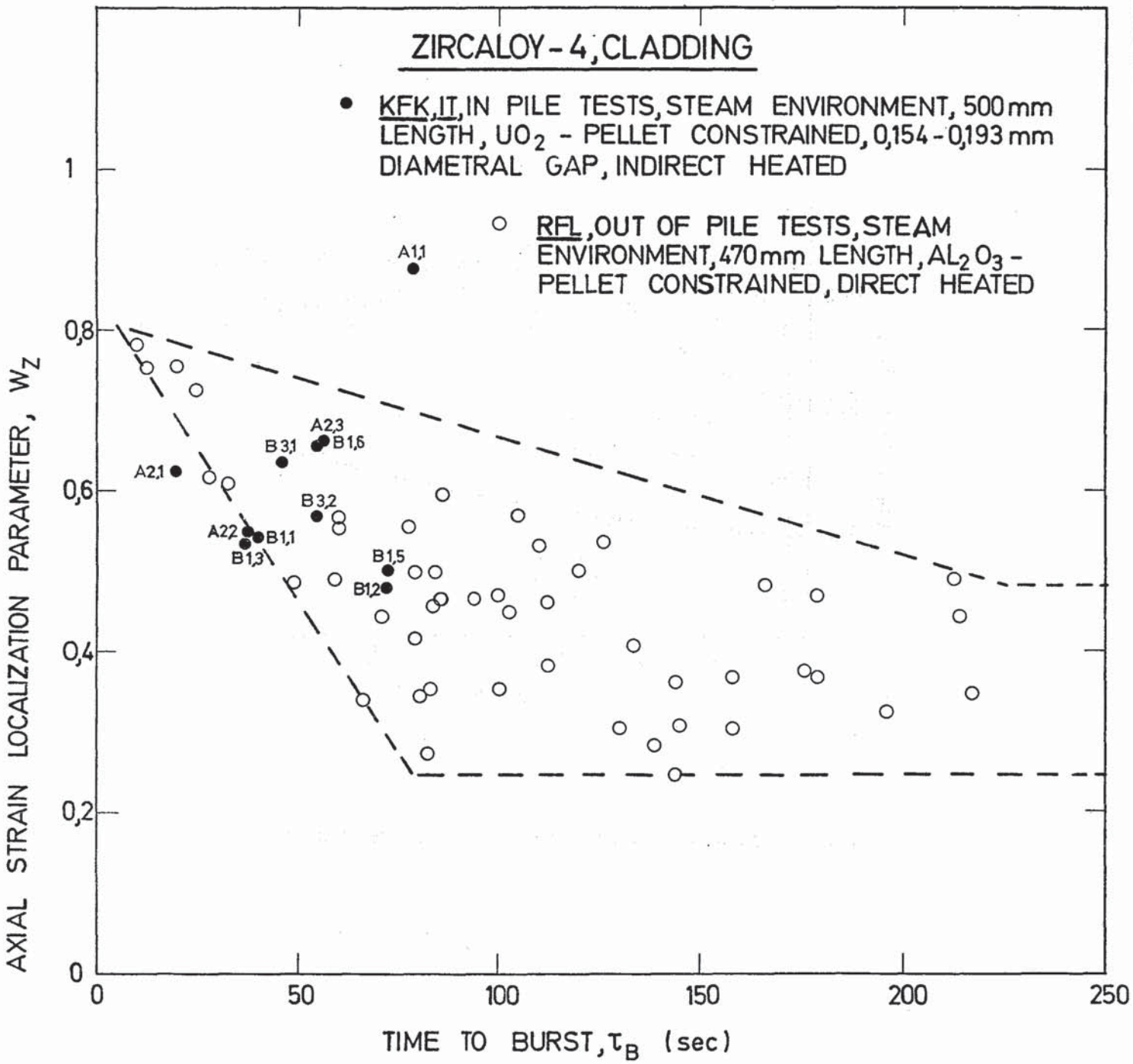

Fig. 6: Time to burst vs W_z. Tests of A and B series compared with RFL-data [2].

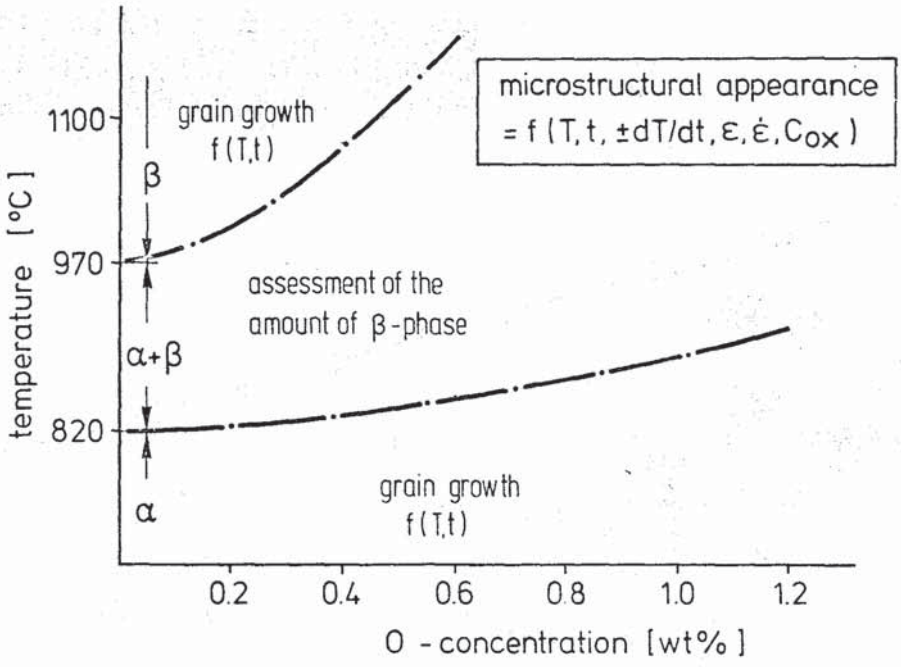

Fig. 7: Pseudobinary Zircaloy-oxygen phase diagram.

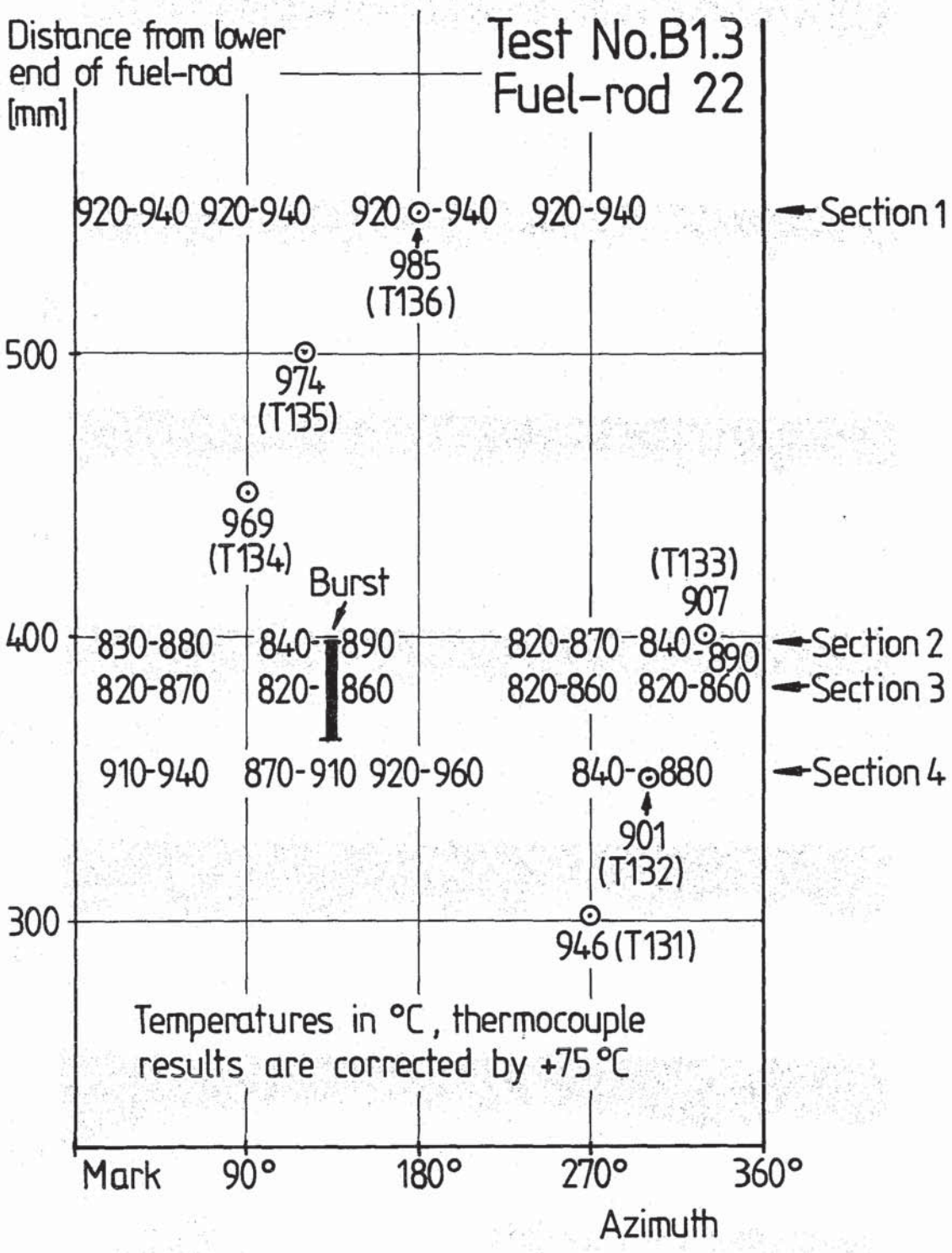

Fig. 8: Field of Zry cladding maximum temperatures, microstructural appearance and measurement.

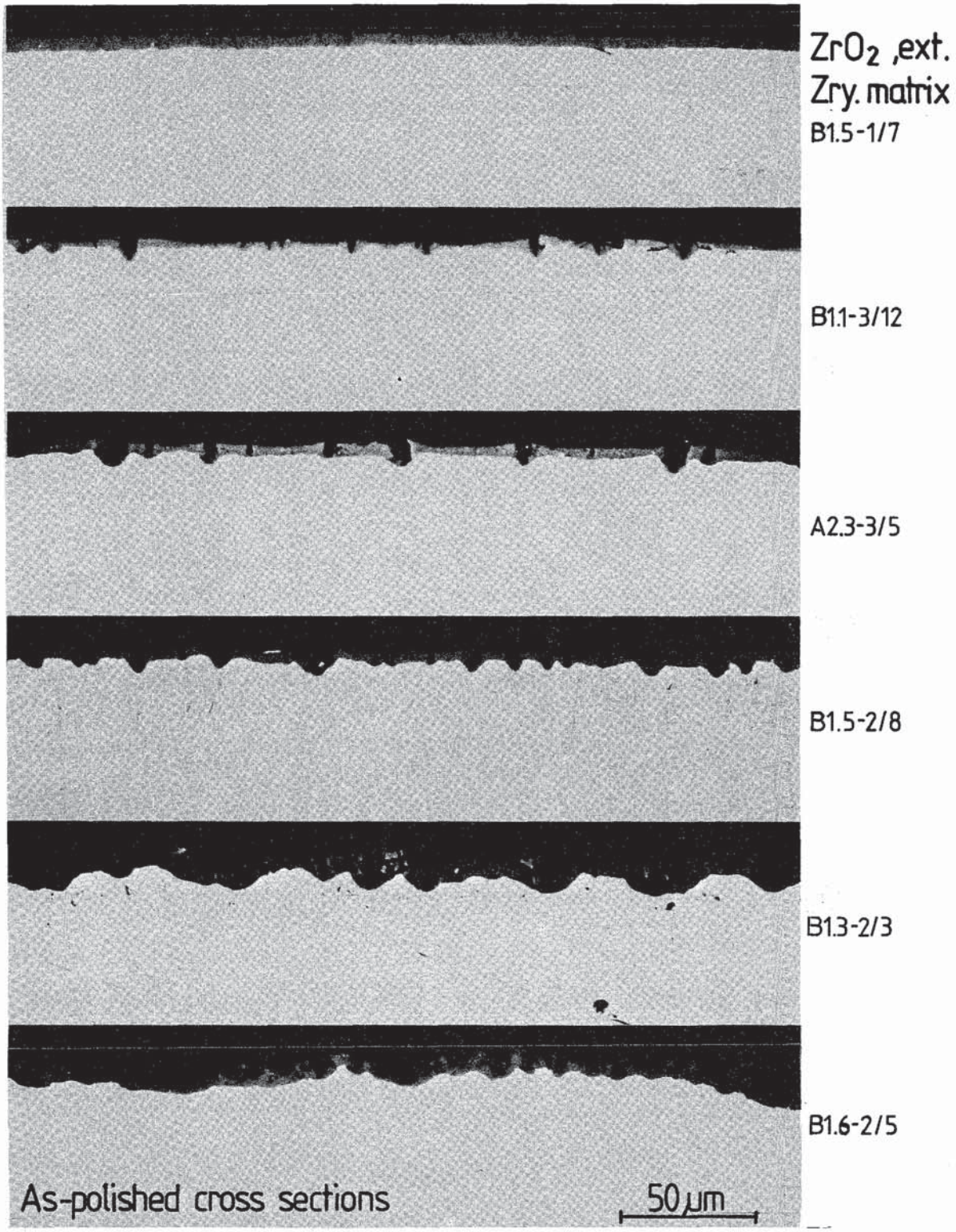

Fig. 9: Zircaloy-4 oxidation during in-pile transients; strain-dependent crack pattern in outer oxide

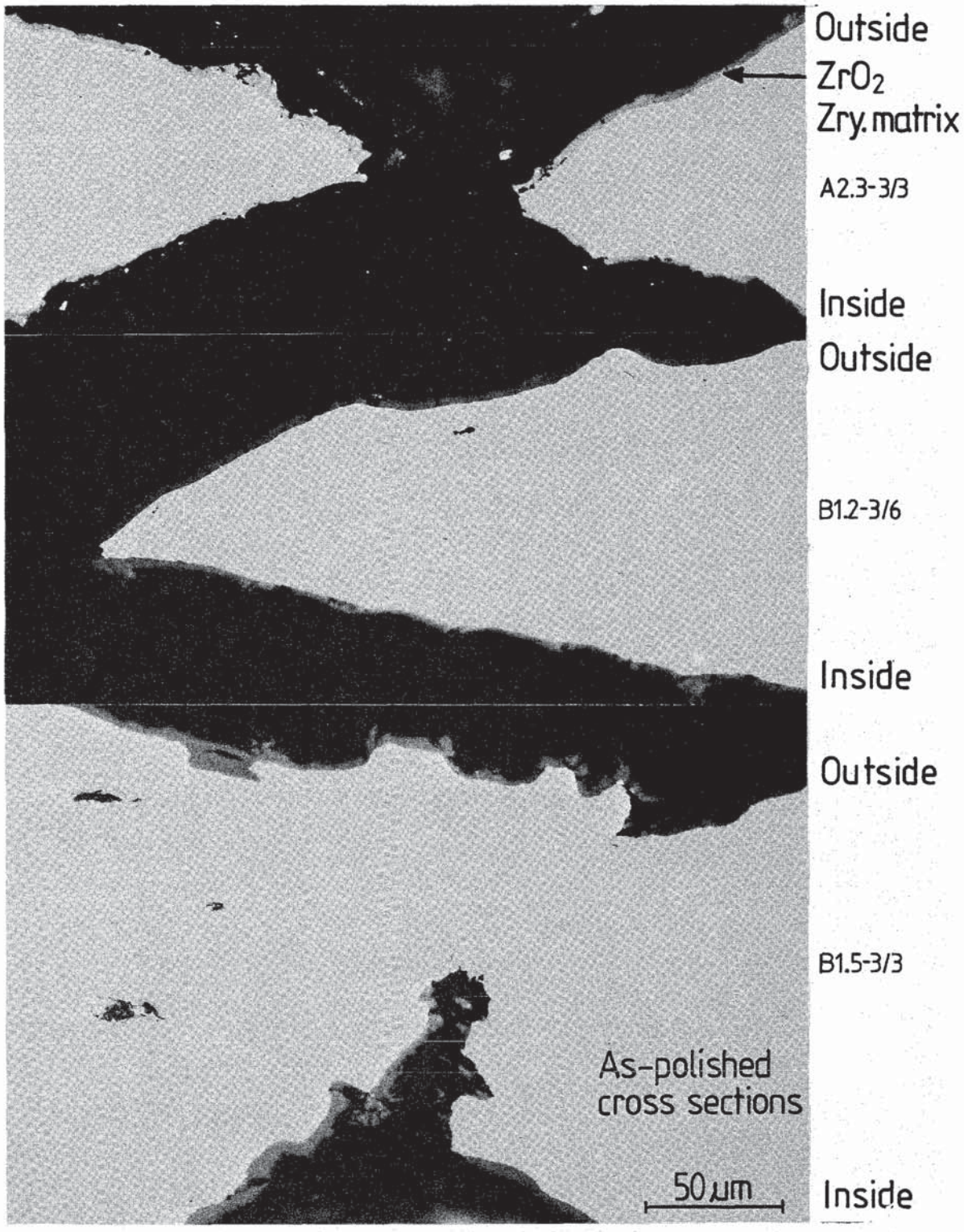

Fig.10: Zircaloy-4 oxidation during in-pile transients; oxide layer at the burst position

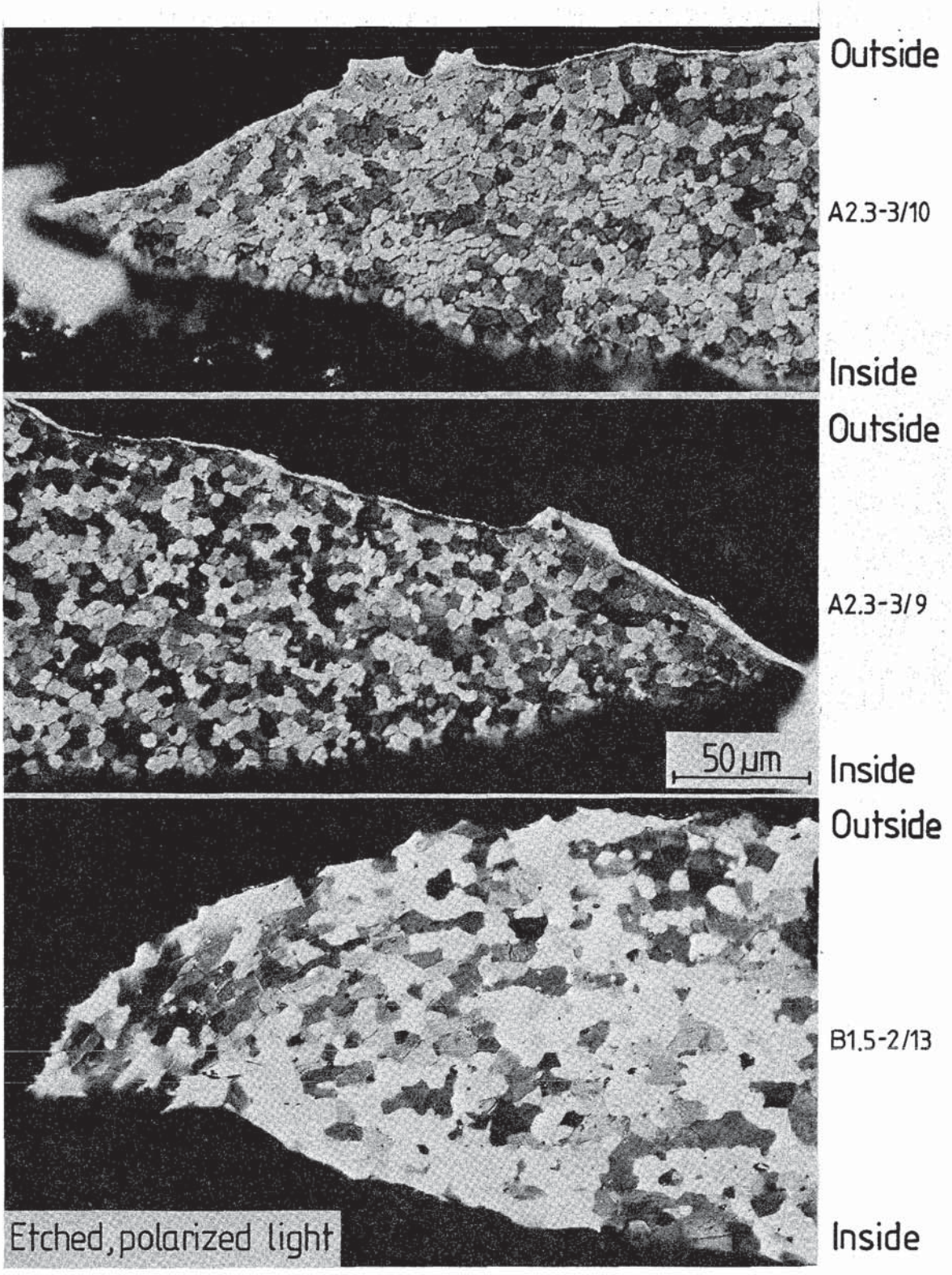

Fig.11: Zircaloy-4 oxidation during in-pile transients; α-Zr(O) layer and matrix at the burst position

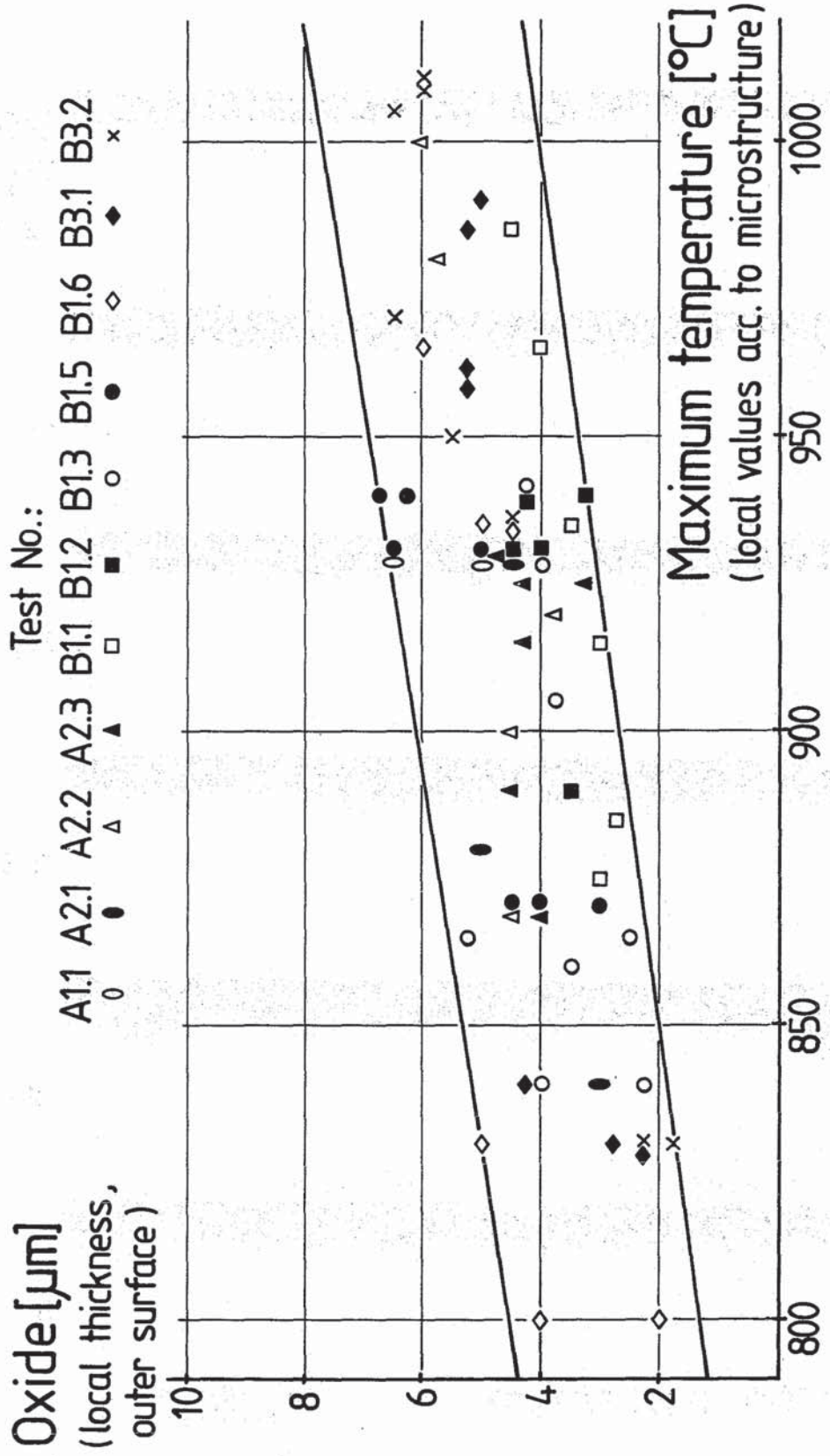

Fig.12: Steam oxidation of Zircaloy cladding tubes during in-pile tests

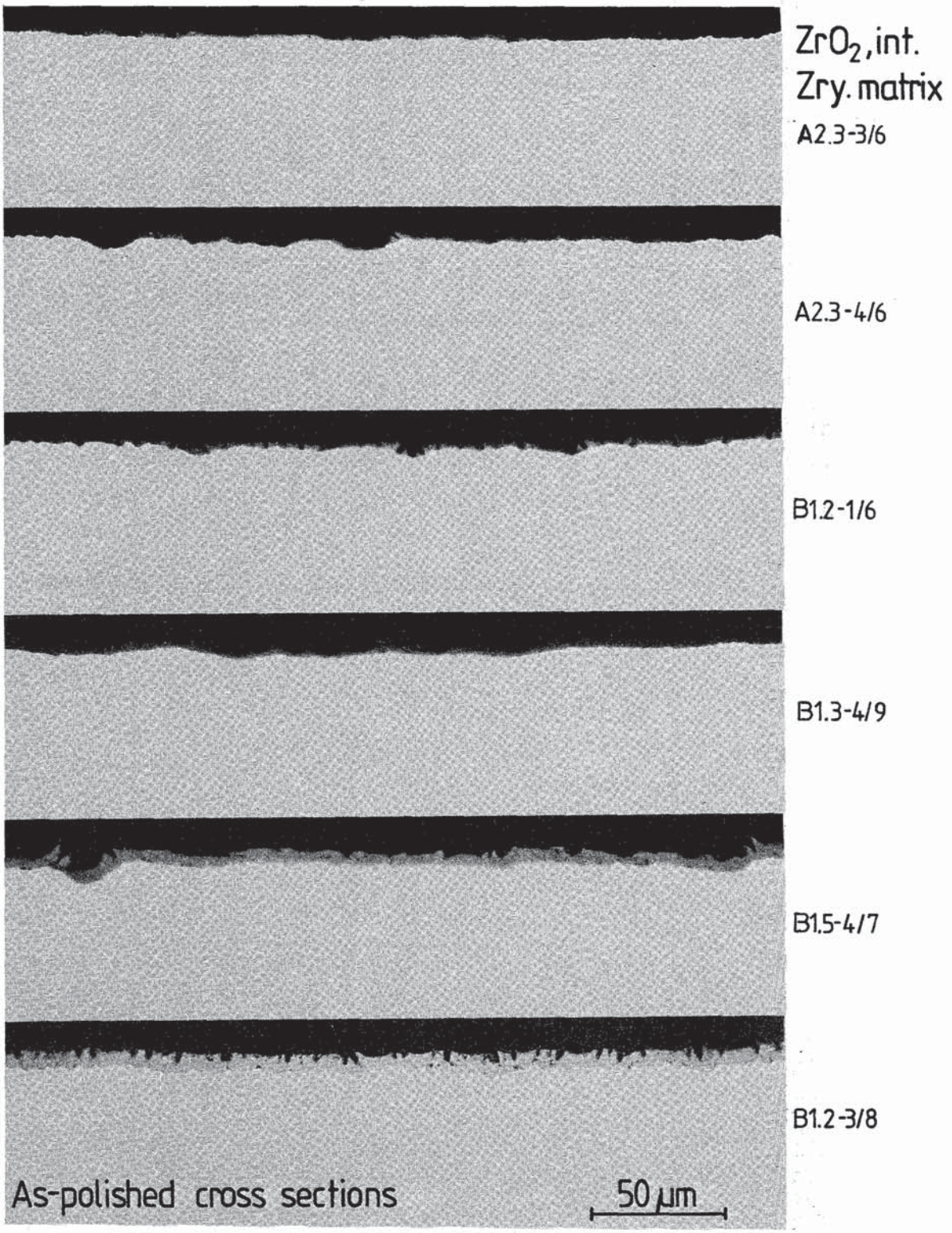

Fig.13: Zircaloy-4 oxidation during in-pile transients; oxide layer at inner cladding surface

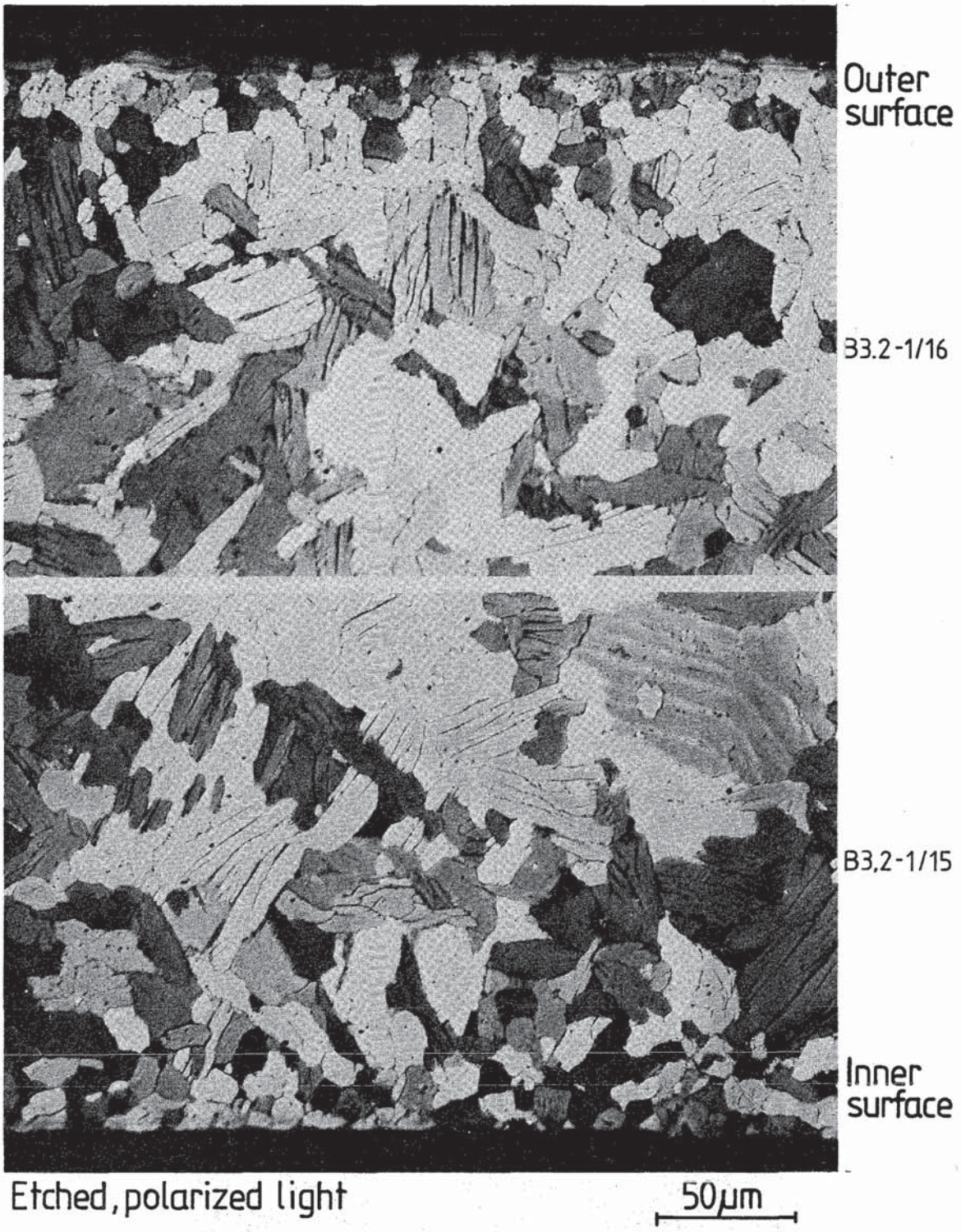

Fig.14: Zircaloy-4 oxidation during in-pile transients; matrix microstructure modified by oxygen uptake

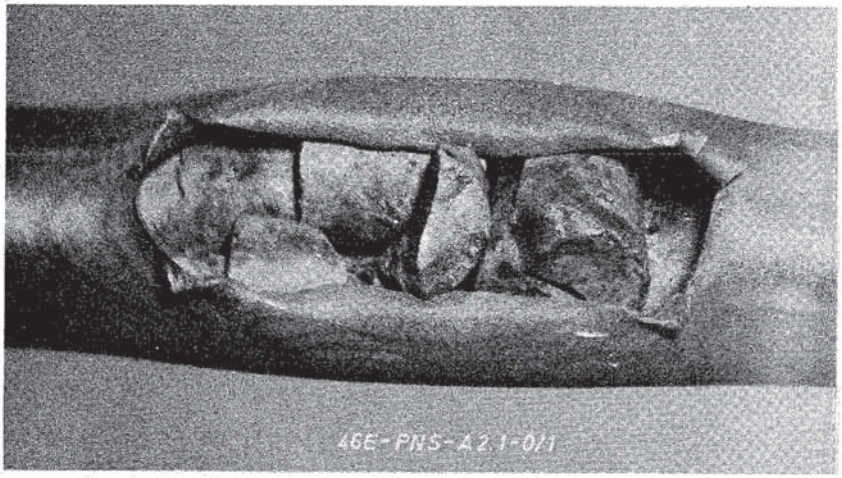

Fig.15: Fragmentation of unirradiated UO_2 pellets in the zone of bursting (Test A 2.1)

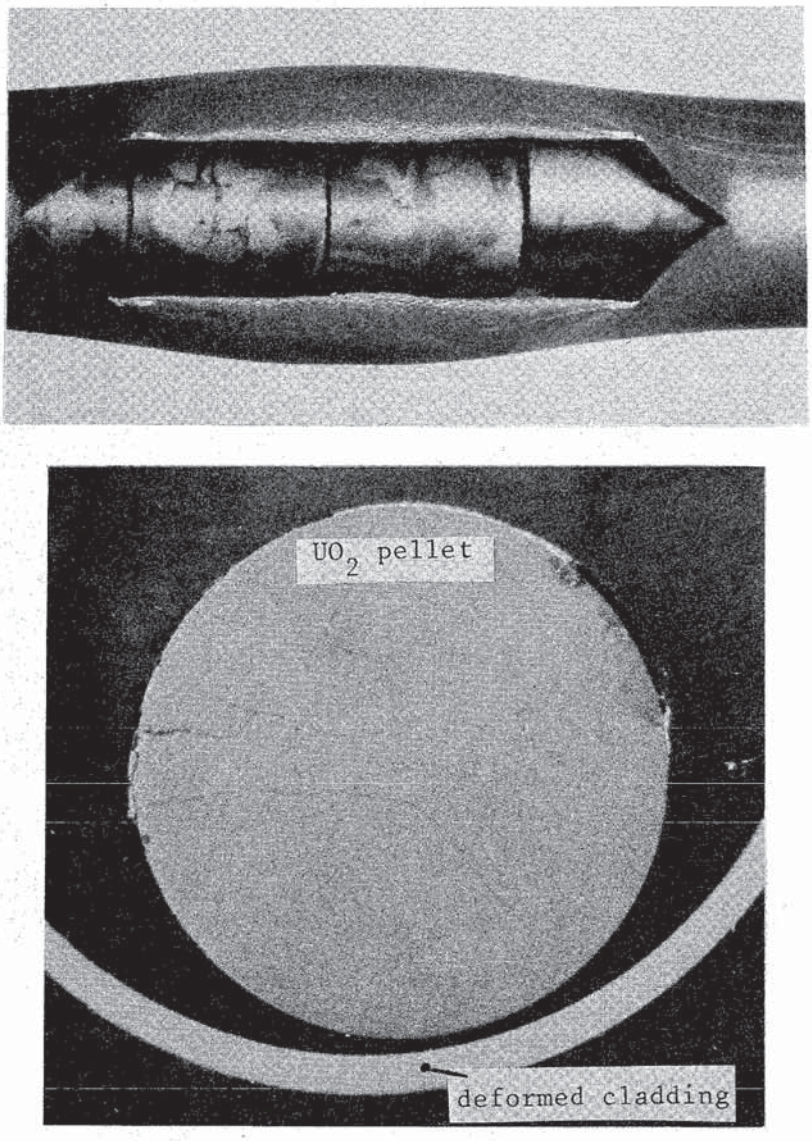

Fig.16: In test B 1.1 no fragmentation of the UO_2 pellets occurred. Only some microcracks could be observed in the pellets at the point of rupture

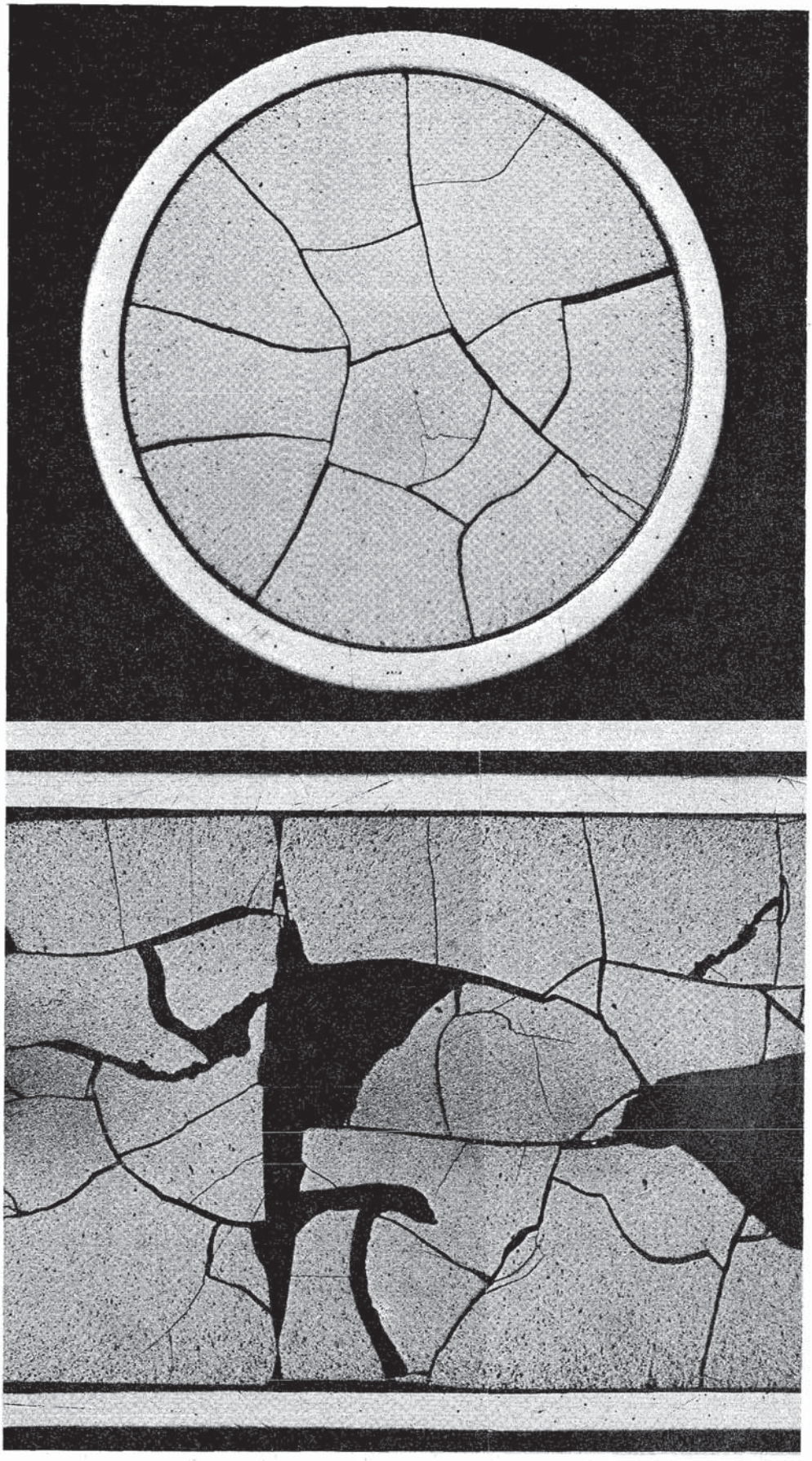

Fig.17: Cross section and longitudinal section of fuel rod F6 after irradiation (burnup: 20000 MWd/t)

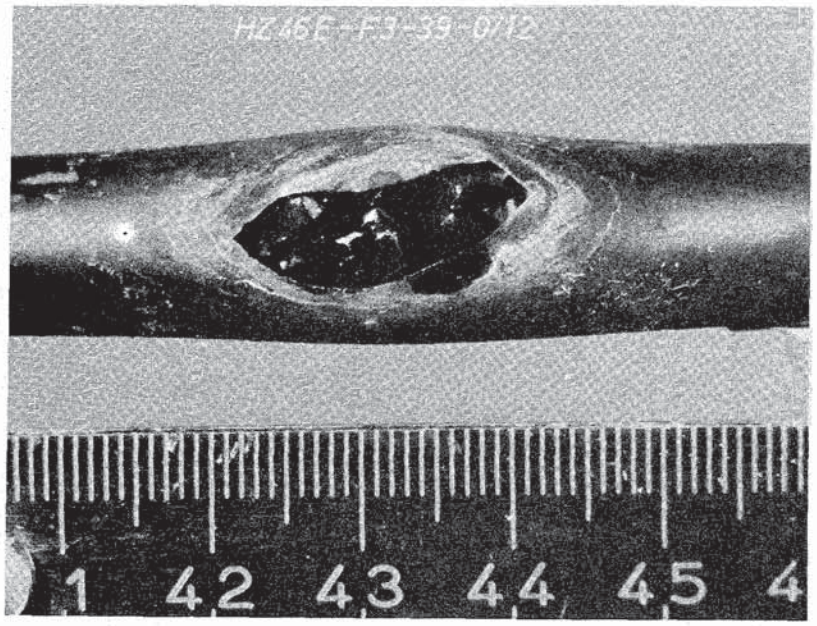

Fig.18: Burst zone of fuel rod F3 (burnup: 20000 MWd/t)

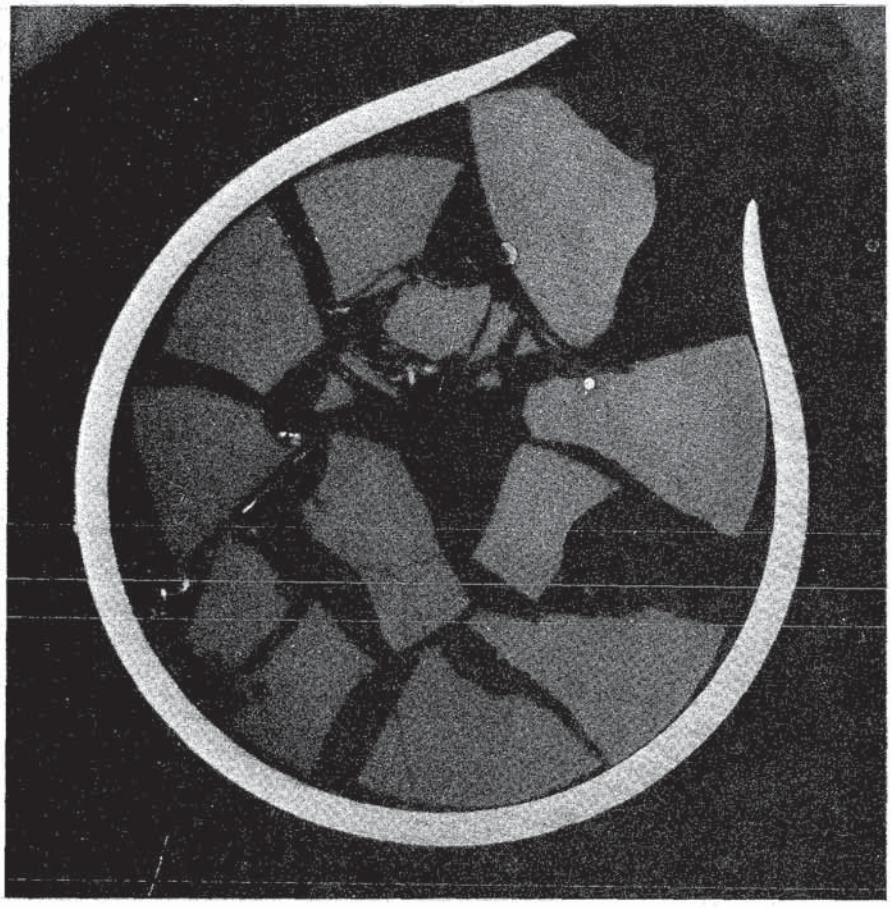

Fig.19: Cross section of the burst fuel rod F3 at the point of rupture. The fragmentation of the UO_2 pellets occurs during pre-irradiation

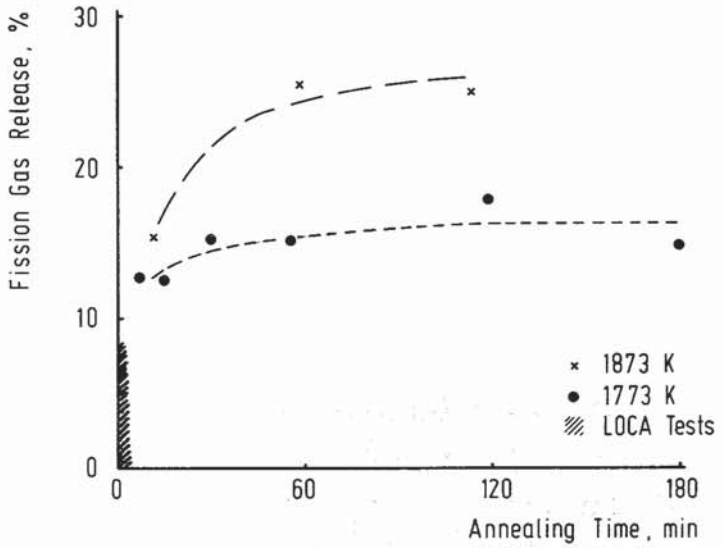

Fig.20: Fission gas release during the annealing tests (2.4% burnup)

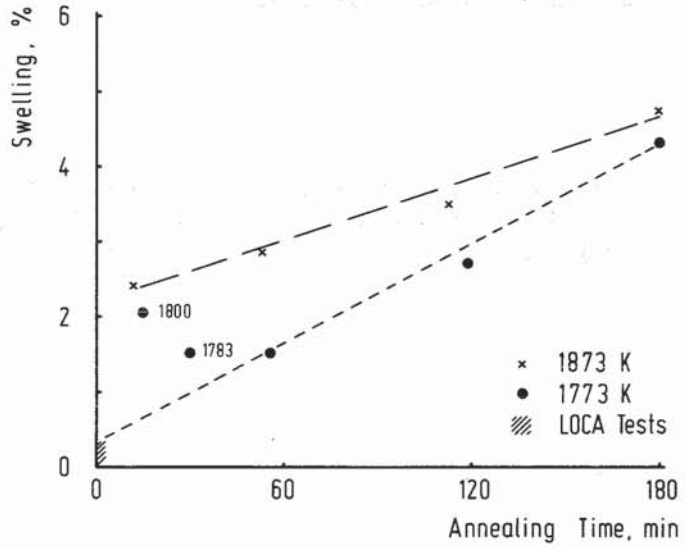

Fig.21: UO_2 swelling during the annealing tests (2.4% burnup)

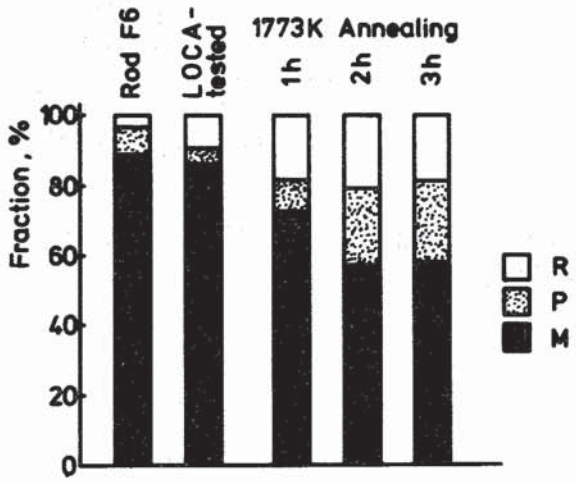

Fig.22: Fission gas fractions in fuel samples of the test series F (2.4% burnup). R: released fission gas, P: gas in pores, M: gas in the matrix

Acknowledgements

The authors are grateful to G. Harbauer, W. Leiling, and M. Prüßmann for technical assistance in the preparation of this report. The authors thank the hot cell personnel for their support of the post-test examinations.